Eur. Phys. J. C manuscript No.
(will be inserted by the editor)

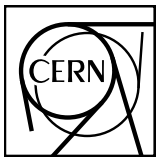

CERN-PH-EP-2015-278
07 October 2015

Measurements of $\pi^{\pm}$, $K^{\pm}$, K^0_S, Λ and proton production in proto 31 GeV/c with the NA61/SHINE spectrometer at the CERN SPS

N. Abgrall[18], A. Aduszkiewicz[23], Y. Ali[21], E. Andronov[14], T. Antićić[3], N. Antoniou[8], B. Baatar[13], F. Bay[16], A. Blondel[18], J. Blümer[5], M. Bogomilov[2], A. Bravar[18], J. Brzychczyk[21], S.A. Bunyatov[13], O. Busygina[12], P. Christakoglou[8], T. Czopowicz[25], N. Davis[8], S. Debieux[18], H. Dembinski[5], M. Deveaux[7], F. Diakonos[8], S. Di Luise[16], W. Dominik[23], T. Drozhzhova[14], J. Dumarchez[4], K. Dynowski[25], R. Engel[5], A. Ereditato[17], G.A. Feofilov[14], Z. Fodor[9,24], M. Gaździcki[7,19], M. Golubeva[12], K. Grebieszkow[25], A. Grzeszczuk[22], F. Guber[12], A. Haesler[18], T. Hasegawa[10], A. Herve[5], M. Hierholzer[17], S. Igolkin[14], A. Ivashkin[12], D. Joković[15], S. Johnson[26], K. Kadija[3], A. Kapoyannis[8], E. Kaptur[22], D. Kiełczewska[23], J. Kisiel[22], T. Kobayashi[10], V.I. Kolesnikov[13], D. Kolev[2], V.P. Kondratiev[14], A. Korzenev[18], K. Kowalik[20], S. Kowalski[22], M. Koziel[7], A. Krasnoperov[13], M. Kuich[23], A. Kurepin[12], D. Larsen[21], A. László[9], M. Lewicki[24], V.V. Lyubushkin[13], M. Maćkowiak-Pawłowska[25], Z. Majka[21], B. Maksiak[25], A.I. Malakhov[13], D. Manić[15], A. Marcinek[21,24], A. D. Marino[26], K. Marton[9], H.-J. Mathes[5], T. Matulewicz[23], V. Matveev[13], G.L. Melkumov[13], S. Morozov[12], S. Mrówczyński[19], S. Murphy[18], T. Nakadaira[10], M. Naskret[24], M. Nirkko[17], K. Nishikawa[10], T. Palczewski[20], A.D. Panagiotou[8], M. Pavin[4,3], O. Petukhov[12], C. Pistillo[17], R. Płaneta[21], J. Pluta[25], B.A. Popov[13,4], M. Posiadała-Zezula[23], S. Puławski[22], J. Puzović[15], W. Rauch[6], M. Ravonel[18], A. Redij[17], R. Renfordt[7], E. Richter-Was[21], A. Robert[4], D. Röhrich[11], E. Rondio[20], M. Roth[5], A. Rubbia[16], A. Rustamov[1,7], M. Rybczynski[19], A. Sadovsky[12], K. Sakashita[10], K. Schmidt[22], T. Sekiguchi[10], A. Seryakov[14], P. Seyboth[19], D. Sgalaberna[16], M. Shibata[10], M. Słodkowski[25], P. Staszel[21], G. Stefanek[19], J. Stepaniak[20], H. Ströbele[7], T. Šuša[3], M. Szuba[5], M. Tada[10], V. Tereshchenko[13], R. Tsenov[2], L. Turko[24], R. Ulrich[5], M. Unger[5], M. Vassiliou[8], D. Veberič[5], V.V. Vechernin[14], G. Vesztergombi[9], L. Vinogradov[14], A. Wilczek[22], Z. Wlodarczyk[19], A. Wojtaszek-Szwarc[19], O. Wyszyński[21], K.Yarritu[27], L. Zambelli[4,10]

(NA61/SHINE Collaboration)

[1] Institute of Radiation Problems, Baku, Azerbaijan
[2] Faculty of Physics, University of Sofia, Sofia, Bulgaria
[3] Ruđer Bošković Institute, Zagreb, Croatia
[4] LPNHE, University of Paris VI and VII, Paris, France
[5] Karlsruhe Institute of Technology, Karlsruhe, Germany
[6] Fachhochschule Frankfurt, Frankfurt, Germany
[7] University of Frankfurt, Frankfurt, Germany
[8] University of Athens, Athens, Greece
[9] Wigner Research Centre for Physics of the Hungarian Academy of Sciences, Budapest, Hungary
[10] Institute for Particle and Nuclear Studies, KEK, Tsukuba, Japan
[11] University of Bergen, Bergen, Norway
[12] Institute for Nuclear Research, Moscow, Russia
[13] Joint Institute for Nuclear Research, Dubna, Russia
[14] St. Petersburg State University, St. Petersburg, Russia
[15] University of Belgrade, Belgrade, Serbia
[16] ETH Zürich, Zürich, Switzerland
[17] University of Bern, Bern, Switzerland
[18] University of Geneva, Geneva, Switzerland
[19] Jan Kochanowski University in Kielce, Poland
[20] National Center for Nuclear Research, Warsaw, Poland
[21] Jagiellonian University, Cracow, Poland
[22] University of Silesia, Katowice, Poland
[23] Faculty of Physics, University of Warsaw, Warsaw, Poland
[24] University of Wrocław, Wrocław, Poland
[25] Warsaw University of Technology, Warsaw, Poland
[26] University of Colorado at Boulder, Department of Physics, Colorado, USA
[27] Los Alamos National Laboratory, Los Alamos, USA

October 5, 2015

Abstract Measurements of hadron production in p+C interactions at 31 GeV/c are performed using the NA61/ SHINE spectrometer at the CERN SPS. The analysis is based on the full set of data collected in 2009 using a graphite target with a thickness of 4% of a nuclear interaction length. Inelastic and production cross sections as well as spectra of $\pi^{\pm}$, $K^{\pm}$, p, K^0_S and Λ are measured with high precision. These measurements are essential for improved calculations of the initial neutrino fluxes in the T2K long-baseline neutrino oscillation experiment in Japan. A comparison of the NA61/SHINE measurements with predictions of several hadroproduction models is presented.

PACS 13.85.Lg,13.85.Hd,13.85.Ni

Keywords proton-Carbon interaction, hadron production

Contents

1 Introduction

The NA61/SHINE (SPS Heavy Ion and Neutrino Experiment) at CERN pursues a rich physics programme in various fields of physics [1–4]. Hadron production measurements in p+C [5, 6] and π+C interactions are needed to improve calculations of neutrino fluxes for the T2K/J-PARC [7] and Fermilab neutrino experiments [8] as well as for simulations of cosmic-ray air showers in the Pierre Auger and KASCADE experiments [9, 10]. The programme on strong interactions investigates p+p [11], p+Pb and nucleus-nucleus collisions at SPS energies, to study the onset of deconfinement and to search for the critical point of strongly interacting matter [12].

First measurements of $\pi^{\pm}$ and K^+ spectra in proton-carbon interactions at 31 GeV/c were already published by NA61/SHINE [5, 6] and used for neutrino flux predictions for the T2K experiment [14–23] at J-PARC. Yields of K^0_S and Λ were also published [13]. All of those measurements were performed using the data collected during the NA61/SHINE pilot run in 2007. A detailed description of the experimental apparatus and analysis techniques can be found in Refs. [5, 24].

This article presents new NA61/SHINE measurements of charged pion, kaon and proton as well as of K^0_S and Λ spectra in p+C interactions at 31 GeV/c, based on eight times larger dataset collected in 2009, after the detector and readout upgrades. These results are important for achieving the future T2K physics goals [25].

T2K – a long-baseline neutrino oscillation experiment from J-PARC in Tokai to Kamioka (Japan) [7] – aims to precisely measure $\nu_\mu \to \nu_e$ appearance [14, 17, 19] and ν_μ disappearance [15, 18, 20]. The neutrino beam is generated by the J-PARC high intensity 30 GeV (kinetic energy) proton beam interacting in a 90 cm long graphite target to produce π and K mesons, which decay emitting neutrinos. Some of the forward-going hadrons, mostly protons, re-interact in the target and surrounding material. To study and constrain the re-interactions in the long target, a special set of data was taken by NA61/SHINE with a replica of the T2K target: the first study based on pilot data is presented in Ref. [26], the analysis of the high-statistics 2009 dataset is finalized [27], while for the ultimate 2010 dataset the analysis is still ongoing.

The T2K neutrino beam [16] is aimed towards a near detector complex, 280 m from the target, and towards the Super-Kamiokande (SK) far detector located 295 km away at 2.5° off-axis from the hadron beam. Neutrino oscillations are probed by comparing the neutrino event rates and spectra measured in SK to predictions of a Monte-Carlo (MC) simulation based on flux calculations and near detector measurements. Until the NA61/SHINE data were available, these flux calculations were based on hadron production models tuned to sparse available data, resulting in systematic uncertainties which are large and difficult to evaluate. Direct measurements of particle production rates in p+C interactions allow for more precise and reliable estimates [16]. Precise predictions of neutrino fluxes are also crucial for neutrino cross section measurements with the T2K near detector, see e.g. Refs. [21–23].

At the first stage of the experiment, the T2K neutrino beamline was set up to focus positively charged hadrons (the

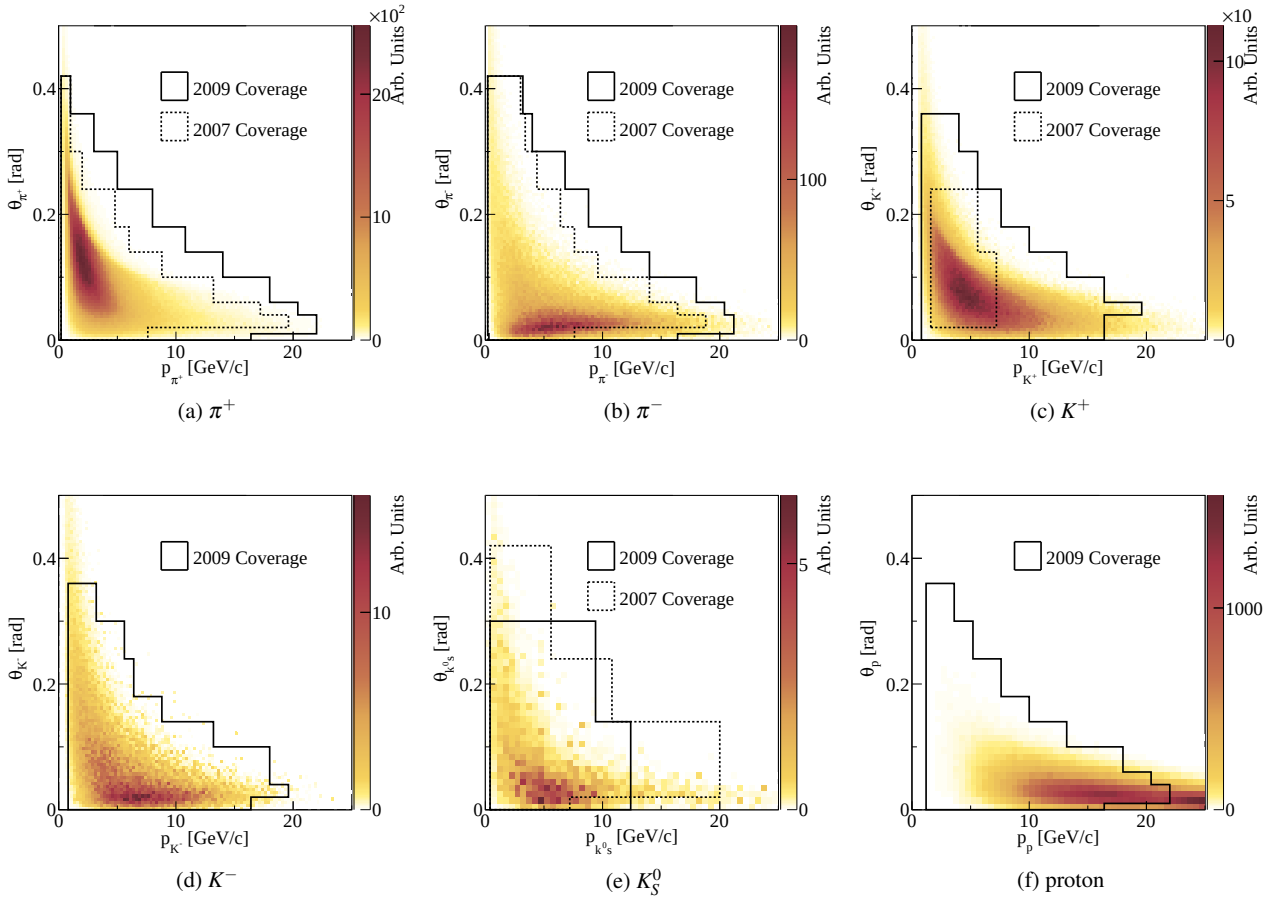

Fig. 1: (Colour online) The $\{p, \theta\}$ phase space of $\pi^{\pm}$, $K^{\pm}$, K^0_S and protons contributing to the predicted neutrino flux at SK in the "positive" focusing configuration, and the regions covered by the previously published NA61/SHINE measurements [5, 6] and by the new results presented in this article. Note that the size of the $\{p, \theta\}$ bins used in the K^0_S analysis of the 2007 data [13] is much larger compared to what is chosen for the K^0_S analysis presented here, see Section 4.3.

so-called "positive" focusing), to produce a ν_μ enhanced beam. While charged pions generate most of the low energy neutrinos, charged kaons generate the high energy tail of the T2K beam, and contribute substantially to the intrinsic ν_e component in the T2K beam. See Ref. [16] for more details. An anti-neutrino enhanced beam can be produced by reversing the current direction in the focusing elements of the beamline in order to focus negatively charged particles ("negative" focusing).

Positively and negatively charged pions and kaons whose daughter neutrinos pass through the SK detector constitute the kinematic region of interest, shown in Figs. 1 and 2 in the kinematic variables p and θ – the momentum and polar angle of particles in the laboratory frame for "positive" and "negative" focusing, respectively. See Refs. [5, 6, 16] for additional information. The much higher statistics available in the 2009 data makes it possible to use finer $\{p, \theta\}$ binning (especially for charged kaons, K^0_S and Λ) compared to our previously published results [5, 6, 13]. The improved statistics of the 2009 data also allows for the first measurements of negatively charged kaons within NA61/SHINE.

The NA61/SHINE results on hadron production are also extremely important for testing and improving existing hadron production models in an energy region which is not well constrained by measurements at present.

The paper is organized as follows: A brief description of the experimental setup, the collected data and their processing is presented in Section 2. Section 3 is devoted to the analysis technique used for the measurements of the inelastic and production cross sections in proton-carbon interactions at 31 GeV/c and the corresponding results. A detailed description of the procedures used to obtain the differential inclusive spectra of hadrons is presented in Section 4. Results on spectra are reported in Section 5. A comparison of these results with the predictions of different hadron pro-

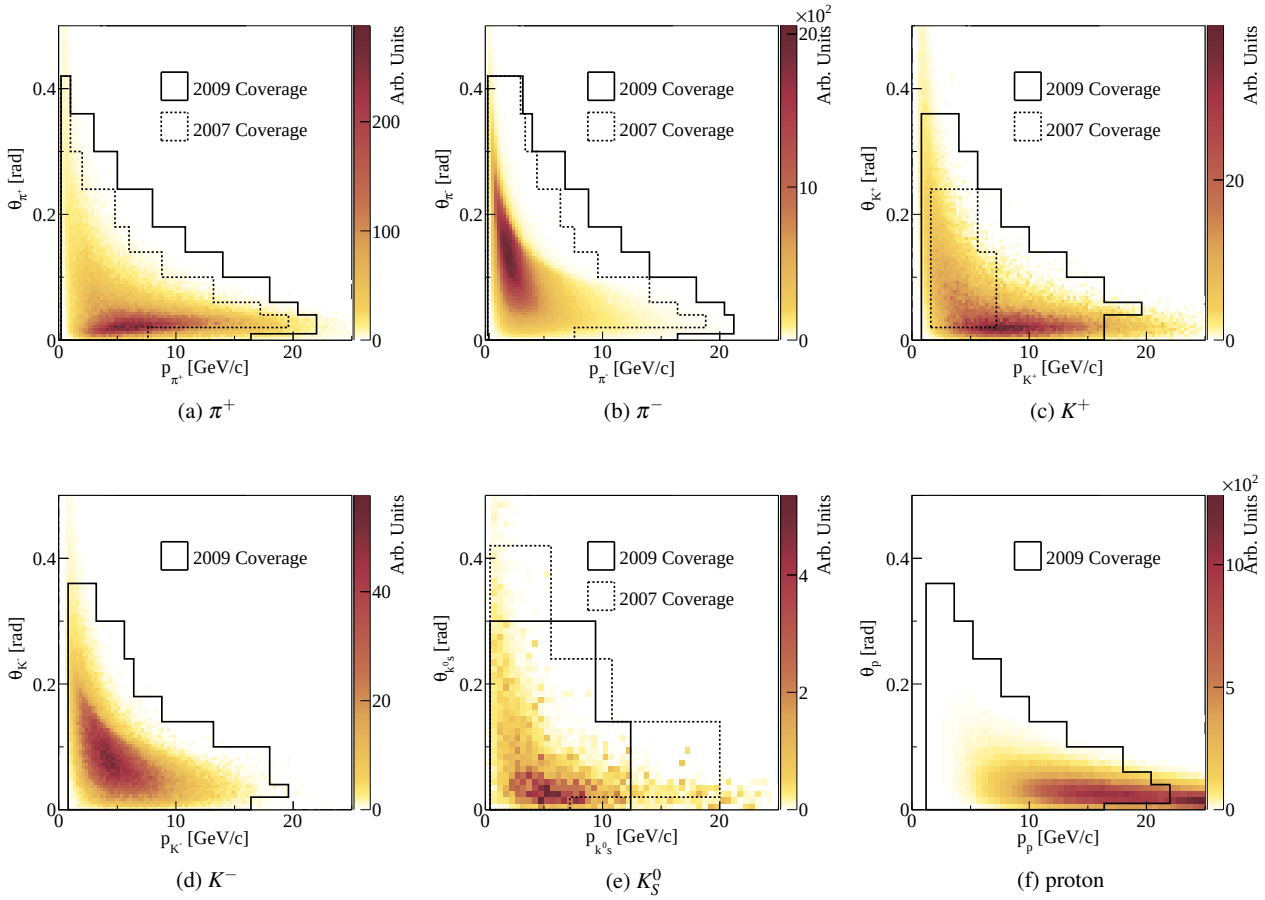

Fig. 2: (Colour online) The $\{p, \theta\}$ phase space of $\pi^{\pm}$, $K^{\pm}$, K^0_S and protons contributing to the predicted neutrino flux at SK in the "negative" focusing configuration, and the regions covered by the previously published NA61/SHINE measurements [5, 6] and by the new results presented in this article. Note that the size of the $\{p, \theta\}$ bins used in the K^0_S analysis of the 2007 data [13] is much larger compared to what is chosen for the K^0_S analysis presented here, see Section 4.3.

duction models is reported in Section 6. A summary and conclusions are given in Section 7.

2 The experimental setup, collected data and their processing

The NA61/SHINE apparatus is a wide-acceptance hadron spectrometer at the CERN SPS. Detailed description of the NA61/SHINE setup is presented in Ref. [24]. Only features relevant for the 2009 running period are briefly mentioned here. The NA61/SHINE experiment has greatly profited from long development of the CERN proton and ion sources, the accelerator chain, as well as the H2 beamline of the CERN North Area. Numerous components of the NA61/SHINE setup were inherited from its predecessors, in particular, the last one – the NA49 experiment [28].

The detector is built arround five Time Projection Chambers (TPCs), as shown in Fig. 3. Two Vertex TPCs (VTPC-1 and VTPC-2) are placed in the magnetic field produced by two superconducting dipole magnets and two Main-TPCs (MTPC-L and MTPC-R) are located downstream symmetrically with respect to the beamline. An additional small TPC is placed between VTPC-1 and VTPC-2, covering the very-forward region, and is referred to as the GAP TPC (GTPC). The GTPC was used for tracking in the analysis described here allowing to extend the kinematic coverage compared to our previously published results.

The TPCs are filled with Ar:CO_2 gas mixtures in proportions 90:10 for the VTPCs and the GTPC, and 95:5 for the MTPCs.

In the forward region, the experimental setup is complemented by a time-of-flight (ToF-F) detector array horizontally segmented into 80 scintillator bars, read out at both ends by photomultipliers [24]. Before the 2009 run, the ToF-F detector was upgraded with additional modules placed on both sides of the beam in order to extend the acceptance for

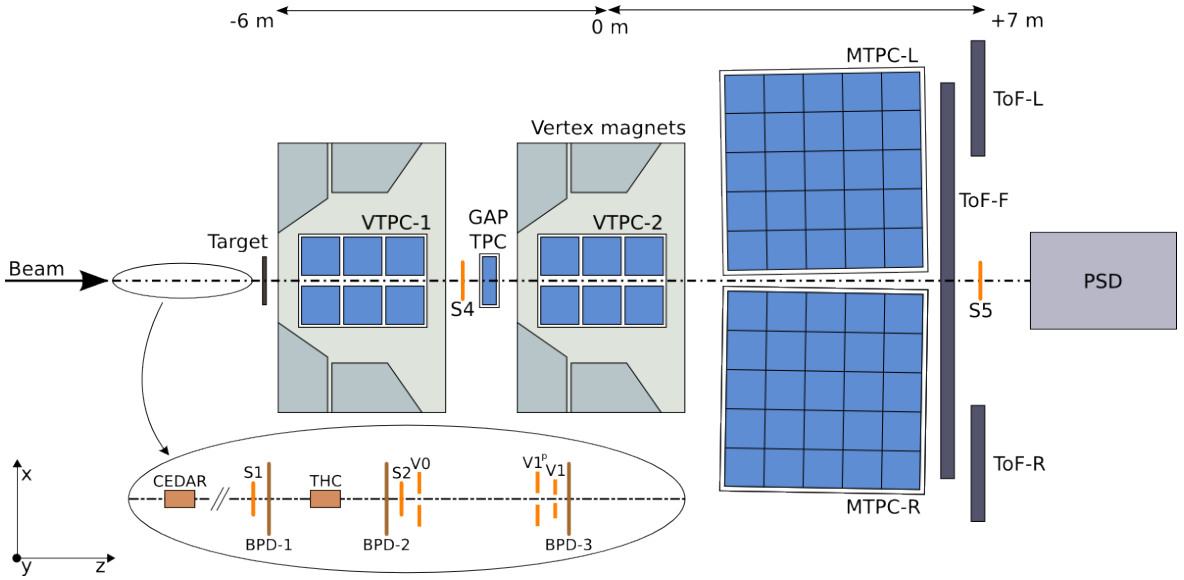

Fig. 3: (Colour online) The schematic layout of the NA61/SHINE spectrometer (horizontal cut, not to scale). The beam and trigger detector configuration used for data taking in 2009 is also presented. The chosen coordinate system is shown on the plot: its origin lies in the middle of the VTPC-2, on the beam axis. The nominal beam direction is along the z axis. The magnetic field bends charged particle trajectories in the x–z (horizontal) plane. Positively charged particles are bent towards the top of the plot. The drift direction in the TPCs is along the y (vertical) axis.

the analysis described here. The intrinsic time resolution of each scintillator is about 110 ps [24]. The particle identification capabilities of the ToF-F are illustrated in Fig. 4.

For the study presented here the magnetic field of the dipole magnets was set to a bending power of 1.14 Tm. This leads to a momentum resolution $\sigma(p)/p^2$ in the track reconstruction of about 5×10^{-3} (GeV/c)$^{-1}$ for long tracks reaching the ToF-F.

Two scintillation counters, S1 and S2, provide the beam definition, together with the three veto counters V0, V1 and V1^p, which define the beam upstream of the target. The S1 counter provides also the start time for all counters. The beam particles are identified by a CEDAR [29] and a threshold Cherenkov (THC) counters. The selection of beam protons (the beam trigger, T_{beam}) is then defined by the coincidence $\mathrm{S1}\wedge\mathrm{S2}\wedge\overline{\mathrm{V0}}\wedge\overline{\mathrm{V1}}\wedge\overline{\mathrm{V1p}}\wedge\mathrm{CEDAR}\wedge\overline{\mathrm{THC}}$. The interaction trigger ($T_{int} = T_{beam}\wedge\overline{\mathrm{S4}}$) is given by the anti-coincidence of the incoming proton beam and S4, a scintillation counter, with a 2 cm diameter, placed between the VTPC-1 and VTPC-2 detectors along the beam trajectory at about 3.7 m from the target, see Fig. 3. Almost all beam protons that interact in the target does not reach S4. The interaction and beam triggers are run simultaneously. The beam trigger events were recorded with a frequency by a factor of about 10 lower than the frequency of interaction trigger events.

The incoming beam trajectory is precisely measured by a set of three Beam Position Detectors (BPDs), placed along the beamline upstream of the target, as shown in the insert in Fig. 3. These detectors are 4.8×4.8 cm^2 proportional chambers operated with an Ar:CO_2 (85:15) gas mixture. Each BPD measures the position of the beam particle on the transverse plane with respect to the beam direction with a resolution of $\sim$100 µm (see Ref. [24] for more details).

The same target as in 2007 was used during the 2009 run – an isotropic graphite sample with a thickness along the beam axis of 2 cm, equivalent to about 4% of a nuclear interaction length, λ_I. During the data-taking the target was placed 80 cm upstream of the VTPC-1.

The TPC read-out and DAQ upgrades were performed before the 2009 run. As a result, to use the new DAQ capacity, a much higher intensity beam was used during the 2009 data-taking compared to the 2007 running period. To cope with a high beam intensity in 2009 data we count the number of through-going beam particles in a given time window and use this information during the data analysis.

The new TPC read-out electronics had been suffering from an additional electronic noise during the p+C data-taking in 2009. The problem was corrected for other settings recorded during the 2009 run.

Reconstruction and calibration algorithms applied to the raw data are briefly presented in Ref. [5]. Similar calibration procedures have also been applied to the 2009 data resulting in a data quality suitable for the analysis, see e.g. Ref. [11].

The calibrated $\mathrm{d}E/\mathrm{d}x$ distributions as a function of particle momentum for positively and negatively charged parti-

cles are presented in Fig. 5. The Bethe-Bloch (BB) parametrization of the mean energy loss, scaled to the experimental data (see Section 4.5), is shown by the curves for positrons (electrons), pions, kaons, (anti)protons, and deuterons. The typical achieved dE/dx resolution is about 4%.

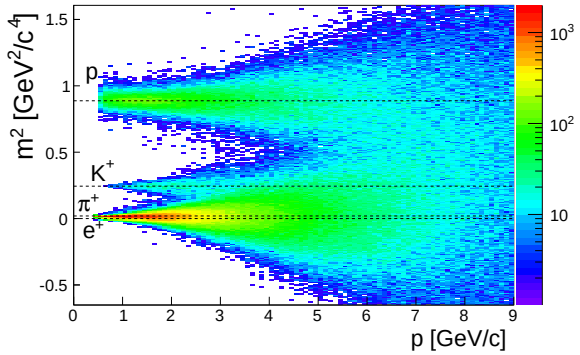

Fig. 4: (Colour online) Mass squared of positively charged particles, derived from the ToF-F measurement and the fitted track parameters, as a function of momentum. The lines show the expected mass squared values for different particles.

Simulation of the NA61/SHINE detector response, used to correct the raw data, is also described in Ref. [5], while some additional details can be found in Ref. [30].

The particle spectra analysis described in Section 4 is based on 4.6×10^6 reconstructed events with the target inserted (I) and 615×10^3 reconstructed events with the target removed (R) collected during the 2009 data-taking period with a beam rate of about 100 kHz, much higher than in 2007 (15 kHz). Only events for which a beam track is properly reconstructed are selected for analysis.

A summary of NA61/SHINE data collected for T2K is presented in Table 1.

3 Inelastic and production cross section measurements

This section presents procedures and results on inelastic and production cross section measurements for p+C interactions at 31 GeV/c. We define the inelastic cross section as a difference between the total and the coherent elastic cross sections, see e.g. [31]. Thus it comprises every reaction which occurs with desintegration of the carbon nucleus

$$\sigma_{\text{inel}} = \sigma_{\text{tot}} - \sigma_{\text{el}} \ . \tag{1}$$

The production processes are defined as those in which new hadrons are produced

$$\sigma_{\text{prod}} = \sigma_{\text{inel}} - \sigma_{\text{qe}} \ . \tag{2}$$

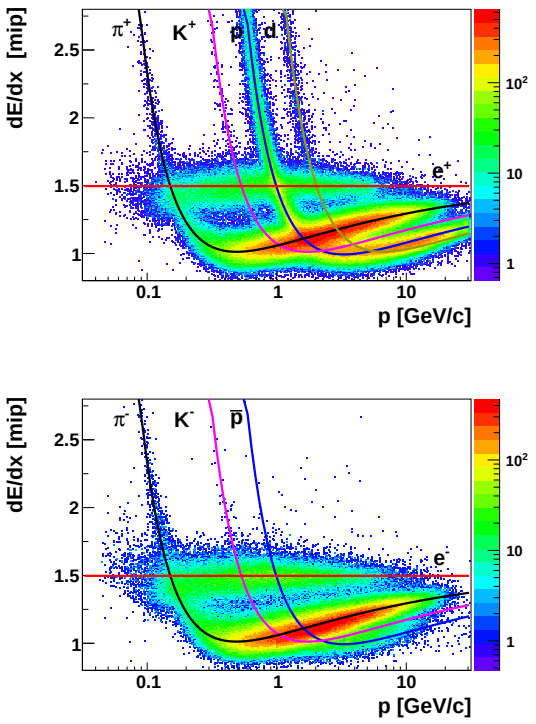

Fig. 5: (Colour online) Specific energy losses in the TPCs for positively (*top*) and negatively (*bottom*) charged particles as a function of momentum. Curves show the Bethe-Bloch (BB) parameterizations of the mean dE/dx calculated for different hadron species. In the case of electrons and positrons, which reach the Fermi plateau, the mean dE/dx is parameterized by a constant.

where σ_{qe} is a quasi-elastic cross section, i.e. a process where the incoming proton scatters off an individual nucleon which, in turn, is ejected from the carbon nucleus.

Since many improvements were made to the trigger logic and much higher beam rate was used during the 2009 data-taking compared to the 2007 run (see Section 2) the normalization analysis of the 2009 data [32] is quite different from the one used for the 2007 data [5, 33].

3.1 Interaction trigger cross section

The simultaneous use of the beam and interaction triggers allows for the direct determination of the interaction trigger probability, P_{Tint}:

$$P_{\text{Tint}} = \frac{N(T_{\text{beam}} \wedge T_{\text{int}})}{N(T_{\text{beam}})} \ , \tag{3}$$

where $N(T_{\text{beam}})$ is the number of events which satisfy the beam trigger condition and $N(T_{\text{beam}} \wedge T_{\text{int}})$ is the number

beam	target	year	triggers $\times 10^6$	status of the NA61/SHINE analysis	usage in the T2K beam MC
protons at 31 GeV/c	thin target	2007	0.7	published: $\pi^{\pm}$ [5], K^{+} [6], K^0_S, Λ [13]	has already been used [16]
	2 cm (0.04λ_I)	**2009**	5.4	$\pi^{\pm}$, $K^{\pm}$, p, K^0_S, Λ (this article)	currently being used
	T2K replica	2007	0.2	published: $\pi^{\pm}$ [26]	method developed
	target	2009	2.8	analysis being finalized [27]	to be integrated
	90 cm (1.9λ_I)	2010	7.2	analysis currently on-going	—

Table 1: A summary of the NA61/SHINE data collected for the T2K physics goals.

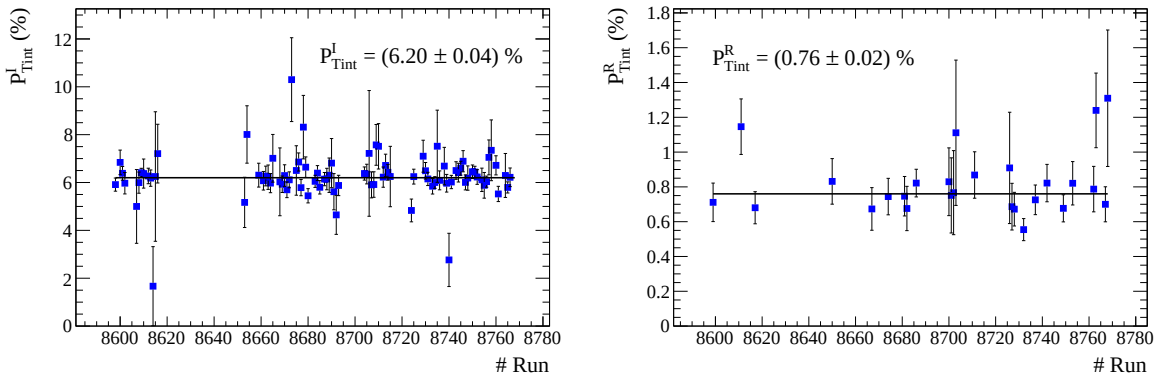

(a) (b)

Fig. 6: (Colour online) The interaction trigger probability as a function of the run number for target inserted (a) and target removed (b) runs. The measured values are shown as well. Points far away from the measured value (solid line) correspond to the runs with low number of events.

	Target inserted	Target removed
N(T_{beam}) before cuts	577894	257430
N($T_{\text{beam}} \wedge T_{\text{int}}$) before cuts	39644	3705
N(T_{beam}) after cuts	331735	145682
N($T_{\text{beam}} \wedge T_{\text{int}}$) after cuts	20578	1110

Table 2: Number of beam and interaction trigger events before and after the event selection. Beam trigger events used for this analysis are a factor of about 10 smaller than the total number of recorded events (see section 2).

of events which satisfy both the beam trigger and interaction trigger conditions. The interaction trigger probability was measured for the target inserted, P^I_{Tint}, and target removed, P^R_{Tint}, configurations. Table 2 summarizes the number of beam and interaction trigger events before and after the event selection.

The interaction probability in the carbon target was calculated as follows:

$$P_{\text{int}} = \frac{P^I_{\text{Tint}} - P^R_{\text{Tint}}}{1 - P^R_{\text{Tint}}}. \tag{4}$$

It is used to obtain the interaction trigger cross section

$$\sigma_{\text{trig}} = \frac{1}{\rho\ L_{\text{eff}}\ N_{\text{A}}/A} P_{\text{int}}, \tag{5}$$

where N_{A}, ρ, A and L_{eff} are the Avogadro's number, the target density, its atomic number and its effective length, respectively. The effective target length accounts for the exponential beam attenuation and can be computed according to

$$L_{\text{eff}} = \lambda_{\text{abs}} \left(1 - \exp^{-L/\lambda_{\text{abs}}}\right), \tag{6}$$

where the absorption length is

$$\lambda_{\text{abs}} = \frac{A}{\rho\ N_{\text{A}}\ \sigma_{\text{trig}}}. \tag{7}$$

Substituting Eqs. (6) and (7) into Eq. (5), the formula for the interaction trigger cross section is obtained:

$$\sigma_{\text{trig}} = \frac{A}{L\ \rho\ N_{\text{A}}} \ln\left(\frac{1}{1 - P_{\text{int}}}\right). \tag{8}$$

3.2 Event selection

An event selection was applied to improve the rejection of out-of-target interactions. The following two quality cuts based on the measurements of the beam position and the beam proton time in the event were applied:

(i) Requirement to have both the x and y positions of a beam particle to be measured by all the three BPDs. This selection is referred to later on as the *standard* BPD selection.

(ii) In order to account for a slow response of BPDs the cut removing all events with at least a second beam particle in the time window $t = [-2,0]\,\mu$s with respect to the triggered time was applied.

After applying these cuts the amount of out-of-target interactions was reduced by about 45% (see Table 2).

3.3 Study of systematic uncertainty on σ_{trig}

The first component of systematic uncertainty was evaluated by varying the event selection criteria described in the previous subsection. It amounts to 1.0 mb.

The elastic scattering of the beam along the beamline was studied. The fraction of events that passes all the event selections, where the beam extrapolation falls outside of the carbon target, was evaluated and found to be negligible.

Another source of potential systematic uncertainty relates to the pile-up. The trigger logic has a time resolution of about 9 ns. If a pile-up particle arrives within this time window it can not be distinguished from the one which caused the trigger. The measured P_{Tint} and corrected unbiased $P_{\text{Tint}}^{\text{corr}}$ interaction trigger probabilities are related as:

$$P_{\text{Tint}}^{\text{corr}} = \frac{P_{\text{Tint}}}{1 - P_{\text{2beam}}}\,, \tag{9}$$

where P_{2beam} is the probability that a pile-up beam is within the trigger logic time window. This probability was found to be $(0.18 \pm 0.07)\%$, thus the correction which it can introduce to σ_{trig} is negligible and no systematic error was assigned.

The beam composition at 31 GeV/c, measured with the CEDAR and the THC, comprises 84% pions, 14% protons and about 2% kaons. The proton component of the beam was selected by requiring respectively the coincidence and the anti-coincidence of the CEDAR and THC counters (see Section 2). In order to verify the purity of the identified proton beam, the beam was deflected to the TPCs with the maximum magnetic field (9 Tm) and its composition was determined using the energy loss measurements in TPC. The fraction of misidentified particles in the proton beam was found to be lower than 0.2% and it was considered to be negligible.

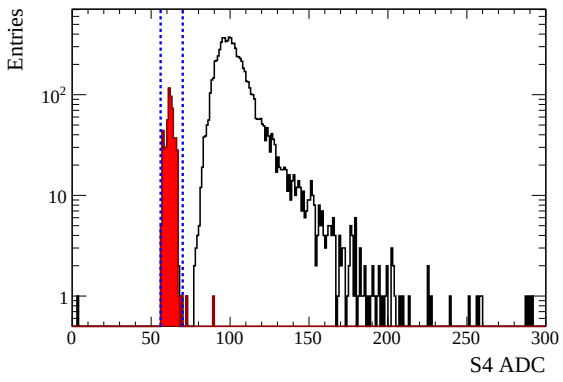

Fig. 7: (Colour online) Distribution of S4 ADC counts for the beam trigger T_{beam}. Red histogram corresponds to the interaction trigger subsample in the beam interaction sample $T_{\text{beam}} \wedge T_{\text{int}}$.

The efficiency of the interaction trigger was estimated using the ADC information from the S4 scintillator counter. The ADC signal of the S4 can be distorted if pile-up beam particles are close in time to the triggered beam. To avoid this effect all the events with at least one pile-up beam within $\pm 4\,\mu$s around the triggered beam were rejected. In Fig. 7 the distribution of the ADC signal is shown for a sample of events tagged by the beam trigger T_{beam}. If a beam proton does not interact in the target, and thus hits S4, the ADC counts will be larger than 70. If both the beam and interaction trigger conditions are satisfied $T_{\text{beam}} \wedge T_{\text{int}}$, the ADC signal corresponds to the pedestal and will be distributed between 56 and 70 counts (Δ_{adc}). The efficiency of the S4 counter as a part of the T_{int} trigger is defined as the ratio between the number of ADC counts in the Δ_{adc} interval for $T_{\text{beam}} \wedge T_{\text{int}}$ events and the total number of ADC counts in the Δ_{adc} interval for T_{beam} events. The measured value is $(99.8 \pm 0.2)\%$. An estimation of the S4 efficiency was also cross-checked using the GTPC, i.e. an extrapolation of track segments reconstructed in the GTPC to the z position of S4 and check of consistency with T_{int}. It was found to be in agreement with the result described above. Any bias given by a possible not perfect functioning of S4 is considered negligible.

3.4 Results on σ_{trig}

The interaction trigger probabilities for the target inserted and target removed samples as a function of the run number are shown in Fig. 6. The mean values of distributions were found to be $P_{\text{Tint}}^{\text{I}} = (6.20 \pm 0.04)\%$ and $P_{\text{Tint}}^{\text{R}} = (0.76 \pm 0.02)\%$. They were submitted to the Eq. (4) to calculate the interaction trigger probability $P_{\text{int}} = (5.48 \pm 0.05)\%$. Finally, the corresponding trigger cross section is:

$$\sigma_{\rm trig} = 305.7 \pm 2.7({\rm stat}) \pm 1.0({\rm det})\,{\rm mb}\ , \quad (10)$$

where "stat" is the statistical uncertainty and "det" is the detector systematic uncertainty. This measurement of $\sigma_{\rm trig}$ overpasses significantly in precision the one obtained with the 2007 data: $298.1 \pm 1.9({\rm stat}) \pm 7.3({\rm det})$ mb [5]. The detector systematic uncertainty of 2009 is significantly smaller. It is a consequence of the fact that in 2009 the beam triggers were recorded by DAQ simultaneously with physics triggers. Thus unique selection cuts could be applied to all triggers (see Section 3.2). On the contrary, during the 2007 run the beam information was read-out by scalers which were not integrated to the main DAQ program and, as a consequence, an evaluation on the event-by-event biases was not possible [33]. To estimate the effect due to this selection, special runs with the beam trigger had been taken. It was also assumed that the effect of the selection was stable over the whole data taking period. On the other hand, the statistical uncertainty on $\sigma_{\rm trig}$ with the 2009 data – as presented in Eq. (10) – is slightly larger because of the smaller number of recorded $T_{\rm beam}$.

The fraction of out-of-target interactions background in the sample of the target inserted events is

$$\varepsilon = \frac{P^{\rm R}_{\rm Tint}}{P^{\rm I}_{\rm Tint}} = (12.3 \pm 0.4)\%. \quad (11)$$

The uncertainty on ε is larger than the one obtained with the 2007 data because of a larger statistical uncertainty on the $P^{\rm R}_{\rm Tint}$.

3.5 Results on inelastic and production cross section

Using Eqs. (1) and (2) one can calculate the inelastic and production cross sections by representing them in the following way:

$$\sigma_{\rm inel} = \left(\sigma_{\rm trig} - \sigma^{\rm f}_{\rm el}\right) \frac{1}{f_{\rm inel}} \quad (12)$$

$$\sigma_{\rm prod} = \left(\sigma_{\rm trig} - \sigma^{\rm f}_{\rm el} - \sigma^{\rm f}_{\rm qe}\right) \frac{1}{f_{\rm prod}}\ , \quad (13)$$

$$\sigma^{\rm f}_{\rm el} = \sigma_{\rm el} f_{\rm el}\ , \quad (14)$$

$$\sigma^{\rm f}_{\rm qe} = \sigma_{\rm qe} f_{\rm qe}\ , \quad (15)$$

where $f_{\rm el}$, $f_{\rm qe}$, $f_{\rm inel}$ and $f_{\rm prod}$ are the fractions of elastic, quasi-elastic, inelastic and production events missing the S4 counter, respectively. Thus the values of $f_{\rm el}$ and $f_{\rm qe}$ would indicate the ability of $T_{\rm int}$ to reject elastic and quasi-elastic events. The values of $f_{\rm inel}$ and $f_{\rm prod}$ depend upon the efficiency of $T_{\rm int}$ for the selection of inelastic and production events. In order to take into account the correlations between $\sigma_{\rm el}$, $f_{\rm el}$ and $\sigma_{\rm qel}$, $f_{\rm qel}$, uncertainties on $\sigma^{\rm f}_{\rm el}$ and $\sigma^{\rm f}_{\rm qe}$ are estimated.

This method differs from the one used in the analysis of the 2007 data [5, 33]. Here the MC simulation is basically only used to extract the fractions. For the absolute values of $\sigma_{\rm inel}$ and $\sigma_{\rm prod}$ one can submit the results of experimental measurements, if available. In addition, in the approach used for the 2007 data the MC values of inelastic and production cross sections were part of the corrections to measure $\sigma_{\rm inel}$ and $\sigma_{\rm prod}$. It is not the case for the method we use now.

The corrections to $\sigma_{\rm trig}$ as well as the corresponding uncertainties were estimated with GEANT4.9.5 [38, 39] using the FTF_BIC physics list (see section 6 for more detailed comparisons of our measurements with the GEANT4 physics lists), except for the elastic cross section, for which large uncertainties in the GEANT4 simulation exist[1]. Since the dependence of the total elastic cross section from the proton beam energy can be very well approximated by a straight line in the momentum range 20-70 GeV/c, the measurements performed by Bellettini *et al.* at 21.5 GeV/c [34] and Schiz *et al.* at 70 GeV/c [40] were used to estimate the elastic cross section at 31 GeV/c beam momentum. The elastic cross section measured by Bellettini *et al.* is

$$\sigma_{\rm el}(21.5\ {\rm GeV}/c) = 81.00 \pm 5.00({\rm sys})\,{\rm mb}$$

Schiz *et al.* reported the measured differential cross section as a function of the momentum transferred with its parametrization. The total elastic cross section can be obtained by integrating the differential cross section over the whole range of momentum transferred and is equal to:

$$\sigma_{\rm el}(70\ {\rm GeV}/c) = 76.6 \pm 6.9({\rm sys})\,{\rm mb}$$

By interpolating with a straight line between the two points the corresponding elastic cross section at the NA61/SHINE momentum is obtained:

$$\sigma_{\rm el}(30.92\ {\rm GeV}/c) = 80.1 \pm 5.4({\rm sys})\,{\rm mb}$$

The $\pm 1\sigma$ range covers the interval $[74.8, 85.5]$ mb. The deviations from the extremes of the interval and the nominal value of σ_{el} estimated with GEANT4 are taken into account as model systematic uncertainty.

The values for the elastic and quasi-elastic cross section, estimated with GEANT4, are (see Ref. [41] for more details):

[1] For $\sigma_{\rm el}$ we found significant differences between various releases of GEANT4 – 4.9.5, 4.9.6 and 4.10 – for different physics lists. The $\sigma_{\rm el}$ values are in the range from 78 mb to 88 mb.

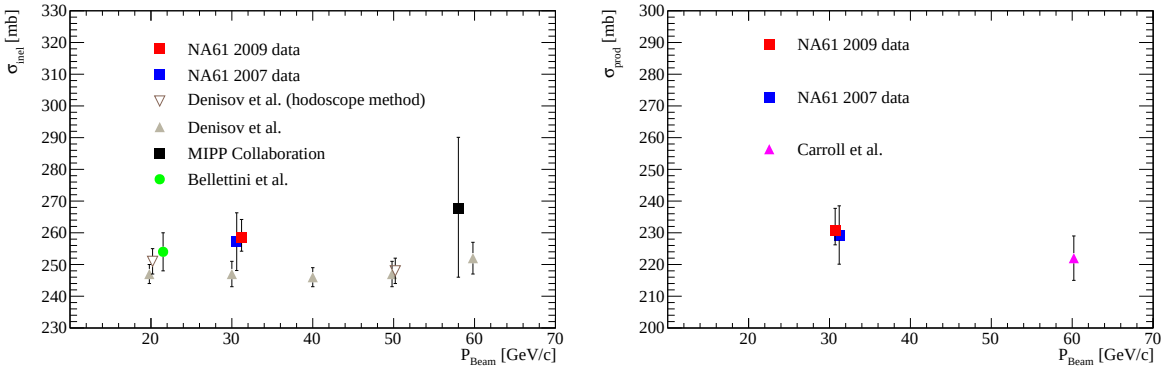

(a) (b)

Fig. 8: (Colour online) A comparison of the measured inelastic (*left*) and production (*right*) cross sections at different momenta with previously published results. Bellettini *et al.* (green full circle) [34], Denisov *et al.* (grey full triangles) [35] and MIPP (black full diamond) [36] measured the inelastic cross section while Carroll *et al.* (pink full triangle) [37] result corresponds to the production cross section. Inelastic cross section measurements performed by Denisov *et al.* with the hodoscope method are shown as well (open inverted triangles). The NA61/SHINE measurements with 2007 (blue full square) and 2009 (red full square) data samples are shown.

$$\sigma^{\mathrm{f}}_{\mathrm{el}} = 50.4\,^{+0.6}_{-0.5}(\mathrm{det})\,^{+4.9}_{-2.0}(\mathrm{mod})\,\mathrm{mb}$$
$$\sigma^{\mathrm{f}}_{\mathrm{qe}} = 26.2\,^{+0.4}_{-0.3}(\mathrm{det})\,^{+3.9}_{-0.0}(\mathrm{mod})\,\mathrm{mb}$$

The fractions are:

$$f_{\mathrm{prod}} = 0.993 \pm 0.000(\mathrm{det})\,^{+0.001}_{-0.012}(\mathrm{mod})$$
$$f_{\mathrm{inel}} = 0.988^{+0.001}_{-0.008}(\mathrm{det})\,^{+0.000}_{-0.008}(\mathrm{mod})$$

where "stat" is the statistical uncertainty of the simulated data sample, "det" is the detector systematic uncertainty obtained by performing the simulation for different positions and sizes of S4, taking also into account the beam divergence measured from the data, and "mod" is the uncertainty on the used physics model, calculated as the largest difference of the estimated contributions between several GEANT4 physics lists for $\sigma^{\mathrm{f}}_{\mathrm{qe}}$ (FTFP_BERT, QBBC, QGSP_BERT) and the FTF_BIC one and from external data for $\sigma^{\mathrm{f}}_{\mathrm{el}}$ as described above.

Using the above given values of the fractions, elastic and quasi-elastic cross sections in Eqs. (12) and (13) the final results are obtained:

$$\sigma_{\mathrm{inel}} = 258.4 \pm 2.8(\mathrm{stat}) \pm 1.2(\mathrm{det})\,^{+5.0}_{-2.9}(\mathrm{mod})\,\mathrm{mb}\,, \qquad (16)$$
$$\sigma_{\mathrm{prod}} = 230.7 \pm 2.7(\mathrm{stat}) \pm 1.2(\mathrm{det})\,^{+6.3}_{-3.4}(\mathrm{mod})\,\mathrm{mb}\,, \qquad (17)$$

where "stat" is the statistical uncertainty, "det" is the total detector systematic uncertainty and "mod" is the physics model uncertainty. The total uncertainty on σ_{prod} is $^{+7.0}_{-4.5}$ mb, significantly smaller than for the NA61/SHINE result obtained using the 2007 data. The dominant uncertainty is the physics model used to recalculate the production cross section from the trigger cross section.

The new NA61/SHINE results on inelastic and production cross section in general agree with the previously published data as shown in Fig. 8. A possible tention with measurements by Denisov *et al.* [35], which are assigned a rather small systematic uncertainty of 1%, could be due to different experimental techniques used to extract σ_{inel}. As discussed in Ref. [31], various approaches to define and measure σ_{inel} could lead to differences up to 8 mb for proton-carbon interactions.

4 Spectra analysis techniques and errors

This section presents analysis techniques developed for the measurements of the differential inclusive spectra of hadrons. It covers details on data selection and binning, particle identification (PID) methods as well as correction factors and systematic uncertainties.

Below we present the procedures used for data analysis consisting of the following steps:

(i) application of event and track selection criteria,
(ii) determination of spectra of hadrons using the selected events and tracks,
(iii) evaluation of corrections to the spectra based on experimental data and simulations,
(iv) calculation of the corrected spectra.

Corrections for the following biases were evaluated and applied:

(i) geometrical acceptance,
(ii) reconstruction efficiency,
(iii) contribution of off-target interactions,
(iv) contribution of other (misidentified) particles produced in inelastic p+C interactions,
(v) feed-down from decays of neutral strange particles,
(vi) analysis-specific effects (e.g. ToF-F efficiency, PID, K^- and $\bar{p}$ contamination, etc.).

All these steps are described in the successive subsections for each analysis technique separately.

The NA61/SHINE measurements refer to hadrons (denoted as *primary hadrons*) produced in p+C interactions at 31 GeV/c and in the electromagnetic decays of produced hadrons. Products of weak decays and secondary interactions are corrected for.

4.1 Event and track selection

Selected events should correspond to the "interaction" (T_{int}) trigger and should have a well-reconstructed incoming beam trajectory (the *standard* BPD selection).

Several criteria were applied to select well-measured tracks in the TPCs and to ensure high reconstruction efficiency as well as to reduce the contamination of tracks from secondary interactions:

(i) track momentum fit at the interaction vertex should have converged,
(ii) the total number of reconstructed points on the track should be greater than N_{point},
(iii) a minimum of N_{field} reconstructed points in the three TPCs used for momentum measurement (VTPC-1, VTPC-2 and GTPC) is required,
(iv) the distance of closest approach of the fitted track to the interaction point (impact parameter) is required to be smaller than D_x (D_y) in the horizontal (vertical) plane.

A summary of cut values for the different analysis techniques, which will be described in the following sections, is given in Table 3.

The adopted $\{p,\theta\}$ binning scheme is chosen based on the available statistics and the kinematic phase-space of interest for T2K. The highest θ limit is analysis-dependent. The angular region down to $\theta = 0$ is covered.

4.2 Derivation of spectra

The raw number of hadron candidates has to be corrected for various effects such that the loss of particles due to reconstruction and selection efficiencies and acceptance. In each of the $\{p,\theta\}$ bins, the correction factor is computed as follows:

Analysis	N_{point}	N_{field}	D_x	D_y
V^0	20	–	4 cm	2 cm
$tof\text{-}dE/dx$	30	6	4 cm	4 cm
dE/dx	30	12	4 cm	4 cm
h^-	30	12	4 cm	4 cm

Table 3: A summary of cuts used by different analysis techniques.

$$C_h(p,\theta) = \left(\frac{\Delta n_h^{\text{rec,fit}}}{\Delta n_h^{\text{sim,gen}}}\right)_{\text{MC}} \Big/ \left(\frac{N^{\text{acc}}}{N^{\text{gen}}}\right)_{\text{MC}}, \tag{18}$$

where the numerator corrects for the loss of candidates of particle type h, where $\Delta n_h^{\text{sim,gen}}$ is the number of true h particles generated in a specific $\{p,\theta\}$ bin, $\Delta n_h^{\text{rec,fit}}$ is the number of h candidates extracted from the reconstructed tracks in the simulation. The denominator accounts for the events lost due to the trigger bias: N^{gen} is the number of generated inelastic events and N^{acc} is the number of accepted ones. The corrected number of candidates is then:

$$\Delta n_h^{\text{corr}}(p,\theta) = \frac{\Delta n_h^{\text{raw}}(p,\theta)}{C_h(p,\theta)}. \tag{19}$$

The procedures presented in Sections 4.3 – 4.6 were used to analyze events with the carbon target inserted and with the carbon target removed. The corresponding corrected numbers of particles (e.g. π^- mesons) in p bins and θ intervals are denoted as Δn_h^{I} and Δn_h^{R}, where h stands for the particle type (e.g. π^-). Note that the same event and track selection criteria as well as the corrections discussed in the previous sections were used in the analysis of events with the target inserted and removed. The latter events allow us to correct the measurements for the contribution of out-of-target interactions.

Then, the double differential inclusive cross section (e.g. of π^- mesons) is calculated as

$$\frac{\mathrm{d}^2\sigma_h}{\mathrm{d}p\mathrm{d}\theta} = \frac{\sigma_{\text{trig}}}{1-\varepsilon}\left(\frac{1}{N^{\text{I}}}\frac{\Delta n_h^{\text{I}}}{\Delta p \Delta\theta} - \frac{\varepsilon}{N^{\text{R}}}\frac{\Delta n_h^{\text{R}}}{\Delta p \Delta\theta}\right), \tag{20}$$

where

(i) $\sigma_{\text{trig}} = (305.7 \pm 2.7 \pm 1.0)$ mb is the "trigger" cross section as given in Section 3.4,
(ii) N^{I} and N^{R} are the numbers of events with the target inserted and removed, respectively, selected for the analysis (see Subsection 4.1),

(iii) Δp ($\Delta\theta$) is the bin size in momentum (polar angle), and

(iv) $\varepsilon = 0.123 \pm 0.004$ is the ratio of the interaction probabilities for operation with the target removed and inserted, Eq. (11).

The particle spectra normalized to the mean particle multiplicity in production interactions was calculated as

$$\frac{\mathrm{d}^2 n_h}{\mathrm{d}p\mathrm{d}\theta} = \frac{1}{\sigma_{\mathrm{prod}}} \frac{\mathrm{d}^2 \sigma_h}{\mathrm{d}p\mathrm{d}\theta} , \tag{21}$$

where σ_{prod} is the cross section for production processes, Eq. (17).

Statistical uncertainty on the measured spectra receives contributions from the finite statistics of both the data as well as the simulated events used to obtain the correction factors. The dominant contribution is the uncertainty of the data which is calculated assuming a Poisson probability distribution for the number of entries in a bin. The Monte Carlo statistics was higher than the data statistics, thus the uncertainty of the Monte Carlo corrections is significantly smaller than the uncertainty of the number of entries in bins.

Systematic uncertainty on the measured spectra was calculated taking into account different contributions discussed in detail in the following sections for each analysis technique separately.

4.3 V^0 analysis

Understanding the neutral strange particle V^0 (here V^0 stands for K^0_S and Λ) production in p+C interactions at 31 GeV/c is of interest for T2K for two reasons. First, it allows us to decrease the systematic uncertainties on measurements of charged pions and protons. Second, measurements of the K^0_S production improve the knowledge of the ν_e and $\bar{\nu}_e$ fluxes coming from the three-body $K^0_L \to \pi^0 e^{\pm} \nu_e(\bar{\nu}_e)$ decays. The following decay channels were studied:

$$K^0_S \to \pi^+ + \pi^- \quad \Gamma = (69.20 \pm 0.05)\% , \tag{22}$$

$$\Lambda \to p \quad + \pi^- \quad \Gamma = (63.9 \pm 0.5)\% . \tag{23}$$

Fits to the invariant mass distributions of selected V^0 candidates were used to extract measured numbers of K^0_S and Λ decays in momentum and polar angle bins. These numbers were corrected for experimental biases using Monte Carlo simulations.

4.3.1 Event and track selection for the V^0 analysis

The track and V^0 candidate selections can be separated into three categories: quality selections, topological selections that are aimed at finding V^0-type candidates, and, finally, the kinematical selections to separate K^0_S and Λ candidates.

The standard quality selections presented in Section 4.1 are used.

The V^0 topological criteria require that a fitted secondary vertex, located downstream of the interaction one, is built out of two tracks with opposite electric charges. Moreover, the distance of closest approach between the daughter tracks and the secondary vertex must be lower than 0.5 cm.

The same quality and topological selections are applied for both Λ and K^0_S analyses.

In order to extract the K^0_S candidates, kinematical cuts are applied to the selected V^0 candidates:

(i) The transverse momentum of the daughter tracks relative to the V^0 momentum must be greater than $p_{\mathrm{T}} > 0.03$ GeV/c in order to remove converted photons from the final selection,

(ii) The cosine of the angle θ^* between the momentum of the V^0 candidate and the momentum of the daughter in the center of mass must be lower than 0.76. This cut allows the rejection of most of the Λ candidates for which the distribution of $\cos\theta^*$ computed under the K^0_S hypothesis is concentrated in the region greater than 0.8,

(iii) The candidates must have an invariant mass under the K^0_S hypothesis within the range of $[0.4, 0.65]$ GeV/c^2,

(iv) The reconstructed proper decay length should be greater than the quarter of the mean proper decay length [42] of K^0_S mesons ($c\tau > 0.67$ cm).

The kinematical cuts used for the Λ analysis are the following:

(i) Transverse momentum of the daughters tracks must be greater than $p_{\mathrm{T}} > 0.03$ GeV/c,

(ii) The candidate must have an invariant mass under the Λ hypothesis within the range of $[1.09, 1.215]$ GeV/c^2,

(iii) The reconstructed proper decay length should be greater than the quarter of the mean proper decay length [42] of Λ hyperons ($c\tau > 1.97$ cm).

Figure 9 shows the Podolanski-Armenteros [43] plots once the event and topological selections are applied, and after all K^0_S and Λ kinematical cuts. One can see that this set of cuts allows for the selection of the desired V^0 candidates.

The measured proper decay length distributions corrected for all experimental biases are shown in Fig. 10 for both K^0_S and Λ. The fitted mean proper decay lengths are in reasonable agreement with the PDG values [42].

4.3.2 Binning, fitting, corrections

The selected V^0 candidates are binned in $\{p, \theta\}$ phase space. Due to the reconstruction efficiency, the momentum range of charged particles starts from 0.4 GeV/c. For the K^0_S analysis, 28 intervals are used, whereas the Λ candidates are

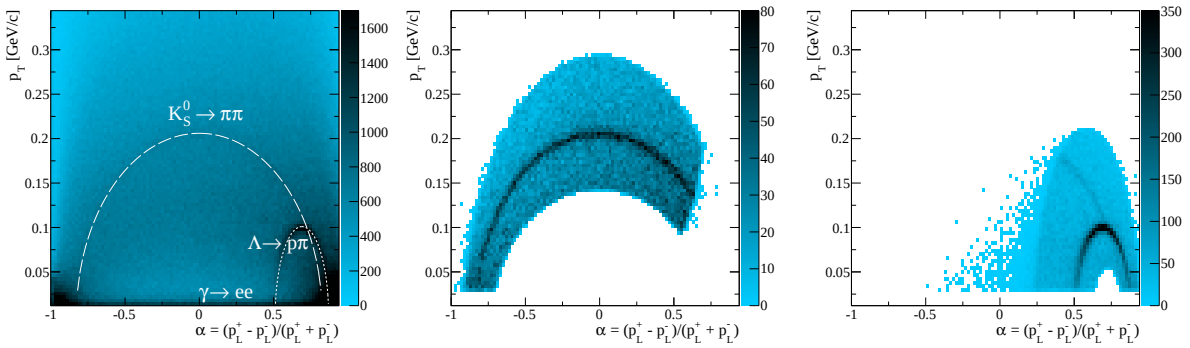

Fig. 9: (Colour online) Podolanski-Armenteros plots for the V^0 candidates after the event and topological cuts (*left*), and after all analysis selections (K^0_S: *middle*, Λ: *right*). Theoretical ellipses for these two V^0 species under study are also presented.

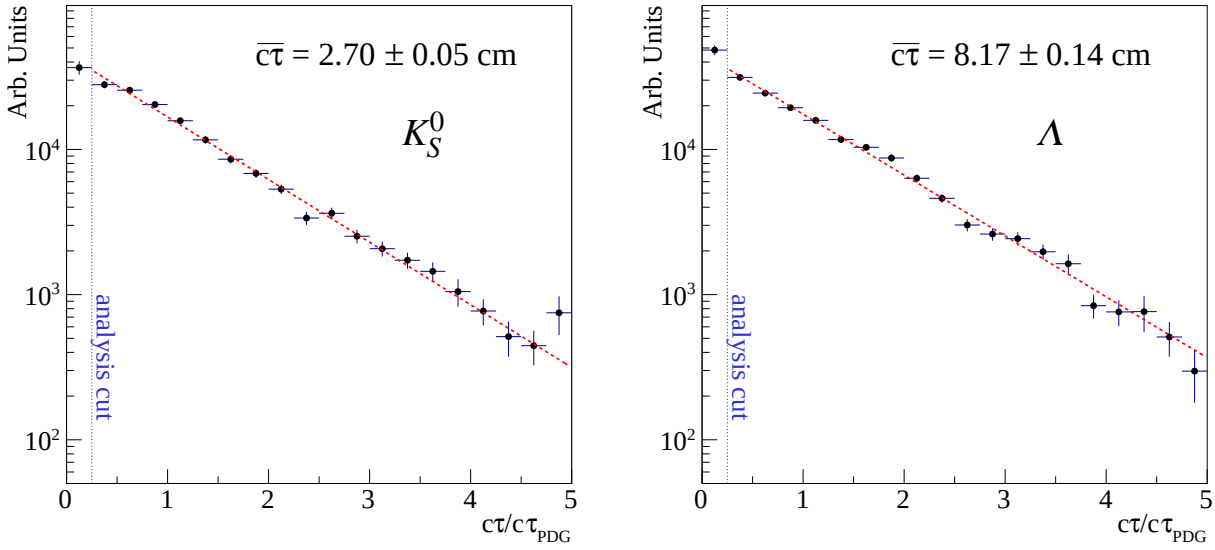

Fig. 10: (Colour online) The measured proper decay length ($c\tau$) distributions for K^0_S (*left*) and Λ (*right*).

divided into 39 bins. The choice of the binning scheme is driven by the available statistics.

In each of these $\{p,\theta\}$ intervals, we performed a fit of the invariant mass distribution. The shape of K^0_S and Λ signal was parametrised by a sum of two Gaussians:

$$L_{sig}(m) = f_{sig}G_W(m;\sigma_W,m_{PDG}) + (1-f_{sig})G_N(m;\sigma_N,m_{PDG}) \quad (24)$$

where m stands for the reconstructed invariant mass, subscripts W and N refer to the wide and narrow Gaussian, respectively. Parameter f_{sig} is the fraction between the two Gaussians. In order to reduce the statistical error on the number of extracted signal, closely related to the number of free parameters, f_{sig} and σ_W were fixed. Also, the central position of the Gaussians was fixed to the well-known PDG value, m_{PDG}.

For the K^0_S analysis the background shape was modeled by an exponential function, while a 3^{rd} order Chebyshev function was used for the Λ analysis.

The $\{p,\theta\}$ binning scheme used for the analysis and an example of a fit in one $\{p,\theta\}$ bin are presented in Figs. 11 and 12 for K^0_S and Λ, respectively.

The same analysis procedure was applied to the Monte-Carlo simulation, where VENUS4.12 [44, 45] was used as the primary generator. The measurements could then be corrected for effects described in Section 4 taking also into account V^0 decay channels that cannot be reconstructed in our detector.

The number of produced V^0 candidates due to interactions in the material surrounding the target can be estimated

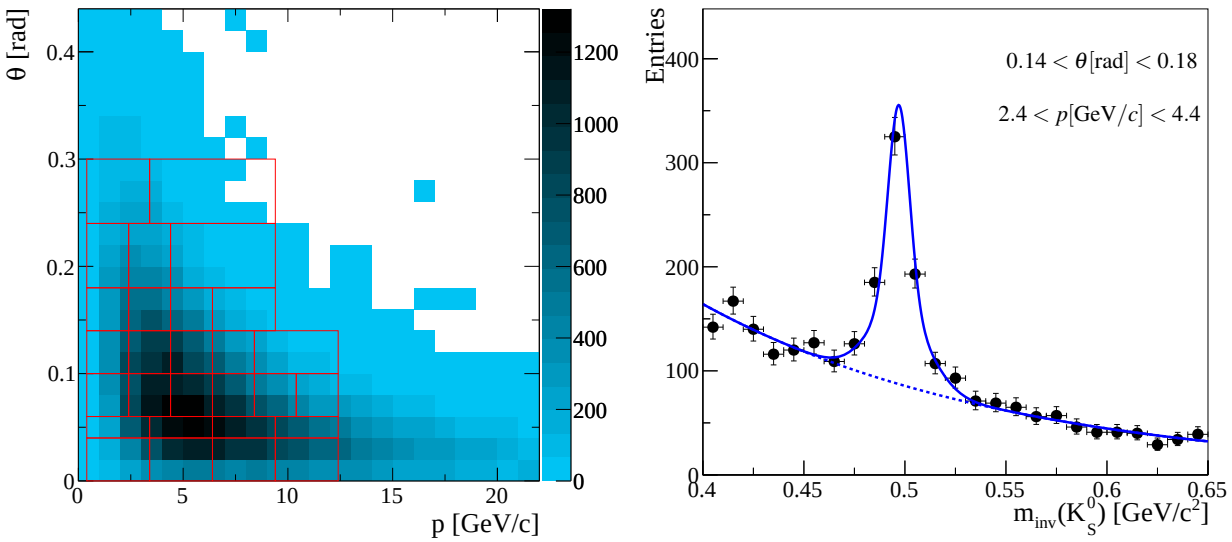

Fig. 11: (Colour online) *Left*: The $\{p, \theta\}$ phase space of interest for T2K. The binning used for the K^0_S analysis is overlaid. *Right*: An example of the K^0_S invariant mass distribution in a selected $\{p, \theta\}$ bin with the fit results overlaid.

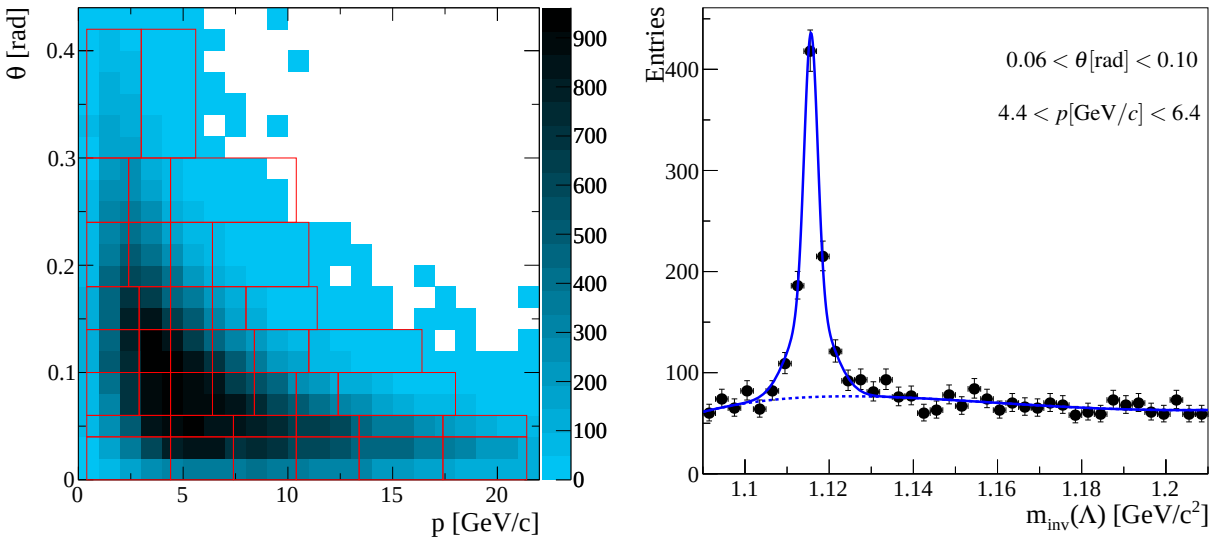

Fig. 12: (Colour online) *Left*: The $\{p, \theta\}$ phase space of interest for T2K. The binning used for the Λ analysis is overlaid. *Right*: An example of the Λ invariant mass distribution in a selected $\{p, \theta\}$ bin with the fit results overlaid.

by using special runs taken with the target removed. The same selections and binning were applied to these events, and a negligible number of candidates was selected.

Spectra were then derived using the standard NA61/SHINE procedure described in Subsection 4.2.

4.3.3 Systematics of the V^0 analysis

The systematic uncertainties associated with this analysis were estimated due to five sources. The adopted procedure was the same for all sources. The relative difference between the standard analysis and the one where the identified systematic contribution is varied was taken as an estimate. The following contributions were considered:

(i) *Correction factors*: The dependence of the MC correction factor values on the generator was tested and included into the systematics. Two other Monte-Carlo simulations with the same statistics were used, based on FLUKA2011 [46–48] and EPOS1.99 [49] as primary generators. The systematic associated with this source is from 7% to 10% for both K^0_S and Λ.

(ii) *Fitting procedure*: Several fitting functions were tested on the invariant mass distributions. A bifurcated Gaussian was used for the peak signal, a 3^{rd} order Chebyshev polynomial and a 4^{th} order polynomial function used for the background description for K^0_S and Λ, respectively. The contribution to the systematics associated with this source is up to 12% (7%) for K^0_S (Λ).

(iii) *Reconstruction algorithm*: Two different reconstruction algorithms to determine the position of the main vertex were used. The uncertainty connected to the algorithm is from 5% to 8% for both analyses.

(iv) *Quality cuts*: All quality cuts were varied independently and the uncertainty connected to this source is up to 10% (5%) for K^0_S (Λ).

(v) *Kinematical cuts*: As for the previous source of errors, all the cuts were varied and the resulting uncertainty is up to 10% (7%) for K^0_S (Λ).

The uncertainty estimates of items (iv) to (v) are strongly correlated since the same datasets and analysis techniques are used. Hence, only the maximum deviation of these sources was taken into account as the total systematic error, where all contributions were added in quadrature.

Comparisons to the 2007 measurement [13] were also done, and compatible results were observed within the attributed errors.

Tables 9 and 10 present the final double differential cross section, $d^2\sigma/(dpd\theta)$, for K^0_S and Λ production in p+C interactions at 31 GeV/c, with the statistical and systematic errors. Fig. 38 (also Fig. 39) and Fig. 40 (also Fig. 41) show the multiplicity spectra.

4.4 The tof-dE/dx analysis method

Depending on a momentum range and a particle specie different analysis techniques for charged hadron spectra can be applied. The method described in this section utilizes the TPCs measurements of the specific energy loss dE/dx and the time-of-flight measurements (tof) using the time-of-flight ToF-F detector. The energy loss information can be used in the full momentum range of NA61/SHINE. The ToF-F detector, which is installed about 13 m downstream of the target (see Fig. 3), contributes to the particle identification up to 10 GeV/c. The mass squared distribution of positively charged particles, derived from the ToF-F measurement and the fitted track parameters, as a function of momentum is shown in Fig. 4.

Use of these two sources of a PID information is particularly important in the momentum range from 1 to 4 GeV/c where the Bethe-Bloch d$E/$dx bands of charged hadrons cross each other (see Fig. 5). Thus the d$E/$dx measurement alone would not be enough to identify particles with sufficient precision and tof is especially important to resolve this complexity.

We apply the combined tof-d$E/$dx analysis technique to determine yields of $\pi^{\pm}$, K$^{\pm}$ and protons for the momentum region above 1 GeV/c. For lower momenta the d$E/$dx-only approach described in Section 4.5 provides a better precision. The spectra of π^- can also be obtained precisely with the so-called h^- analysis techniques described in Section 4.6.

Event and track selection common to all hadron analyses is described in Section 4.1. The following additional cuts are applied in the tof-d$E/$dx analysis:

(i) exclusion of kinematic regions where the spectrometer acceptance changes rapidly, thus small mismatch in the MC description can cause a large effect for the hadron spectra. Basically, these are regions at the edges of the hadron phase space where the reconstruction capability is limited by the ToF-F acceptance, by the magnet aperture or by the presence of uninstrumented regions in the VTPCs. To exclude these regions we apply the cut on the hadron azimuthal angle ϕ. Since the spectrometer acceptance drop quickly with increase of the emission angle of hadron, θ, typical values of ϕ intervals for low and high θ are $\pm 60^\circ$ and $\pm 6^\circ$, respectively.

(ii) every track must have an associated ToF-F hit. Since particles can decay or interact before reaching the detector, the z position of the last reconstructed TPC cluster of a track should be reasonably close to the ToF-F wall, thus the cut $z_{\text{last}} > 6$ m is applied to all tracks. This requirement is especially important for $K^{\pm}$ ($c\tau \approx 3.7$ m), while pions have higher chances to reach the ToF-F ($c\tau \approx 7.8$ m). Moreover a muon produced in the pion decay follows a parent pion trajectory. Such a topology is in general reconstructed as a single track.

Having ToF-F slabs oriented vertically, the position of a hit is measured only in the x direction. The precision is determined by the width of the scintillator slab producing the signal. A ToF-F hit is then associated with a track if the trajectory can be extrapolated to the pertaining slab.

Another important reason for using the ToF-F information is a time tag which ensures that all selected tracks have originated from the same event. The ToF-F time resolution of 110 ps [24] with the event rate of 100 kHz (one beam proton per 10 μs) guaranties an unambiguous separation of tracks from different events.

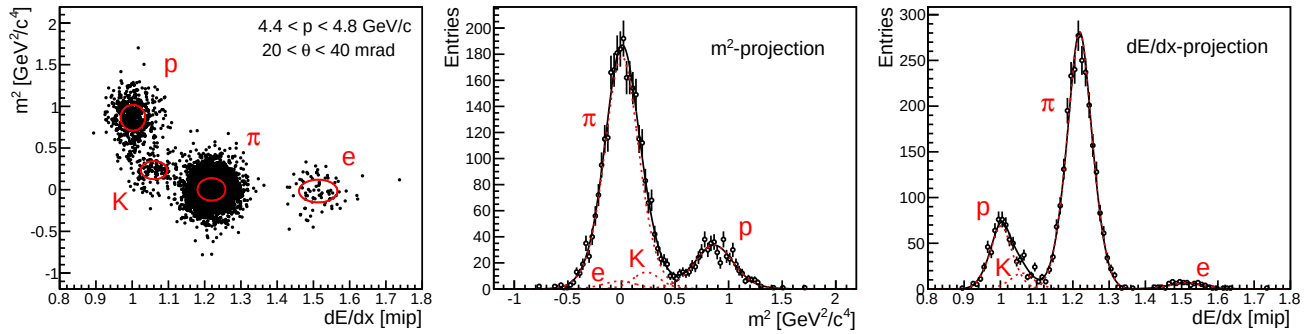

Fig. 13: (Colour online) Example of a two-dimensional fit to the $m^2 - dE/dx$ distribution of positively charged particles (*left*). The m^2 (*middle*) and dE/dx (*right*) projections are superimposed with the results of the fitted functions. Distributions correspond to the $\{p, \theta\}$ bin: $4.4 < p < 4.8$ GeV/c and $20 < \theta < 40$ mrad.

The tof-dE/dx analysis performed separately for positively and negatively charged particles follows the procedure described in detail in Refs. [5, 6, 50]. For every $\{p, \theta\}$ bin the two-dimensional histogram of m^2 and $\mathrm{d}E/\mathrm{d}x$ is filled, where a particle mass squared, m^2, is calculated using measurements of tof, momentum and length of a track. An example of such a distribution is shown in Fig. 13. In this distribution particles of different types form regions which are parametrized by a product of two-dimensional Gaussian functions in m^2 and $\mathrm{d}E/\mathrm{d}x$. The binned maximum likelihood method is applied to fit the distribution with 20 parameters (4 particle types $\times$ 5 parameters of a two-dimensional Gaussian). Depending on the momentum range and particle specie, some of these parameters are fixed or constrained. In particular, this is important for K^+ which are covered by protons at higher momenta. Thus, the mean $\langle \mathrm{d}E/\mathrm{d}x \rangle$ position of kaons is fixed and the width of the $\mathrm{d}E/\mathrm{d}x$ peak is constrained from above by using information from pions and protons.

As a result of the fit one obtains raw yields of particles ($e^{\pm}$, $\pi^{\pm}$, $K^{\pm}$, p, $\bar{\mathrm{p}}$) which are further corrected using the NA61/SHINE Monte Carlo simulation program with VENUS4.12 [44, 45] for primary interactions and a GEANT3-based part for tracking of secondary particles through the detector.

4.4.1 Feed-down corrections and Λ re-weighting

The hadrons which were not produced in the primary interaction can amount to a significant fraction of the selected track sample. Thus a special effort was undertaken to evaluate and subtract this contribution. Hereafter we will refer to this correction as a feed-down.

According to the MC simulation with VENUS4.12 as a primary generator, the correction reaches 12% for π^+, 40% for π^- and up to 60% for protons at low polar angles and small momenta. For kaons it is not significant ($\lesssim$2%). Figure 14 shows the distribution of the feed-down correction for π^- and protons as a function of momentum for one of the θ bins. Decomposition reveals that the main contribution to the correction comes from Λ-hyperon decays:

$$p + \mathrm{C} \to \Lambda + \mathrm{X}$$
$$\hookrightarrow \pi^- + p \,.$$

For π^- mesons these decays are responsible for about $2/3$ of the non-primary contribution at $p = 1$ GeV/c. Moreover for protons, they amount to about $1/2$ for the whole momentum range. Our own measurements of Λ spectra described in Section 4.3 can be used to improve a precision of the correction. Therefore the feed-down contribution of Λ is calculated separately from the feed-down correction due to other weak decays.

Technically the data-based Λ feed-down correction was evaluated by weighing the VENUS4.12 spectra of Λ to force the weighed spectra follow the measured ones. The resulting change of the π^- and proton spectra is shown in Fig. 15. Once the VENUS4.12 spectra of Λ are corrected, the π^- spectra are scaled up by a maximum of 8% at $p = 2$ GeV/c. For protons the effect is spread out along the whole momentum range with a maximum at $p = 9$ GeV/c.

Let us also note that the correction of the VENUS4.12 K^0_S spectra based on the NA61/SHINE measurements impacts final charged pion spectra by less than 2%. The correction was neglected in the results presented here.

4.4.2 Systematic uncertainties of the tof-dE/dx analysis

Systematic uncertainties on the hadron spectra were estimated by varying track selection and identification criteria as well as the parameters used to calculate the corrections. The following sources of systematic uncertainties have been considered:

– *PID* ($\mathrm{d}E/\mathrm{d}x$). A Gaussian function is used to parametrize the $\mathrm{d}E/\mathrm{d}x$ distribution at a fixed value of momentum. The width of the distribution decreases with increasing

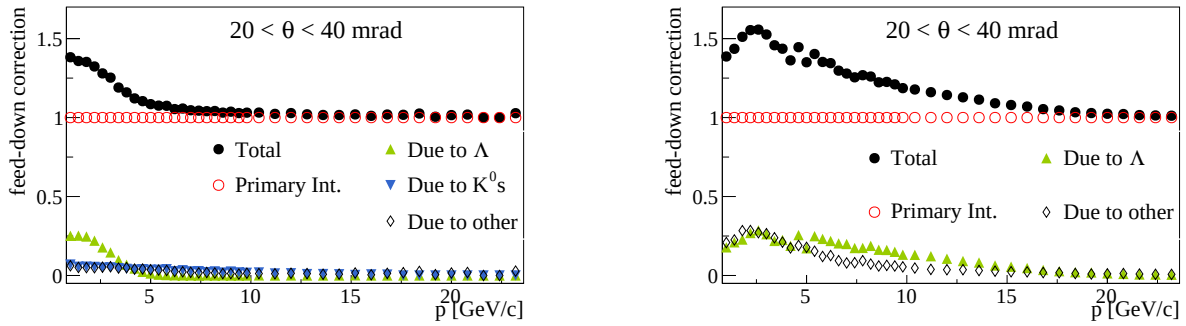

Fig. 14: (Colour online) An example of the feed-down correction dependence on momentum for π^- mesons (*left*) and protons (*right*) for the [20,40] mrad angular interval. Contributions due to Λ and K^0_S decays are shown separately.

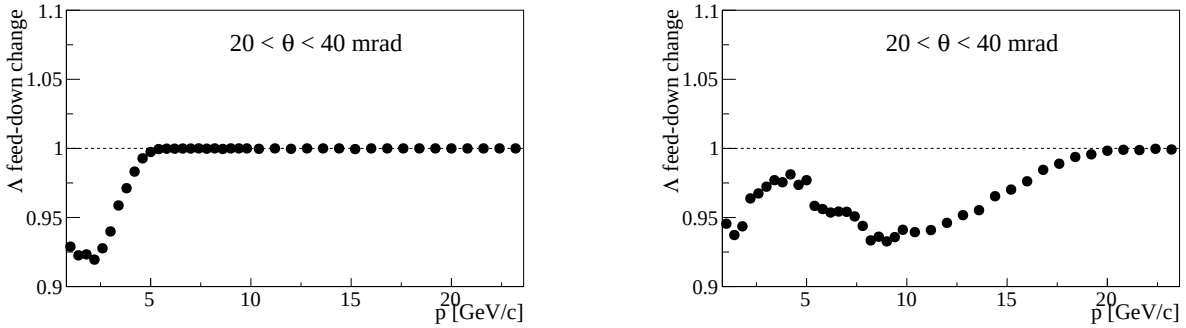

Fig. 15: (Colour online) The effect of the Λ re-weighting. The ratio of multiplicities calculated using the VENUS4.12 model alone and the VENUS4.12 model with the Λ spectra corrected by the NA61/SHINE measurements. Graphs are shown as a function of momentum for π^- mesons (*left*) and protons (*right*).

number of TPC clusters used to determine the $\langle \mathrm{d}E/\mathrm{d}x \rangle$ value of a track. Having in one $\{p, \theta\}$ bin tracks with different number of clusters would cause a deviation from the single-Gaussian shape. The contribution of this effect to the uncertainty of the fitted number of particles of a certain species has been estimated by performing an alternative fit by a sum of two Gaussians.

At low momenta the ToF-F resolution assures an unambiguous particle identification. Thus small distortions of the $\mathrm{d}E/\mathrm{d}x$ shape in general are not relevant for the final results. The $\mathrm{d}E/\mathrm{d}x$ uncertainty becomes significant only starting from about 3 GeV/c. For pions it steadily increases up to 2% at $p = 20$ GeV/c. However for kaons, the uncertainty is an order of magnitude larger: up to 20% for K^+ at high momentum.

– *Hadron loss.* To ensure a high quality match of tracks and ToF-F hits the last point of a track should be within 1.6 m from the ToF-F wall ($z_{\mathrm{last}} > 6$ m). This implies that a track segment is reconstructed in the MTPC-L or MTPC-R detectors. Possible imperfections in the description of the spectrometer can introduce a difference in the acceptance and reconstruction efficiency (merging track segments between VTPC-2 and MTPC-L/R) between MC and real data which can be important for the reconstruction of long tracks. To check how sensitive the results are to the z_{last} cut, it was relaxed down to $z_{\mathrm{last}} > -1.5$ m for pions and $z_{\mathrm{last}} > -3$ m for kaons. The difference in the resulting final spectra has been assigned as the systematic error. It reaches up to 2% at 1 GeV/c and it drops quickly with increasing momentum.

– *Reconstruction efficiency.* To estimate the reconstruction efficiency the following track selection criteria were varied: the minimum number of points measured on the track, the azimuthal angle and the impact parameter cuts. We also compared results obtained with two independent track topologies, results obtained with two different algorithms for merging track segments from different TPCs into global tracks, and results obtained with two different algorithms for the vertex reconstruction. It was found that the influence of such changes is small compared to the statistical errors. The corresponding systematic uncertainty was estimated to be 2%.

– *Forward acceptance.* As stated in Section 2, the GTPC detector was used for the first time in the reconstruction

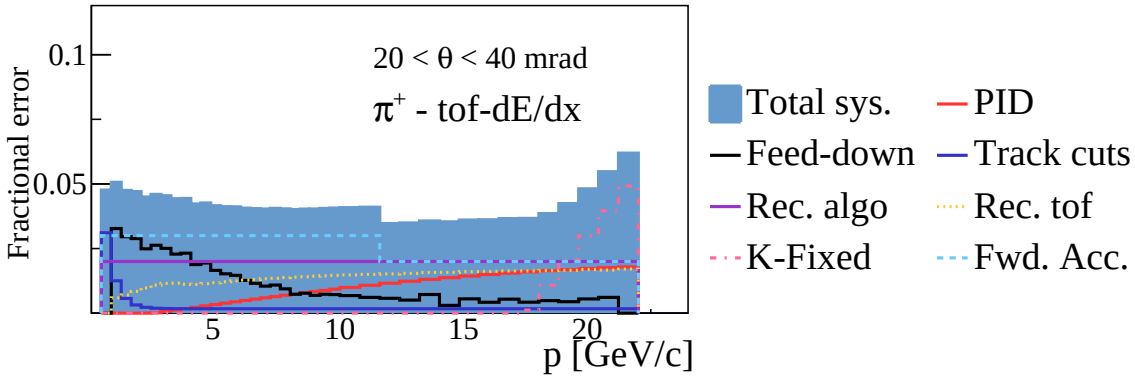

Fig. 16: (Colour online) Breakdown of π^+ systematic uncertainties for the *tof*-dE/dx analysis, presented as a function of momentum for the [20,40] mrad angular interval.

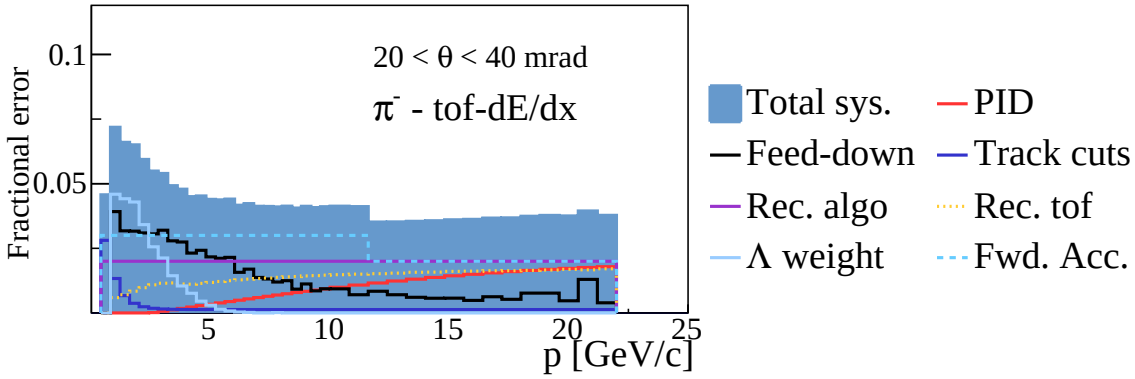

Fig. 17: (Colour online) Breakdown of π^- systematic uncertainties for the *tof*-dE/dx analysis, presented as a function of momentum for the [20,40] mrad angular interval.

algorithms. The GTPC increases the number of reconstructed tracks mainly for smaller angles, $\theta < 40$ mrad, and it allows improvement in the phase space granularity in the forward region up to 20 mrad. The systematic uncertainty in the forward region was based on the comparison of results with and without the GTPC included in the reconstruction algorithms and the variation of the required number of GTPC clusters in the analysis. The later one takes into account the loss of information coming from the GTPC electronic readout which was not simulated. The number of clusters in the GTPC was varied between 4 and 6. The described above sources of *forward acceptance* uncertainties were added in quadrature. The same procedure was used by all three charged hadron analyses.

In case of $tof - dE/dx$ studies, the difference in spectra obtained with and without the GTPC information used in the reconstruction was found to be 4% up to $\theta < 20$ mrad and about 3% for $20 < \theta < 40$ mrad. The variation on the number of GTPC clusters resulted in the systematic error up to 4% for $0 < \theta < 10$ mrad and up to 2% for $10 < \theta < 20$ mrad for tracks at higher momentum $p > 12$ GeV/c. In this region the majority of tracks does not cross the VTPC-1/2 detectors thus the reconstruction in the magnetic field totally relies on the GTPC.

– *ToF-F reconstruction.* The ToF-F reconstruction efficiency was estimated using a sample of events with a very strict event selection which guaranteed no incoming beam-proton within a $\pm 20\,\mu$s time window around the triggered interaction. The inefficiency was found to vary from 4% in the central region to a fraction of percent in the ToF-F slabs far away from the beamline. This behavior in general correlates with a higher particle density in the near-to-beam region where several particles can hit a single slab thus contributing to inefficiency. The value of 50% of the inefficiency correction as a conservative limit has been assigned to the uncertainty of hadron spectra.
– *Secondary interactions and non-Λ feed-down corrections.* As in the case of the h^- (Section 4.6) and dE/dx (Section 4.5) approaches, the important contribution to the systematics at low momenta comes from the uncertainty on the MC-based correction for secondary interactions and weak decays of strange particles (non-Λ hyperons). Following arguments described in Ref. [5] we assigned an uncertainty of 30% of the correction value for both of these sources.

– *Λ feed-down correction.* The data-based correction for the feed-down from pions and protons originated from Λ decays has been calculated separately (see Section 4.4.1). The uncertainty assigned to this correction was estimated to be 30% which is an upper limit on the overall uncertainty of the Λ spectra.
Among different feed-down contributions presented for π^- in Fig. 14 the one from Λ is the largest at low momentum. Due to the fact that the yield of Λ is strongly overestimated by VENUS at low θ (see Fig. 41) the feed-down correction for π^- weighted with data is reduced by about a factor of 2. The systematic uncertainty associated with this correction is reduced by the same amount.

Figures 16 and 17 show a breakdown of the total systematic uncertainty in the *tof*-d$E/$dx analysis in a selected angular interval [20,40] mrad.

4.5 The d$E/$dx analysis method

An analysis of charged pion production at low momentum was performed by means of particle identification via measurements of specific energy loss in the TPCs. For a large fraction of tracks measurements of *tof* can not be applied to low-momentum particles since the majority of them do not reach the ToF-F detector. A reliable identification of π^+ mesons was not possible at momenta above 1 GeV/c where the BB curves for pions, kaons, and protons cross each other (see Fig. 5). On the other hand, for π^- mesons, since the contamination from K^- and antiprotons is almost negligible, the d$E/$dx analysis could be extended in momentum up to 3 GeV/c allowing consistency checks with the other analysis methods in the region of overlap.

The procedure of particle identification, described below, is tailored to the region where a rapid change of energy loss with momentum is observed. This procedure was used already with the 2007 data analysis and more details can be found in Ref. [51]. Here we just describe the most important steps of the analysis.

In order to optimize the parametrization of the BB function, samples of $e^\pm$, $\pi^\pm$, $K^\pm$, p, and d tracks with reliable particle identification were chosen in the $\beta\gamma$ range from 0.2 up to 100. The dependence of the BB function on $\beta\gamma$ was then fitted to the data using the Sternheimer and Peierls parametrization of Ref. [52]. This function was then used to calculate for every track of a given momentum the expected $\langle$d$E/$d$x\rangle_{\rm BB}$ values for all possible identification hypotheses for comparison with the measured mean $\langle$d$E/$d$x\rangle_{\rm data}$. A small (a few percent) dependence of the mean $\langle$d$E/$d$x\rangle_{\rm data}$ on the track polar angle had to be corrected for.

The identification procedure was performed in $\{p,\theta\}$ bins. Narrow momentum intervals (of 0.1 GeV/c for $p < 1$ GeV/c and 0.2 GeV/c for $1 < p < 3$ GeV/c) were chosen to account for the strong dependence of d$E/$dx on momentum. The event and track selection criteria presented in Section 4.1 were applied. In each $\{p,\theta\}$ bin an unbinned maximum likelihood fit (for details see Ref. [53]) was performed to extract yields of π^+ and π^- mesons. The probability density functions were assumed to be a sum of Gaussian functions for each particle species, centered on $\langle$d$E/$d$x\rangle_{\rm BB}$ with variances derived from the data. The d$E/$dx resolution is a function of the number of measured points and the particle momentum. In the π^+ analysis three independent abundances were fitted (π^+, K^+ and proton), while in the π^- analysis we were

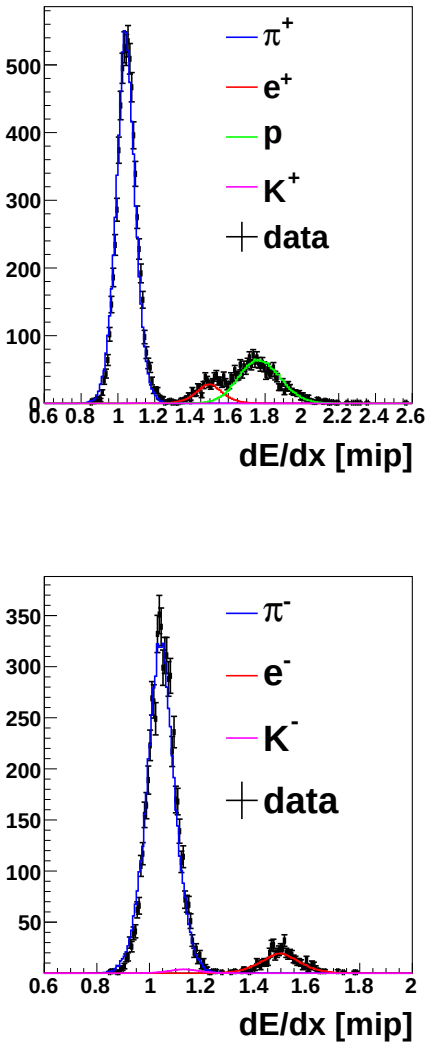

Fig. 18: (Colour online) The d$E/$dx distributions for positively (*top*) and negatively (*bottom*) charged particles in the momentum bin [0.8,0.9] GeV/c and angular bin [180,240] mrad compared with the distribution calculated using the fitted relative abundances.

left with only two independent abundances (π^- and K^-). The e^+ and e^- abundances were determined from the total number of particles in the fit.

As an example, the $\mathrm{d}E/\mathrm{d}x$ distribution for positively charged particles in the momentum bin [0.8,0.9] GeV/c and angular bin [180,240] mrad is shown in Fig. 18 compared with the distribution obtained using the fitted parameters.

Finally, the VENUS MC simulation was used to calculate bin-by-bin corrections for pions from weak decays and interactions in the target and the detector material. The corrections include also track reconstruction efficiency and resolution as well as losses due to pion decays and the limited geometrical acceptance of the detector. In addition to the approach used for the 2007 data, we took also into account all μ tracks coming from π decay. Studies based on MC showed that this additional category of tracks turned out to have non-negligible impact on the value of corrections increasing it by about $\sim$8% in comparison to a situation when no μ are taken into account. Moreover, μ tracks from $\pi \to \mu$ decays can not be separated from π candidates in data, as both particles have similar $\mathrm{d}E/\mathrm{d}x$ values due to small differences in their masses.

4.5.1 Systematic uncertainties of the $\mathrm{d}E/\mathrm{d}x$ *analysis*

In the $\mathrm{d}E/\mathrm{d}x$ analysis we considered several sources of systematic errors. Some of them were already described in previous sections and some were specific to the $\mathrm{d}E/\mathrm{d}x$ analysis. The main contributors to the systematic uncertainties are:

- *Feed-down corrections.* We assigned an uncertainty of 30% on the corrections for feed-down from non-Λ (MC-based) and Λ (data-based) decays. This uncertainty is particularly significant in the low momentum region studied in this analysis. For further information see Section 4.4.1.
- *PID (*$\mathrm{d}E/\mathrm{d}x$*).* The BB parametrization used in the analysis was fitted to the experimental data. In order to estimate the uncertainty related to the precision of the prametrization the results were calculated using the BB curves shifted by $\pm 1\%$. This value was selected by comparing the expected distributions of energy loss for pions with the measured ones. The resulting relative systematic uncertainty (p_{BB}) was calculted as:

$$p_{\mathrm{BB}} \equiv \frac{n_{\mathrm{iden,BB},\pi^\pm}}{n_{\mathrm{iden},\pi^\pm}} , \tag{25}$$

  where $n_{\mathrm{iden,BB},\pi^\pm}$ represents the number of identified $\pi^\pm$ when the BB curves are shifted by $\pm 1\%$, while $n_{\mathrm{iden},\pi^\pm}$ gives the original number of identified charged pions.
  Clearly BB calibration uncertainty is important only for the momentum bins where the BB curves for two particle hypotheses are close to each other. A particularly difficult momentum region is [0.8-2.2] GeV/c where the BB curve for kaons approaches and crosses that for pions. The kaon relative abundance is low which causes additional instability in the fit. Therefore we looked for a conservative estimate of an error on pions in this momentum range allowing the kaon abundance m_K to change within 0 to 0.5%. The limit was adjusted while studying neighboring bins with $p = [0.7, 0.9]$ GeV/c, where returned m_K was not larger than 0.1%. The corresponding relative systematic uncertainty (p_{m_K}) was calculated as:

$$p_{m_K} \equiv \frac{n_{\mathrm{iden},m_K,\pi^\pm}}{n_{\mathrm{iden},\pi^\pm}} , \tag{26}$$

  where $n_{\mathrm{iden},m_K,\pi^\pm}$ represents the fitted number of identified $\pi^\pm$ with the 0.5% limit set on the fitted relative kaon fraction.
  One has to keep in mind that both results p_{BB} and p_{m_K} are correlated. Thus for the final value of the systematic coming from the identification procedure (denoted as p_f) we took the largest value among the two ($p_f \equiv \max[p_{\mathrm{BB}}, p_{m_K}]$).
- *Forward acceptance.* The sources of *forward acceptance* uncertainties described in Section 4.4.2 were considered for low momentum tracks. Systematic uncertainty of 5% was assigned for low angle intervals ($\theta < 60$ mrad), and 3% for other intervals.
- *Reconstruction efficiency.*
  For these studies we were comparing final results on π multiplicities coming from $\mathrm{d}E/\mathrm{d}x$ analysis obtained with different reconstruction algorithms. For most θ angles uncertainty coming from *reconstruction efficiency* is below 2%.
- *Track cuts.*
  We studied the impact of the dominant track cut in the $\mathrm{d}E/\mathrm{d}x$ analysis by changing the selection cut on the measured number of points by 10% from the starting value of 30. Obtained results show that uncertainty coming from *track cuts* is moslty negligible, below 1%.

Figures 19 and 20 show a breakdown of the total systematic uncertainty in the $\mathrm{d}E/\mathrm{d}x$ analysis in a selected angular interval ([20,40] mrad) for π^+ and π^-, respectively.

4.6 The h^- analysis method

The h^- method utilizes the observation that the negatively charged pions account for more than 90% of primary negatively charged particles produced in p+C interactions at 31 GeV/c. Therefore π^- spectra can be obtained by correcting data for a small non-pion contribution calculated from Monte-Carlo without the use of particle identification. The method is limited to negatively charged hadrons due to larger contribution of K^+ and protons for positively

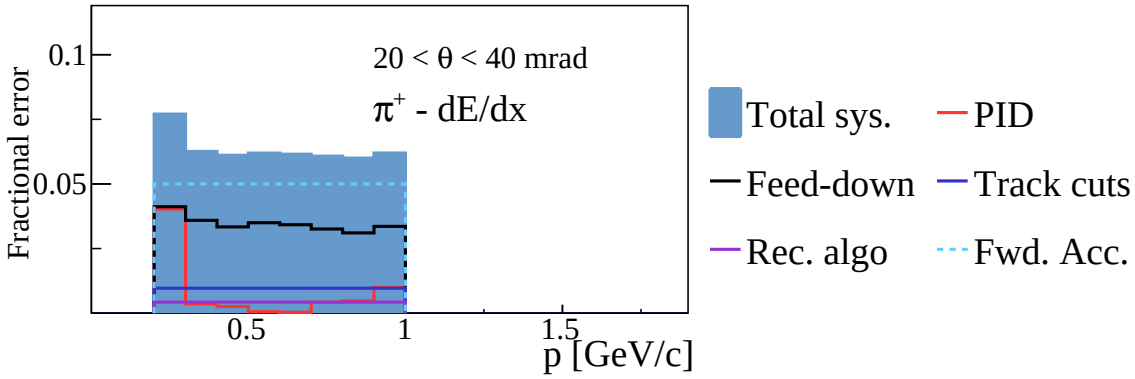

Fig. 19: (Colour online) Breakdown of π^+ systematic uncertainties for the dE/dx analysis, presented as a function of momentum for the [20,40] mrad angular interval.

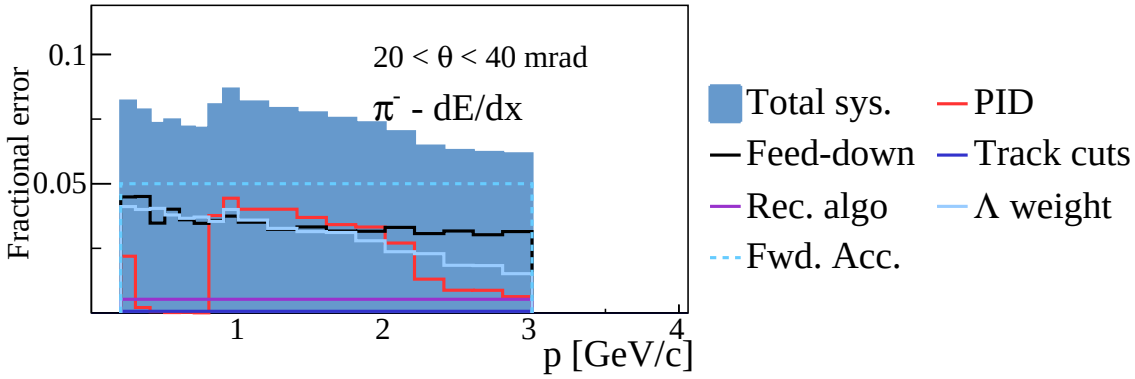

Fig. 20: (Colour online) Breakdown of π^- systematic uncertainties for the dE/dx analysis, presented as a function of momentum for the [20,40] mrad angular interval.

charged particles. Obtained π^- spectra cover a wide momentum range from about 0.2 GeV/c to 20 GeV/c, providing an independent cross-check in the region of overlap with the other two analyses discussed above.

The analysis follows the previously developed procedure [5, 54]. In the first step, the raw yields were obtained for selected data sample in the $\{p, \theta\}$ bins. Standard cuts, described in Section 4.1, were applied to provide good quality events and tracks. In case the track has less than 12 hits in the VTPCs, the required number of hits in GTPC was at least $N_{field(GTPC)} \geq 4$ to ensure a long enough track segment in the first part of the spectrometer, which is important for a good estimate of the track parameters, particularly for tracks that start in GTPC and continue to MTPCs. An additional selection to remove electrons was added as compared to the previous analysis applied to the 2007 data. A dE/dx-based selection to remove electrons was introduced to improve the purity of the sample and to reject electrons mostly at low θ angles. This was done particularly to remove electrons emitted by incident protons passing through the NA61/SHINE detector that were not accounted for in Monte-Carlo. The effect was not prominent for the analysis of 2007 data because the intensity of the beam was significantly lower compared to the 2009 year. The separation between electrons and mostly pions was found to be sufficient for all θ bins, and a momentum-dependent cut was applied for each θ bin separately. The contribution from electrons was the largest for θ up to 20 mrad and momentum below 4 GeV/c with the fraction reaching 10% as compared to 2% calculated for larger θ bins.

In the next step, the raw yields of selected negatively charged hadrons were then corrected using the standard NA61/SHINE Monte-Carlo chain with VENUS model for primary interactions and GEANT3 for particle propagation and secondary interactions. As in the previous analysis one global correction factor was calculated for the same $\{p, \theta\}$ binning as in data. The correction included the contribution of primary K^- and $\bar{p}$, the contribution from weak decays of strange particles and secondary interactions in the target as well as in the detector material. Furthermore, it included track reconstruction efficiency and losses due to the limited geometrical acceptance.

Given the large available statistics, the h^- analysis technique allows for the best precision for the π^- spectra in the full $\{p, \theta\}$ range covered.

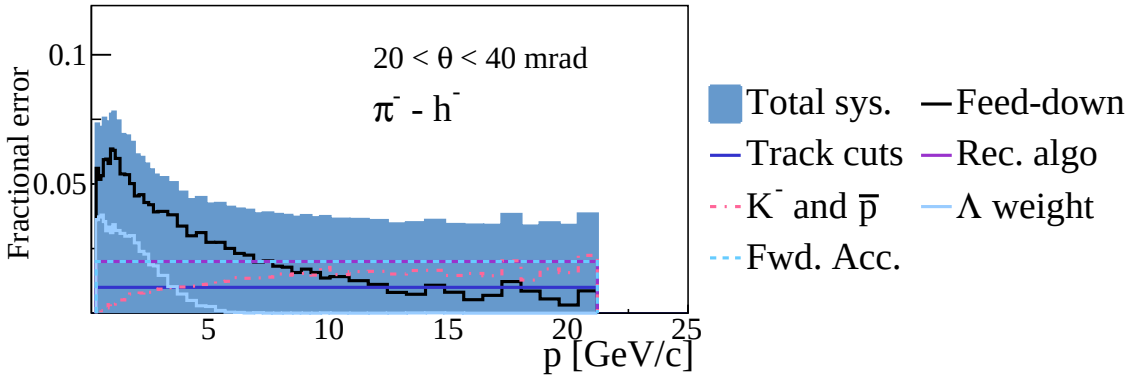

Fig. 21: (Colour online) Breakdown of π^- systematic uncertainties for the h^- analysis, presented as a function of momentum for the [20,40] mrad angular interval.

4.6.1 Systematic uncertainties of the h^- analysis

Most of the systematic errors were evaluated in the same way as for the other charged hadron spectra analyses. Error sources which are specific only to the h^- analysis include K^-, $\bar{p}$ contamination and an error associated with cuts to reject electrons. The following effects were taken into account when calculating systematics errors:

- *Feed-down.* The uncertainty related to the correction for the secondary interactions and weak decays of strange particles remains the dominant contribution at low momentum. For both of these sources, the 30% error was assigned as described in [5]. The significant reduction of the error as compared to the 2007 analysis comes from the use of our own measurements of the Λ production (see subsection 4.4.1 for more details) and the removal of electrons at low θ and low momentum.
- *Forward acceptance.* The impact of the GTPC detector was evaluated following the procedure described in Section 4.4.2. The systematic uncertainty related to the comparison of the reconstruction algorithms with and without the GTPC was found to be 4% for $0 < \theta < 10$ mrad and 2% for $10 < \theta < 40$ mrad in the overlapping momentum regions. The variation on the number of hits for tracks starting in the GTPC resulted in the systematic uncertainty up to 4-5% for the most forward region below $\theta < 20$ mrad and at higher momentum $p > 5$ GeV/c.
- *K^- and $\bar{p}$ contamination.* The uncertainty related to the admixture of K^- and $\bar{p}$ was estimated based on simulation with VENUS, assuming a 20% error on the correction. The contribution of K^- and $\bar{p}$ varies with momentum from 5% to 10% at low θ angles. At higher θ (above 100 mrad) it increases and varies from 5% to 20% at higher momentum.
- *Reconstruction efficiency.* The reconstruction efficiency was evaluated by comparing results for different reconstruction algorithms used in the experiment. The constant error value was assigned since no dependence was observed on momentum and the θ angle.
- *Track selection method.* The uncertainty was estimated by varying the following selections: the total number of hits on track, electron cuts, and the impact parameter. The number of clusters on the track was changed by 10% from the nominal value of 30 clusters. The error associated with the cut to reject electrons was estimated by varying in data the constant parameter of the linear cut used for each of the θ bins by $\pm 3\%$. The separation of electrons and mostly pions is good so the impact of the selection is negligible compared to the cut on the number of hits. In the case of the impact parameter, the analysis was repeated with the cut removed and the effect was found to be negligible.

Figure 21 shows a breakdown of the total systematic uncertainty in a selected angular interval ([20,40] mrad) for π^- in the h^- analysis.

5 Results on spectra

This section presents results on spectra for $\pi^\pm$, $K^\pm$, and protons, as well as K^0_S and Λ. The large statistics of the 2009 dataset resulted not only in improved precision and larger coverage compared to the published 2007 data but, in addition, allowed measurements of K^- spectra for the first time in NA61/SHINE. The comparison between the 2009 and 2007 results is shown and discussed. The new measurements are presented along with predictions of hadron production models, which are described in Section 6. For the purpose of the data comparison with model predictions, the spectra were normalized to the mean particle multiplicity in all production interactions. The experimental measurements are shown with total uncertainties which correspond to the statistical and systematic errors added in quadrature.

5.1 $\pi^{\pm}$ results

The spectra of $\pi^{\pm}$ mesons were obtained using three different analysis techniques *tof*-d$E/$dx, d$E/$dx and h^- described in Sections 4.4, 4.5 and 4.6. Within the corresponding systematic uncertainties, the results of various methods were found to be in a good agreement as shown in Fig. 22 and Fig. 23 for π^+ and π^-, respectively. In order to present a single spectrum for positively and negatively changed pions, the results were combined. For π^+ mesons, we use complementarity of acceptance for differfent analysis techniques: in the momentum range below 1 GeV/c results from the d$E/$dx analysis are used for all angular intervals up to 420 mrad, while the momentum region above 1 GeV/c is covered by the *tof*-d$E/$dx analysis for angular intervals up to 360 mrad. In case of π^- mesons, results of the h^- analysis are used in the full angular range up to 420 mrad since they provide the smallest total uncertainty in the region of the overlap between methods. The final spectra are shown for π^+ in Fig. 28 (also Fig. 29) and for π^- in Fig. 30 (also Fig. 31). Numerical results are given in Tables 4 and 5 for π^+ and π^-, respectively. Thus, the final results span a broad kinematic range. The new $\pi^{\pm}$ results have been compared to the previously published measurements based on the 2007 data [5]. One should note here that the present results are shown in the form of $d^2\sigma/(dpd\theta)$, while the $d\sigma/(dp)$ spectra were used in our previous publications [5, 6]. As illustrated in Fig. 24, the 2009 and 2007 results are in agreement. Thus, the new measurements confirm the published 2007 results which have been questioned in [55]. Both the statistical and the total systematic uncertainties have been considerably reduced for the new 2009 results as presented for π^+ in Fig. 25 and for π^- in Fig. 26. At low momentum systematic errors dominate whereas at higher momentum the statistical error still has the largest contribution to the total uncertainty.

5.2 $K^{\pm}$ results

The *tof*-d$E/$dx analysis technique was used to obtain results on the K^+ spectra shown in Fig. 32 (also Fig. 33) and on the K^- spectra in Fig. 34 (also Fig. 35). The large 2009 dataset allowed for the first measurements of K^- yields in p+C interactions within NA61/SHINE. In the case of K^+, large statistics made it possible to use narrow $\{p,\theta\}$ bins in the analysis which is of importance for the flux tunning in T2K. Numerical results are given in Tables 6 and 7 for K^+ and K^-, respectively. The analysis of K^+ was repeated, as a cross-check, with a coarser $\{p,\theta\}$ binning that corresponds to the previously published measurements based on the 2007 data [6] and a good agreement was found. The total uncertainty for the 2009 data remains dominated by the statistical error as shown in Fig. 27 for K^+ as an example.

5.3 Proton results

Similarly to charged kaons, the *tof*-d$E/$dx analysis technique was the only method used to extract proton spectra in a wide kinematic range above 1 GeV/c. These measurements, shown in Fig. 36 (also Fig. 37), are important for T2K since they provide a possibility to constrain re-interactions in the long carbon target and in the elements of the beamline. Numerical results are given in Table 8. The new proton spectra are in a good agreement with preliminary results obtained using the 2007 data [56].

5.4 V^0 results

The K^0_S and Λ spectra are shown in Fig. 38 (also Fig. 39) and Fig. 40 (also Fig. 41) respectively. Numerical results are given in Tables 9 and 10 for K^0_S and Λ, respectively. As explained in Section 4.4.1, those measurements are used to reduce the dominant systematic uncertainties due to the feed-down correction in the charged hadron analyses. Results are consistent within the quoted systematic uncertainties with previously published measurements [13] which were obtained with a much coarser $\{p,\theta\}$ binning due to the lower statistics of the 2007 data.

The spectra of K^0_S can be cross-checked by measurements of $K^{\pm}$ yields, thanks to the unique capability to measure these three types of kaons simultaneously in the NA61/SHINE experiment. So far, only a few experiments have been able to perform such measurements and to verify two different theoretical hypotheses that predict K^0_S yields from $K^{\pm}$ production rates but neither of those models was disfavored. The first approach assumes isospin symmetry in kaon production and predicts (see e.g. Ref. [57]):

$$N(K^0_S) = \frac{1}{2}\left(N(K^+) + N(K^-)\right) . \tag{27}$$

While the second method uses a quark-counting argument [58], with a simplified quark parton model. The following assumptions are made on the number of sea and valence quarks:

$$u_{\mathrm{s}} = \bar{u}_{\mathrm{s}} = d_{\mathrm{s}} = \bar{d}_{\mathrm{s}},\ s_{\mathrm{s}} = \bar{s}_{\mathrm{s}} , \tag{28}$$

$$n \equiv u_{\mathrm{v}}/d_{\mathrm{v}} . \tag{29}$$

Taking into account that interactions are with a carbon nucleus ($n = 2$ for p+p collisions, $n = 1$ for p+n), the relation between mean multiplicity of K^0_S, K^+ and K^- is:

$$N(K^0_S) = \frac{1}{8}\left(3N(K^+) + 5N(K^-)\right) . \tag{30}$$

This method is currently the one used to tune K^0_L production in the T2K flux simulation chain [16]. Figure 39 shows a

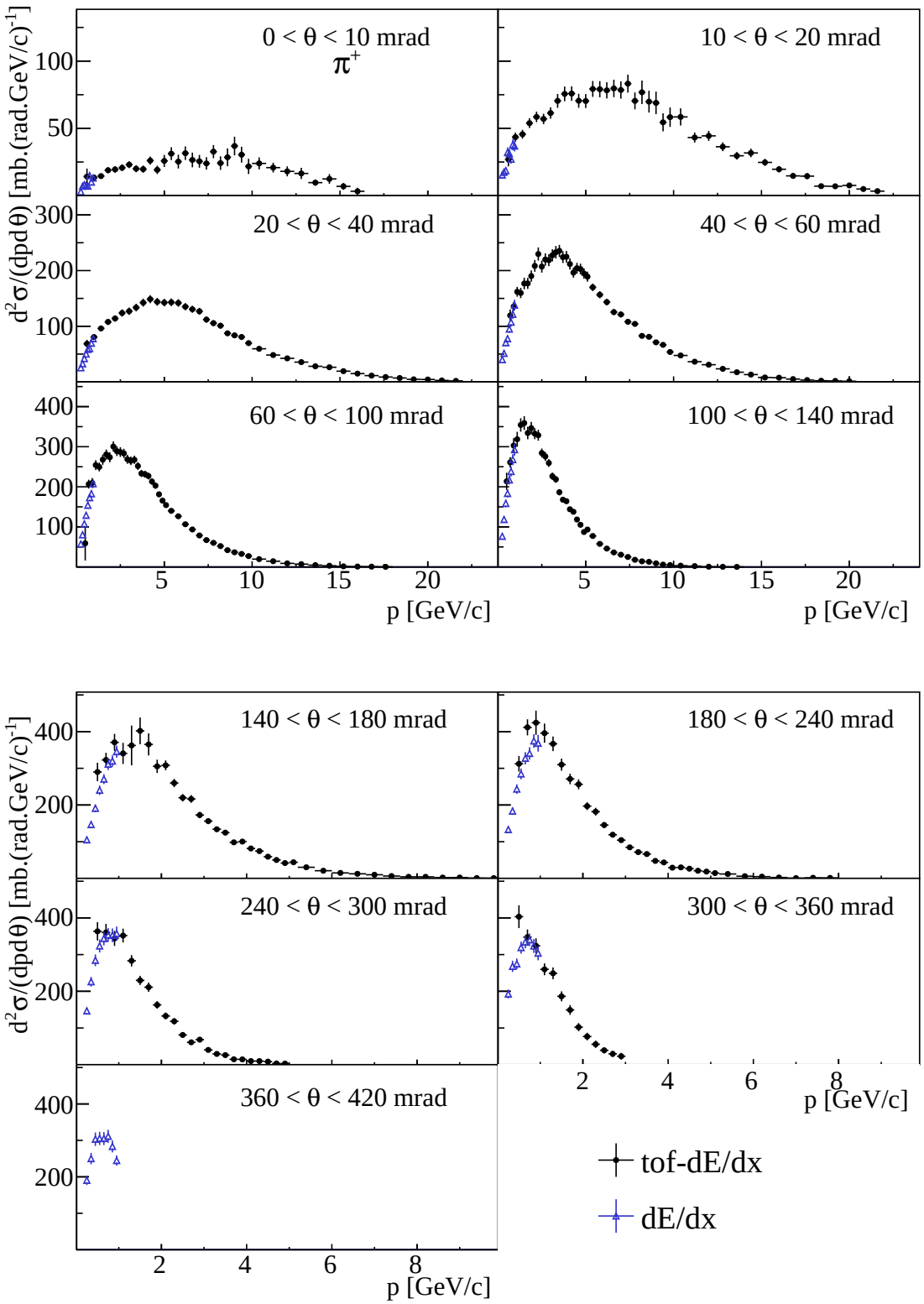

Fig. 22: (Colour online) Laboratory momentum distributions of π^+ produced in p+C interactions at 31 GeV/c production processes in different polar angle intervals (θ). Error bars indicate the total uncertainty. Results obtained with two different analysis techniques are presented: open blue triangles are the dE/dx analysis and full black circles are the $tof\text{-}dE/dx$ analysis.

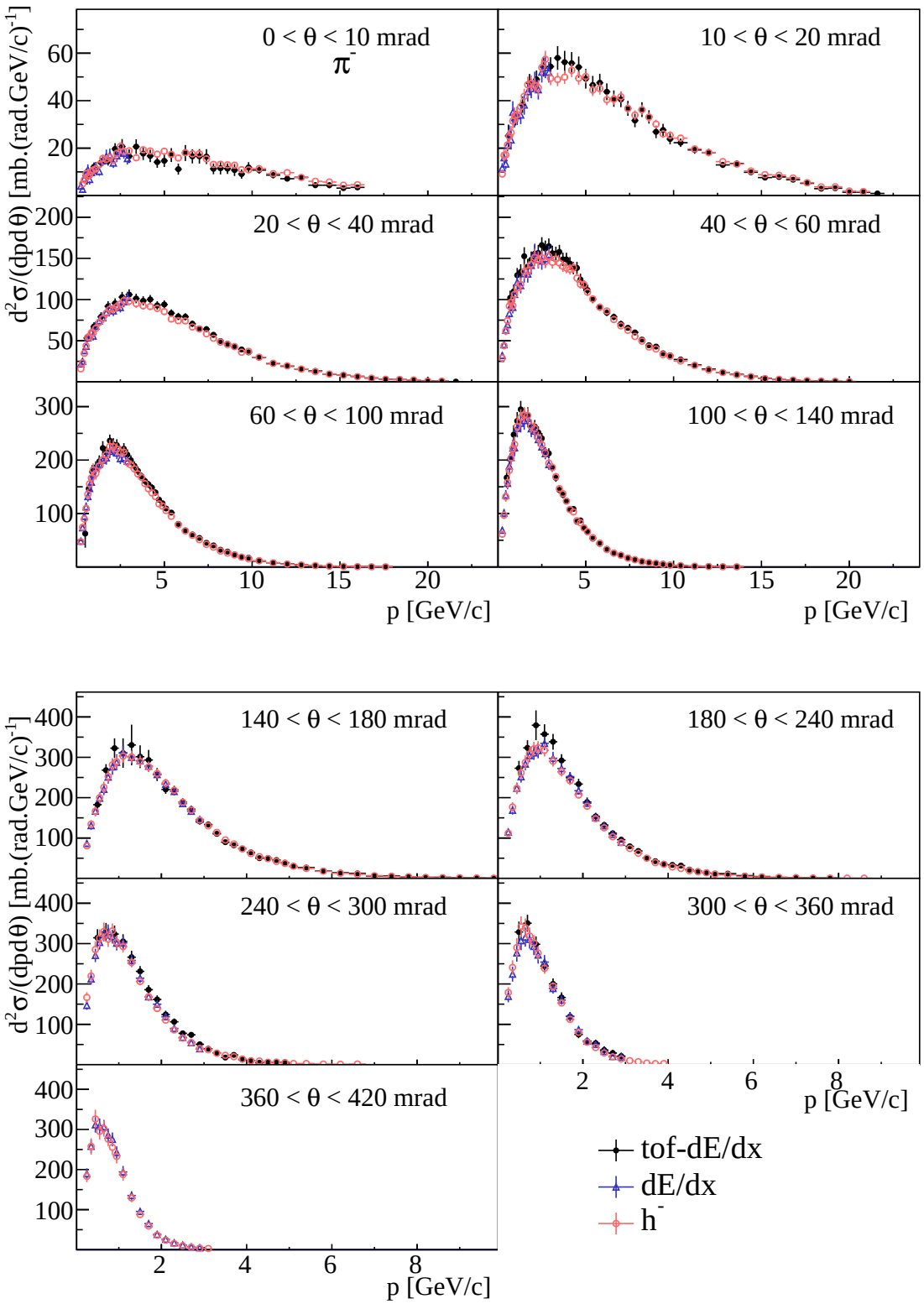

Fig. 23: (Colour online) Laboratory momentum distributions of π^- produced in p+C interactions at 31 GeV/c production processes in different polar angle intervals (θ). Error bars indicate the total uncertainty. Results obtained with three different analysis techniques are presented: open blue triangles are the dE/dx analysis, open red circles are the h^- analysis and full black circles are the $tof\text{-}dE/dx$ analysis.

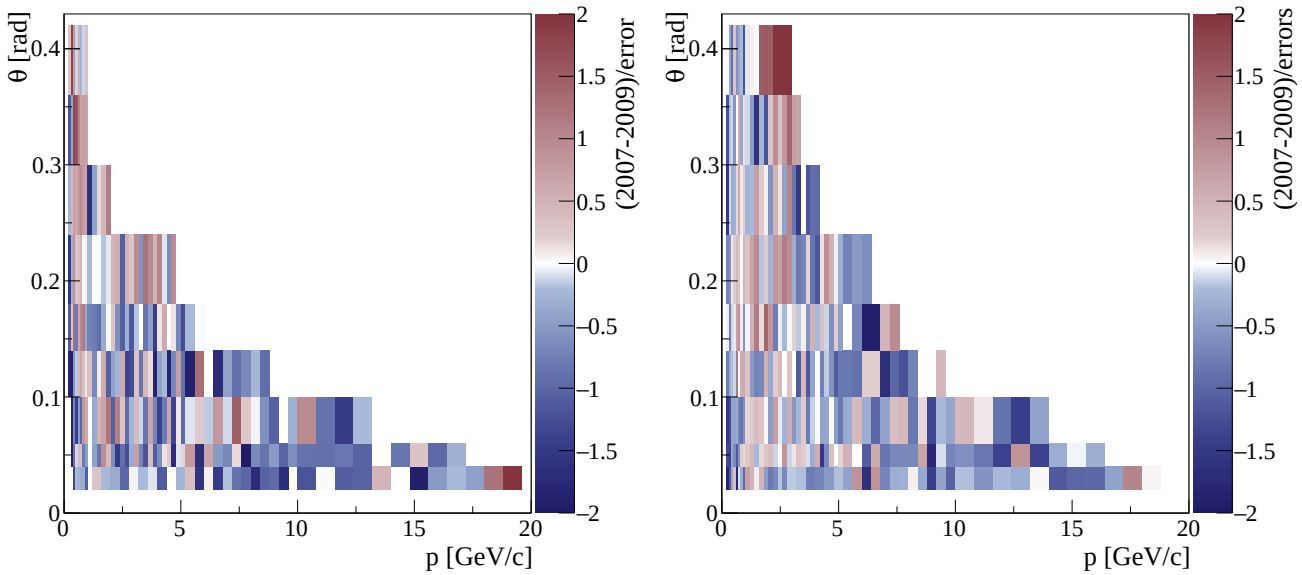

Fig. 24: (Colour online) Comparison between NA61/SHINE results obtained using the 2007 [5] and the 2009 data-sets for π^+ (*left*) and π^- (*right*). The difference between the 2007 and 2009 results is divided by its total uncertainty and plotted as a function of θ and p.

comparison of the measured spectra of K^0_S to the predictions from measured charged kaon yields and a reasonable agreement is observed between those results. Unfortunately, the large uncertainties associated with the K^0_S measurements do not allow us to discriminate between the two hypothesis.

6 Comparisons with hadron production models

In this section we compare the measured particle spectra in p+C interactions at 31 GeV/c with the predictions of different hadronic event generators. The comparisons are presented for a few selected GEANT4 physics lists [38, 39] (FTF_BIC [2] and QGSP_BERT) as well as for some hadroproduction models used within NA61/SHINE – VENUS4.12 [44, 45], EPOS1.99 [49] [3] and GIBUU1.6 [59].

The results of these comparisons are presented in Figs. 28–41. In order to avoid uncertainties related to the different treatment of quasi-elastic interaction and to the absence of predictions for inclusive cross sections, spectra are normalized to the mean particle multiplicity in all production interactions. For the data, the normalization relies on the p+C inclusive production cross section σ_{prod} which was found to be 230.7 mb (see Section 3.5).

The production cross section is calculated from the inelastic cross section by subtracting the quasi-elastic contribution. Therefore production processes are defined as those in which only new hadrons are present in the final state. Details of the cross section analysis procedure can be found in Section 3 and in Refs. [5, 33].

From the model comparison plots shown here one concludes that none of the models describes properly all spectra presented here. Some models provide a reasonable description in some regions but fail in some other areas. The FTF-based physics list of GEANT4 provides a reasonable description of NA61/SHINE data for $\pi^\pm$ and K^+, but it has difficulties in reproducing K^- and proton spectra. The EPOS and GIBUU models show a good agreement with the measured $K^\pm$ spectra. The best description of the measured proton spectra is achieved by the VENUS event generator which is used to calculate the corrections for all analyses presented here.

[2] The predictions of this physics list are significantly different between the consecutive releases of the GEANT4 toolkit - 4.9.5, 4.9.6 and 4.10

[3] Please, note that the EPOS model is used here in the energy domain for which it has not been designed (below 100 GeV in the lab)

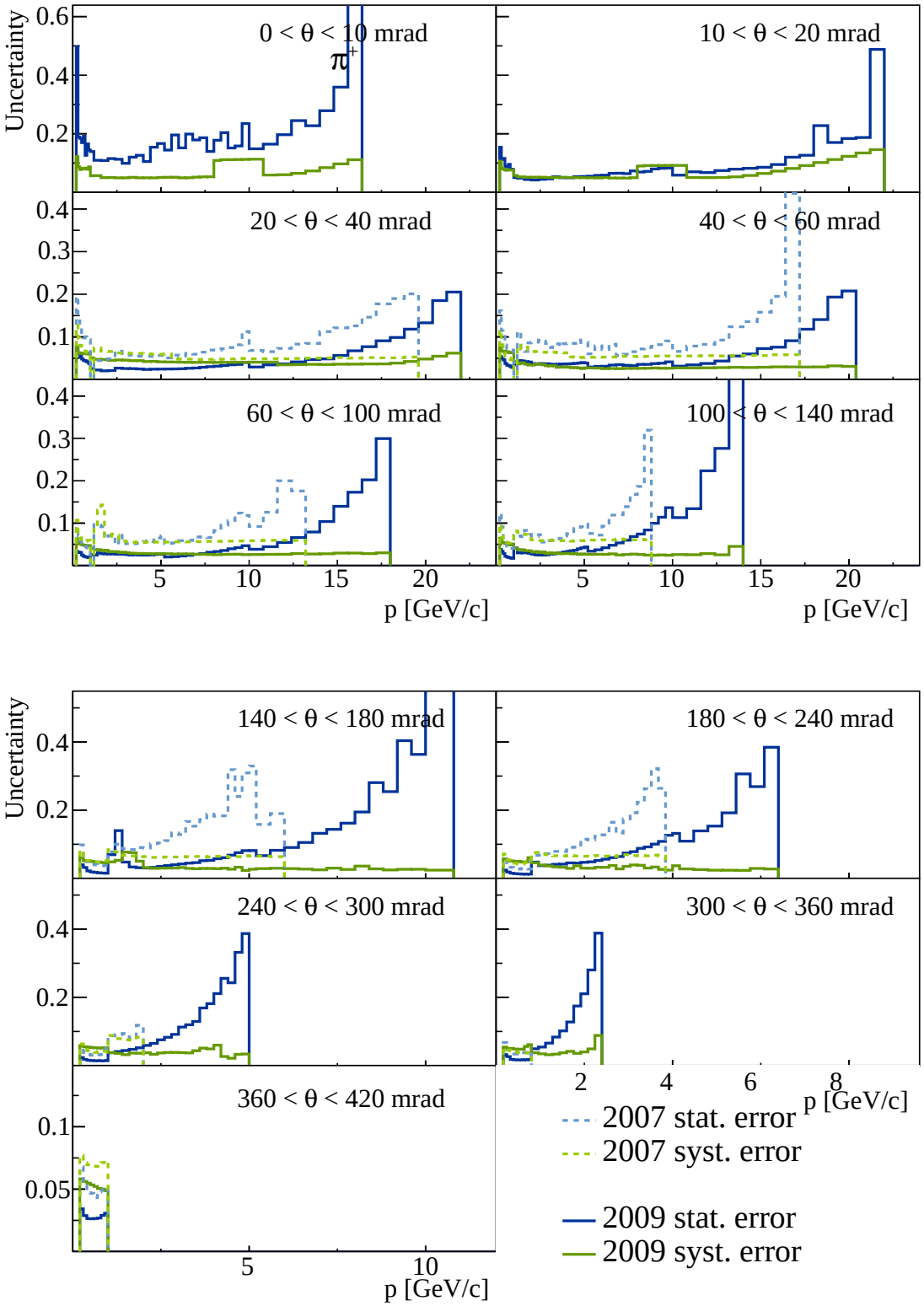

Fig. 25: (Colour online) Comparison between NA61/SHINE statistical and systematic uncertainties obtained using the 2007 [5] and the 2009 data-sets for π^+.

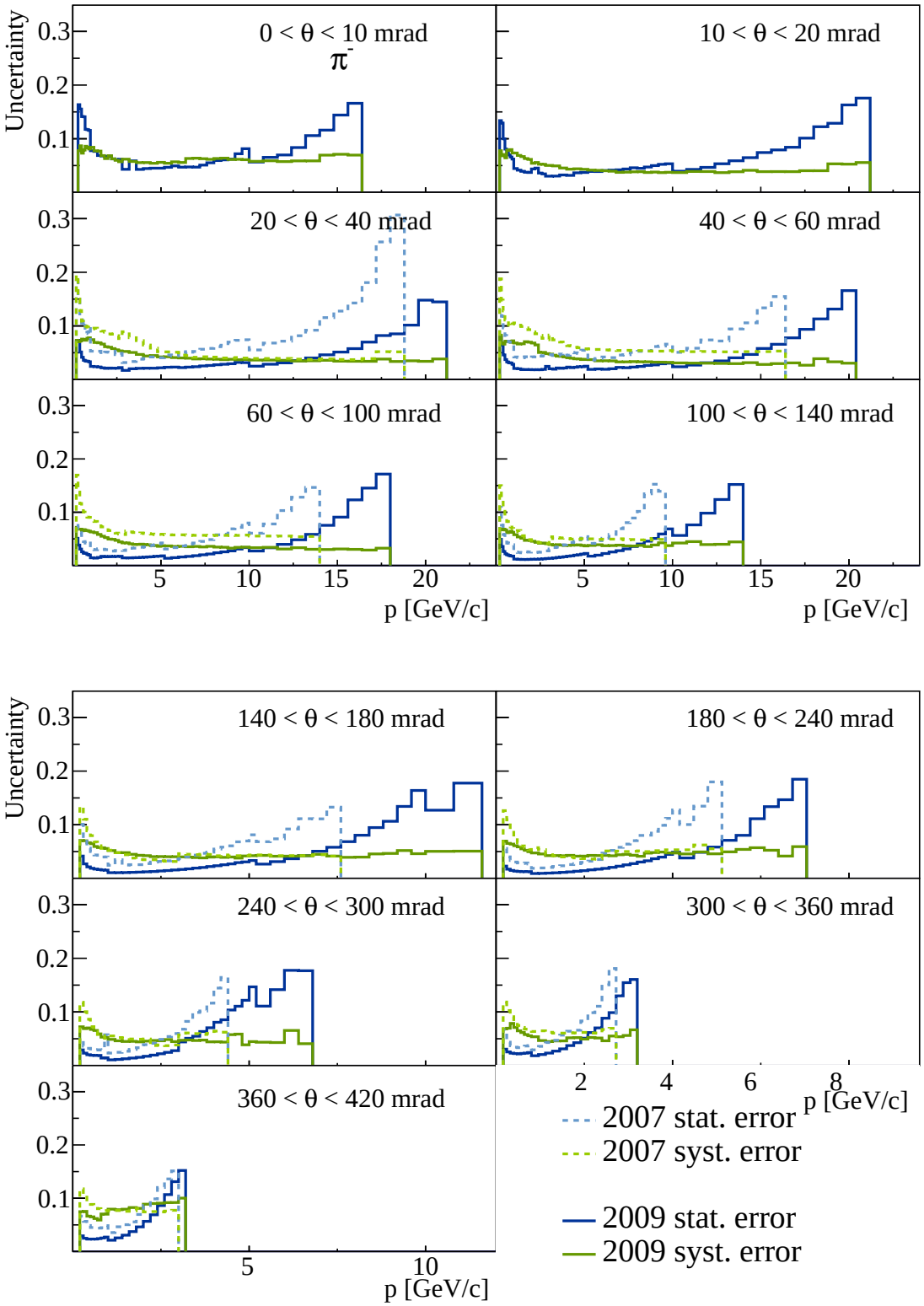

Fig. 26: (Colour online) Comparison between NA61/SHINE statistical and systematic uncertainties obtained using the 2007 [5] and the 2009 data-sets for π^-.

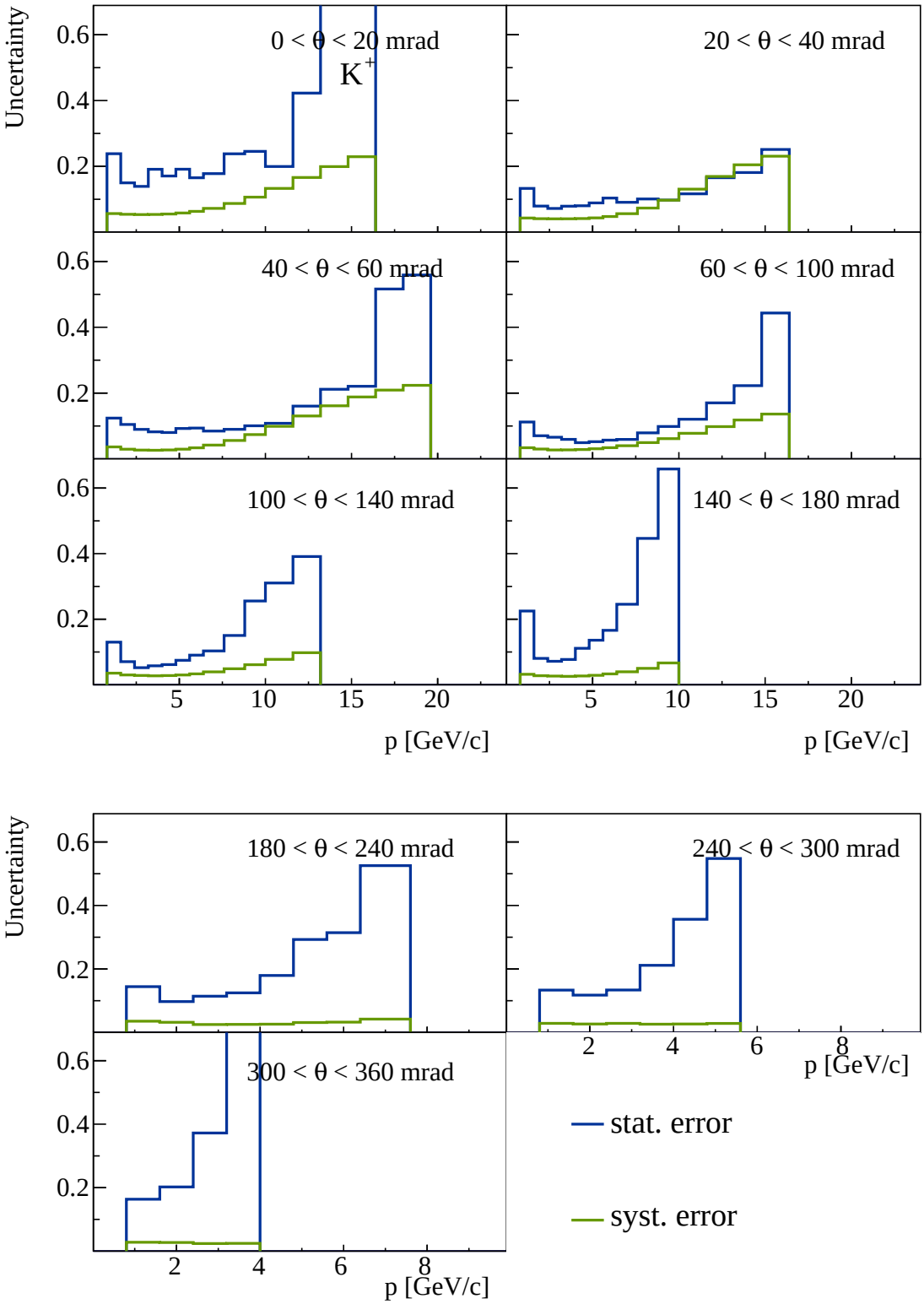

Fig. 27: (Colour online) Statistical and systematic uncertainties obtained using the 2009 data-set for K^+.

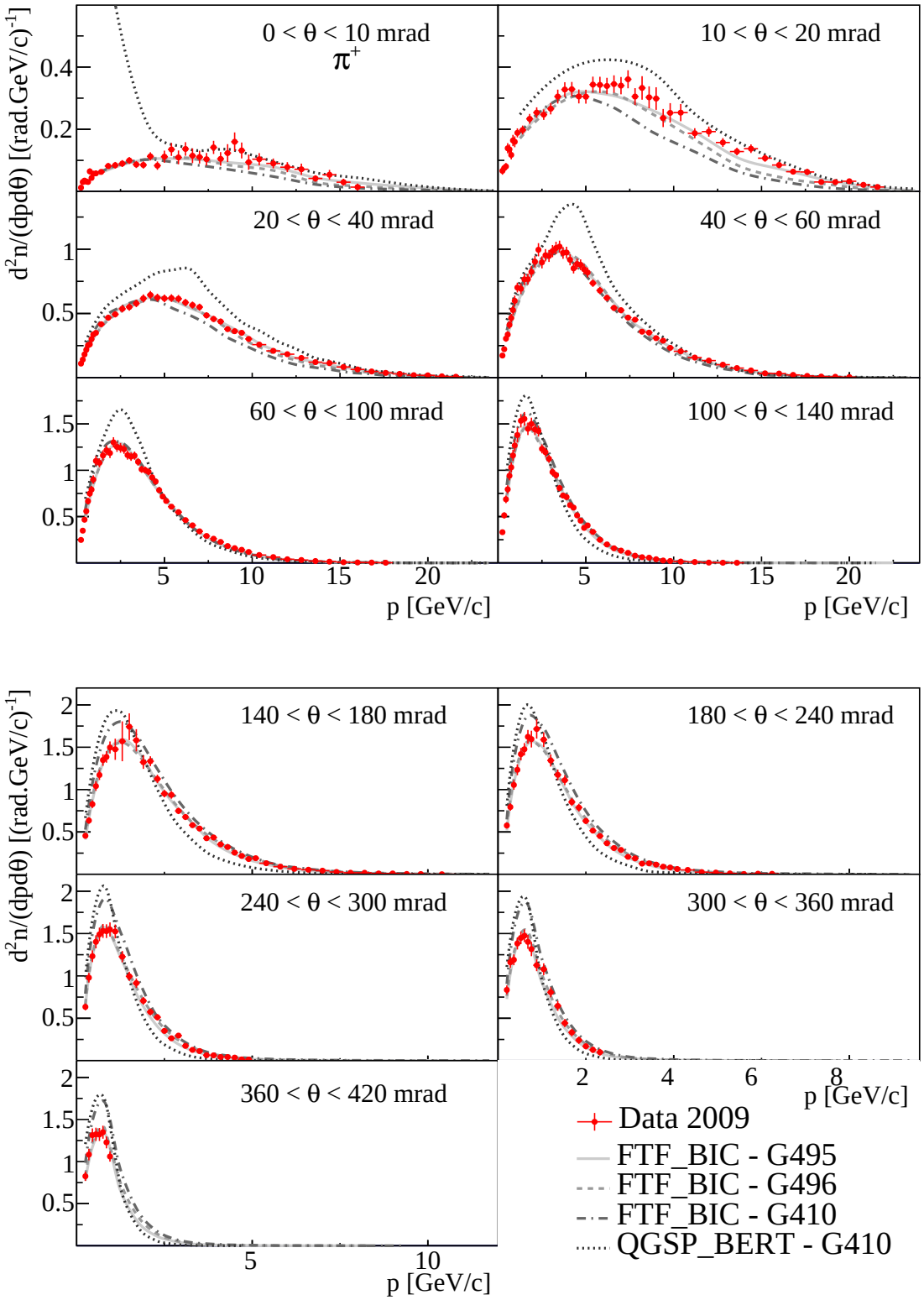

Fig. 28: (Colour online) Comparison of measured π^+ spectra with predictions of some selected GEANT4 physics lists. Distributions are normalized to the mean π^+ multiplicity in all production p+C interactions. The vertical error bars on the data points show the total (stat. and syst.) uncertainty. The horizontal bars indicate the bin size in momentum.

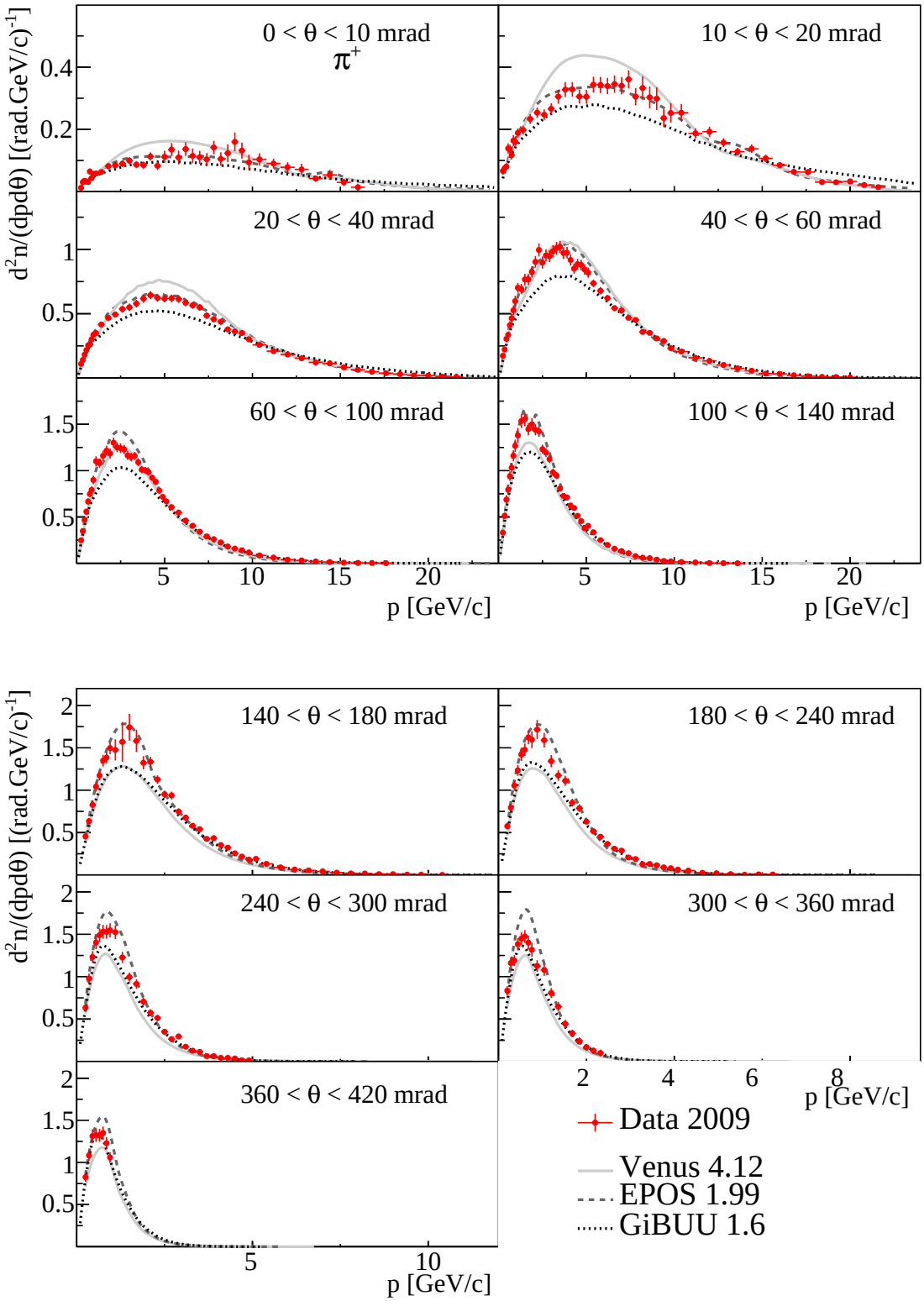

Fig. 29: (Colour online) Comparison of measured π^+ spectra with model (VENUS, EPOS, GIBUU) predictions. Distributions are normalized to the mean π^+ multiplicity in all production p+C interactions. The vertical error bars on the data points show the total (stat. and syst.) uncertainty. The horizontal bars indicate the bin size in momentum.

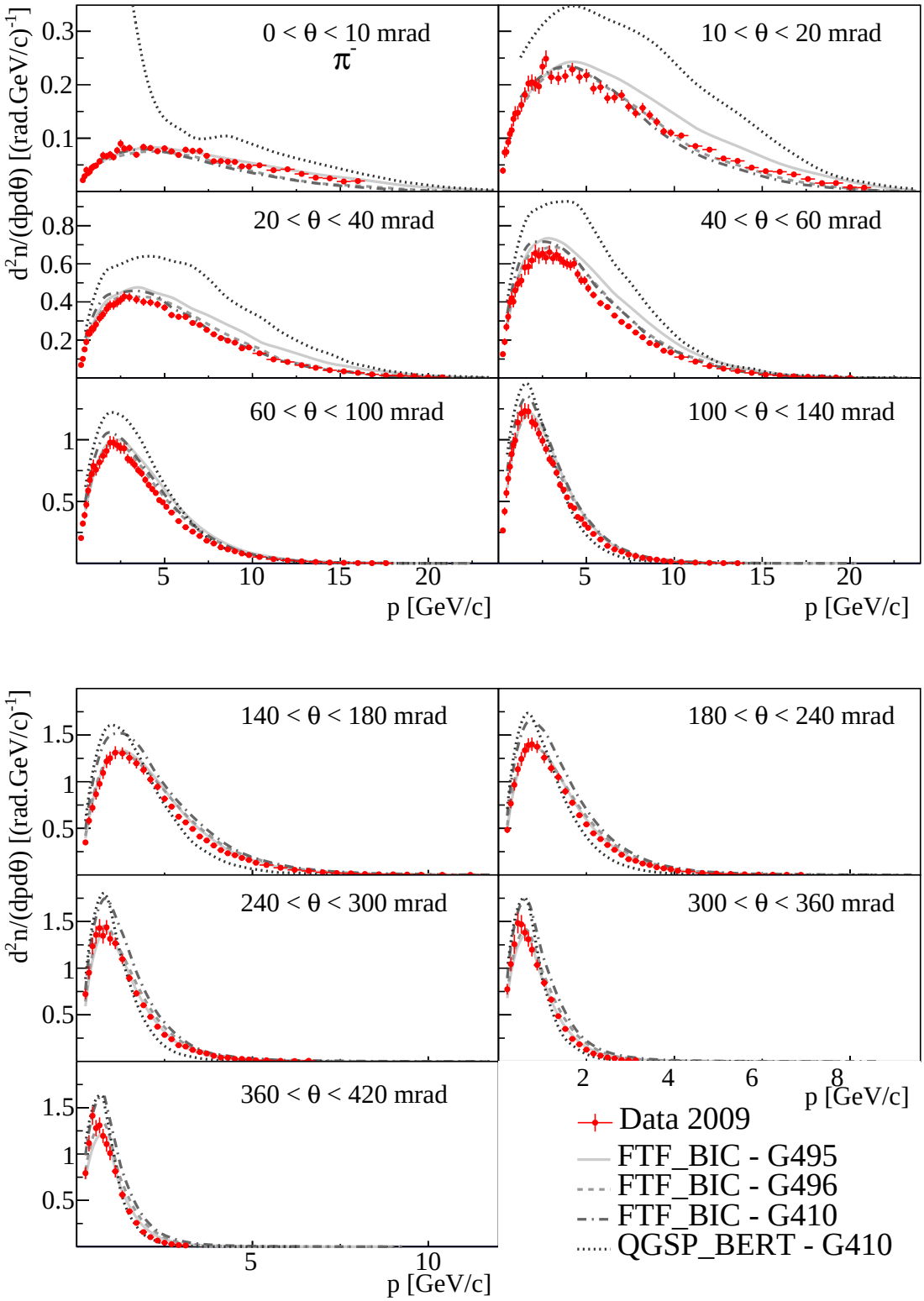

Fig. 30: (Colour online) Comparison of measured π^- spectra with predictions of some selected GEANT4 physics lists. Distributions are normalized to the mean π^- multiplicity in all production p+C interactions. The vertical error bars on the data points show the total (stat. and syst.) uncertainty. The horizontal bars indicate the bin size in momentum.

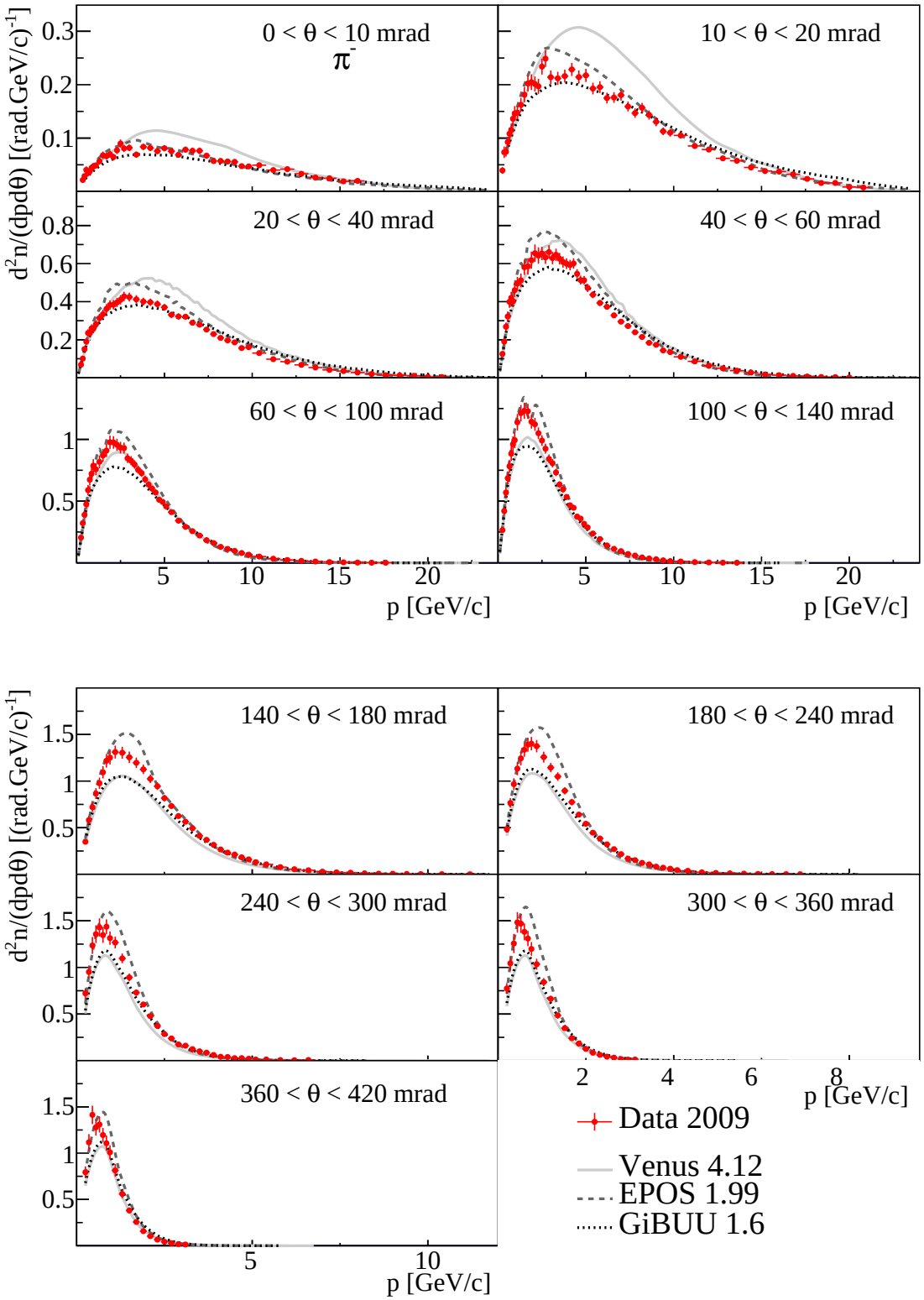

Fig. 31: (Colour online) Comparison of measured π^- spectra with model (VENUS, EPOS, GIBUU) predictions. Distributions are normalized to the mean π^- multiplicity in all production p+C interactions. The vertical error bars on the data points show the total (stat. and syst.) uncertainty. The horizontal bars indicate the bin size in momentum.

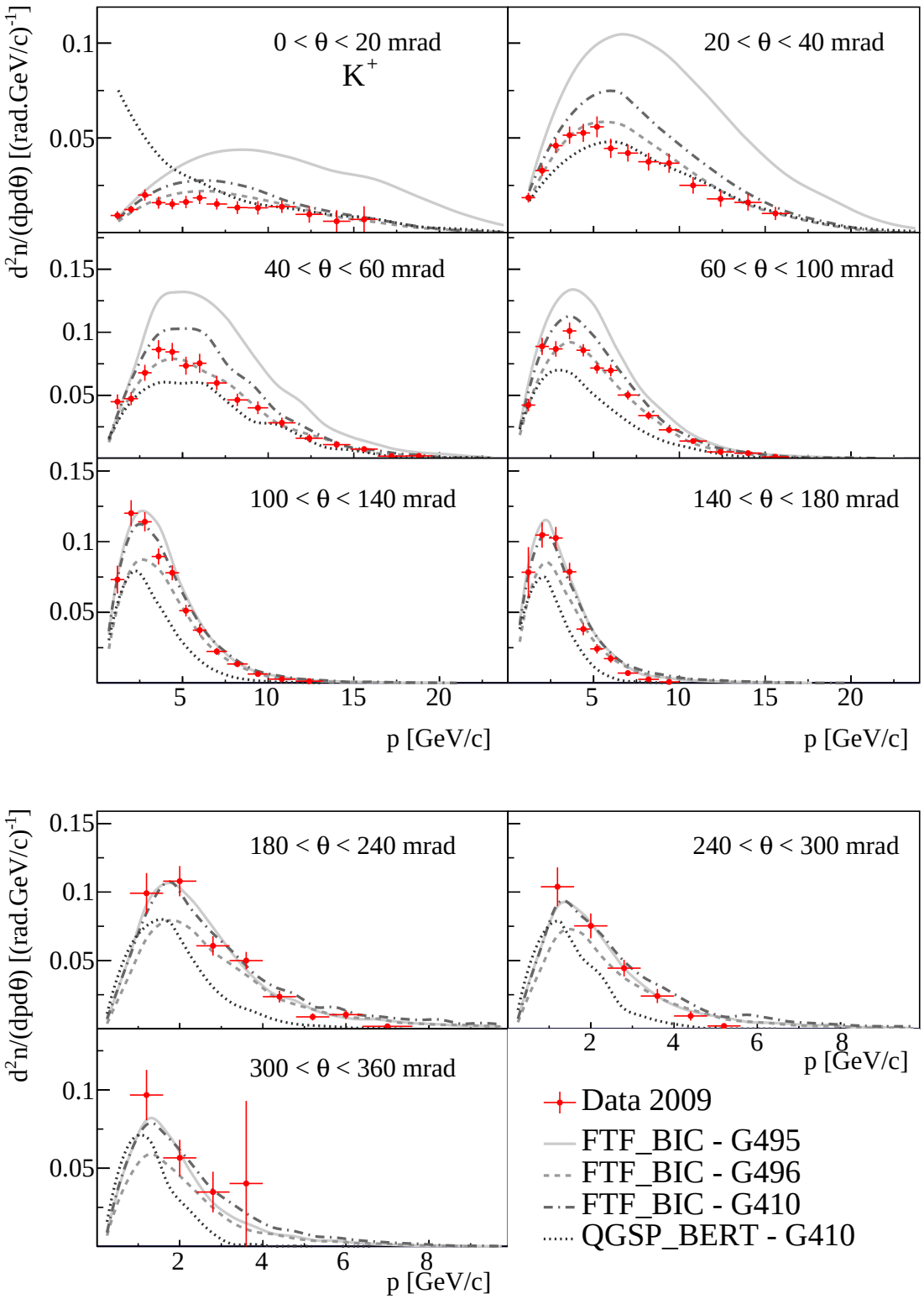

Fig. 32: (Colour online) Comparison of measured K^+ spectra with predictions of some selected GEANT4 physics lists. Distributions are normalized to the mean K^+ multiplicity in all production p+C interactions. The vertical error bars on the data points show the total (stat. and syst.) uncertainty. The horizontal bars indicate the bin size in momentum.

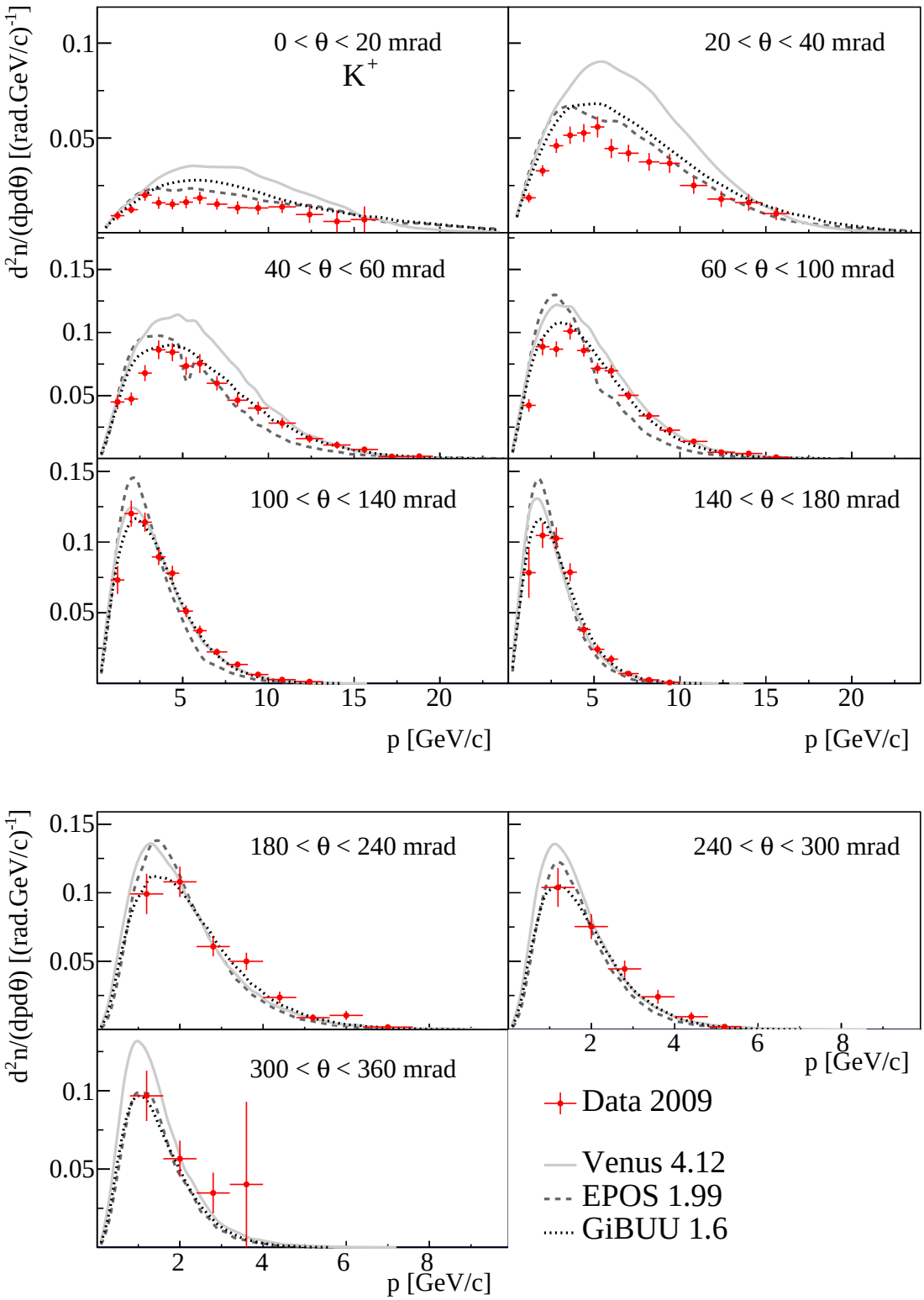

Fig. 33: (Colour online) Comparison of measured K^+ spectra with model (VENUS, EPOS, GIBUU) predictions. Distributions are normalized to the mean K^+ multiplicity in all production p+C interactions. The vertical error bars on the data points show the total (stat. and syst.) uncertainty. The horizontal bars indicate the bin size in momentum.

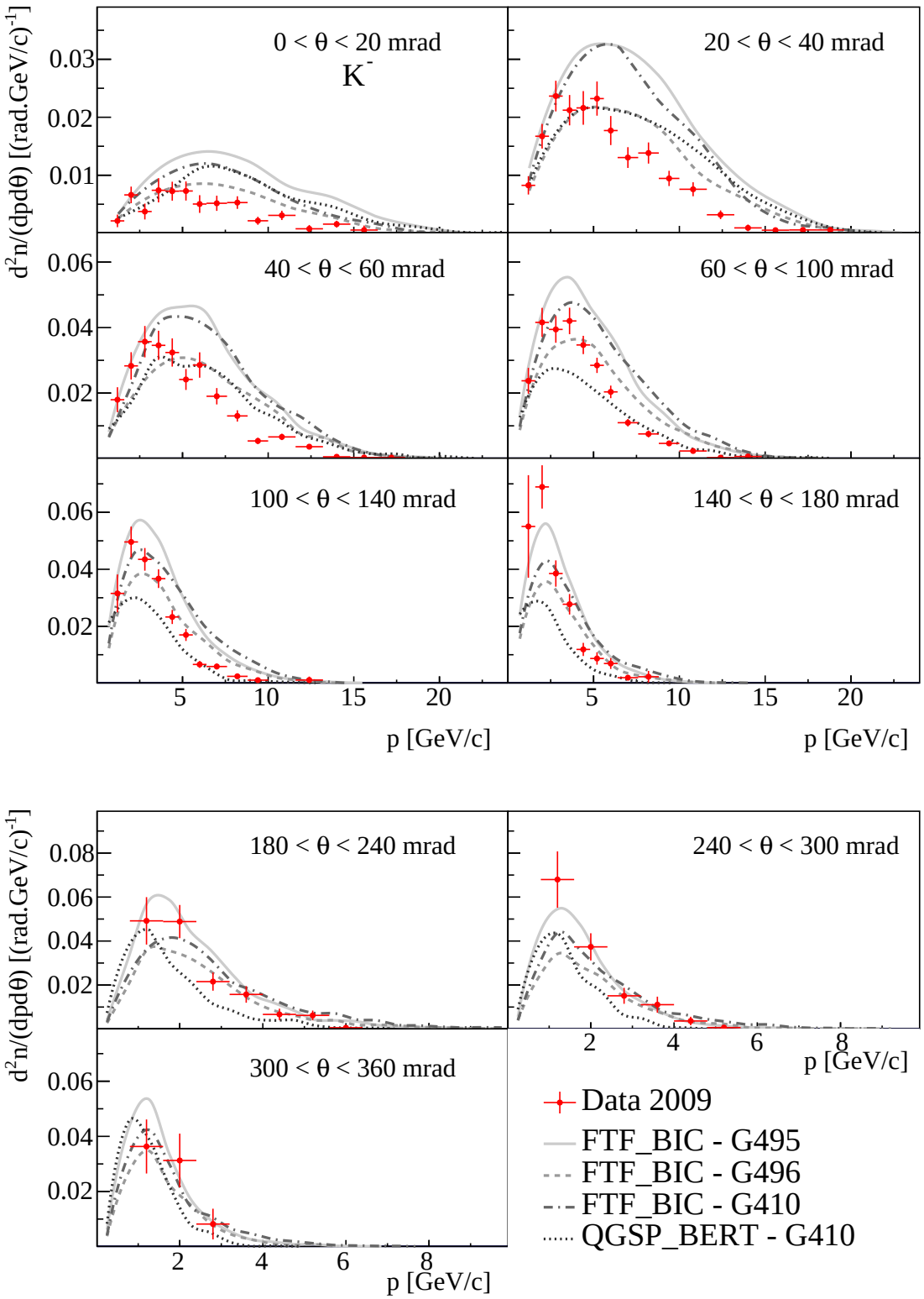

Fig. 34: (Colour online) Comparison of measured K^- spectra with predictions of some selected GEANT4 physics lists. Distributions are normalized to the mean K^- multiplicity in all production p+C interactions. The vertical error bars on the data points show the total (stat. and syst.) uncertainty. The horizontal bars indicate the bin size in momentum.

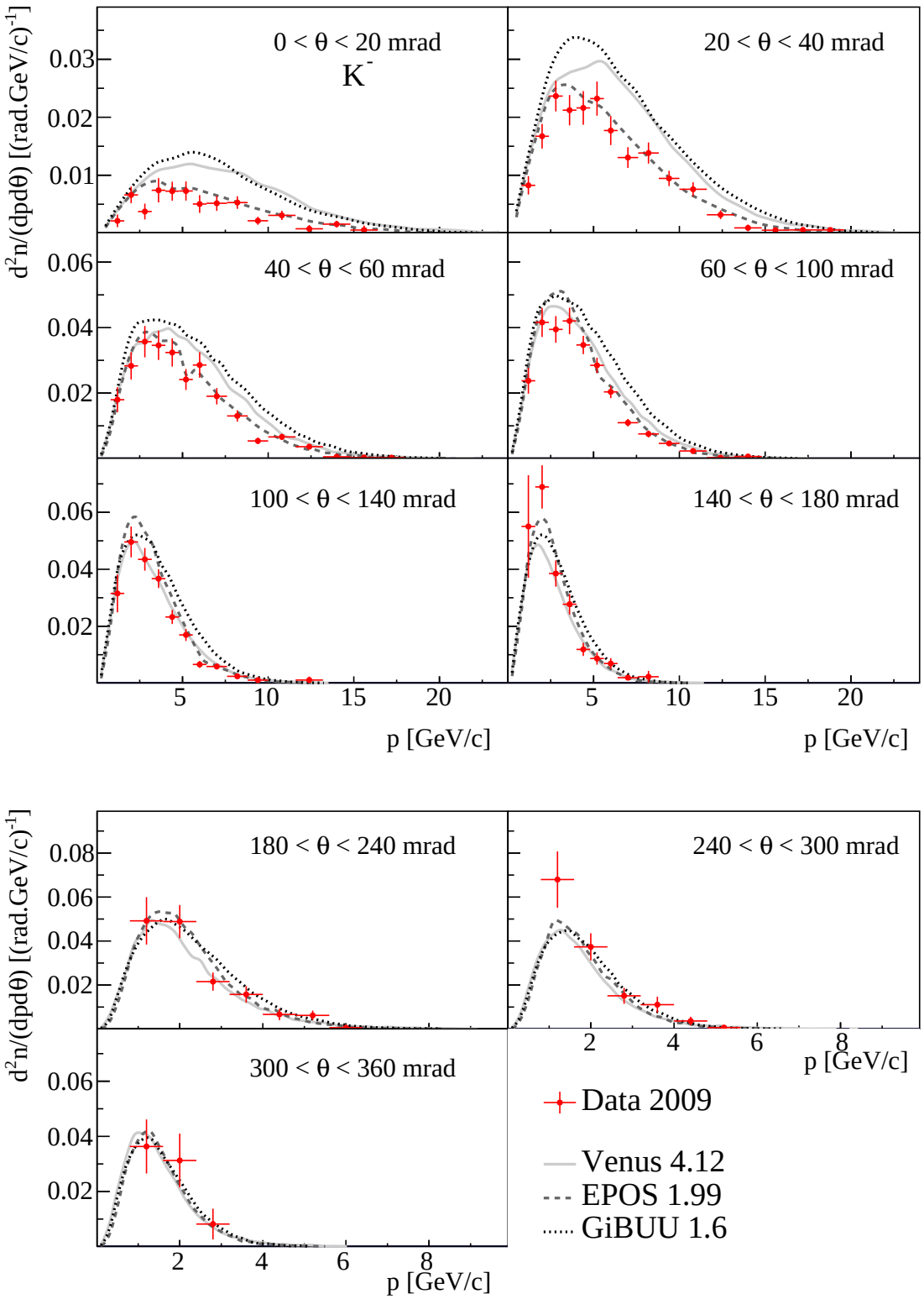

Fig. 35: (Colour online) Comparison of measured K^- spectra with model (VENUS, EPOS, GIBUU) predictions. Distributions are normalized to the mean K^- multiplicity in all production p+C interactions. The vertical error bars on the data points show the total (stat. and syst.) uncertainty. The horizontal bars indicate the bin size in momentum.

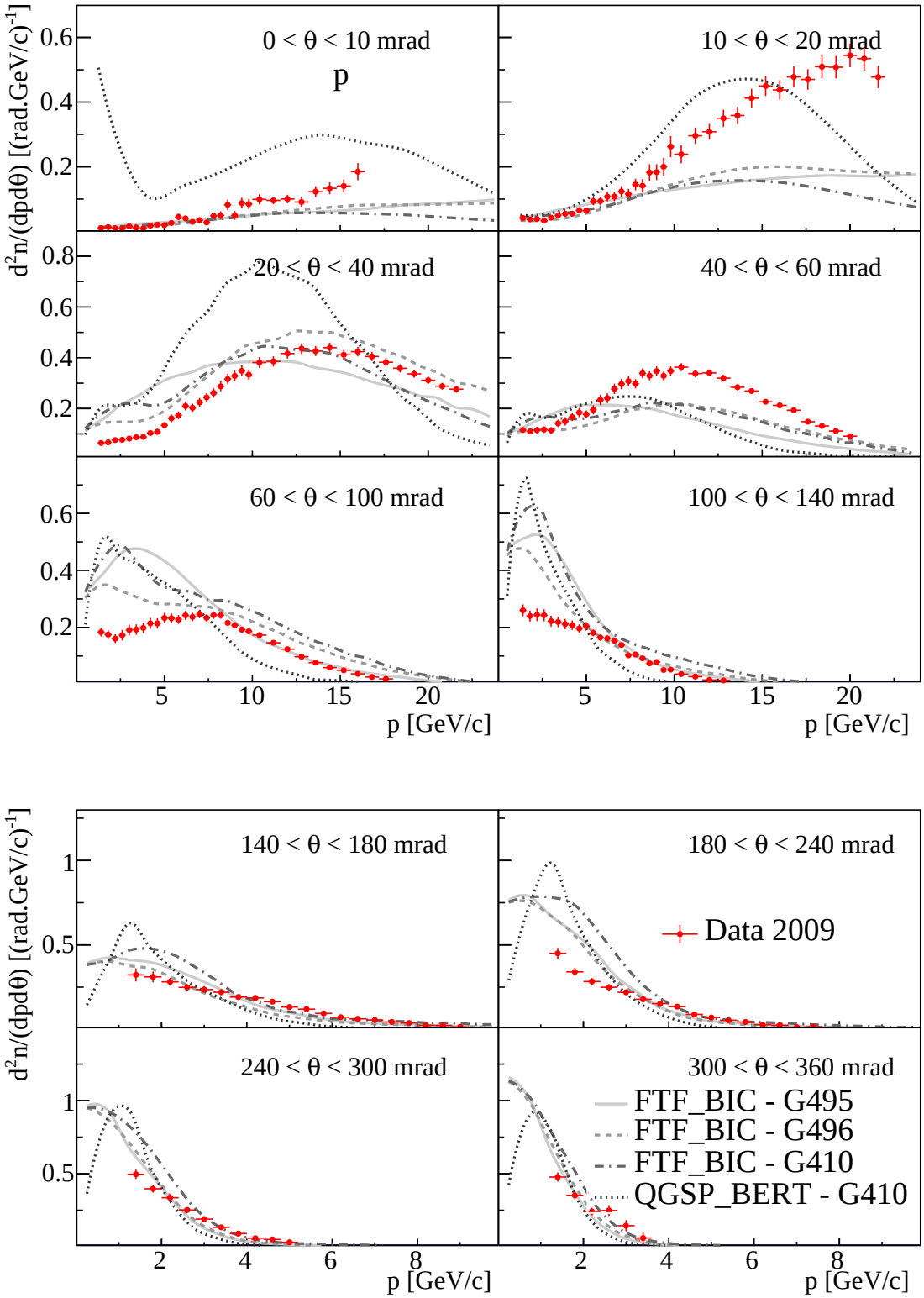

Fig. 36: (Colour online) Comparison of measured proton spectra with predictions of some selected GEANT4 physics lists. Distributions are normalized to the mean proton multiplicity in all production p+C interactions. The vertical error bars on the data points show the total (stat. and syst.) uncertainty. The horizontal bars indicate the bin size in momentum.

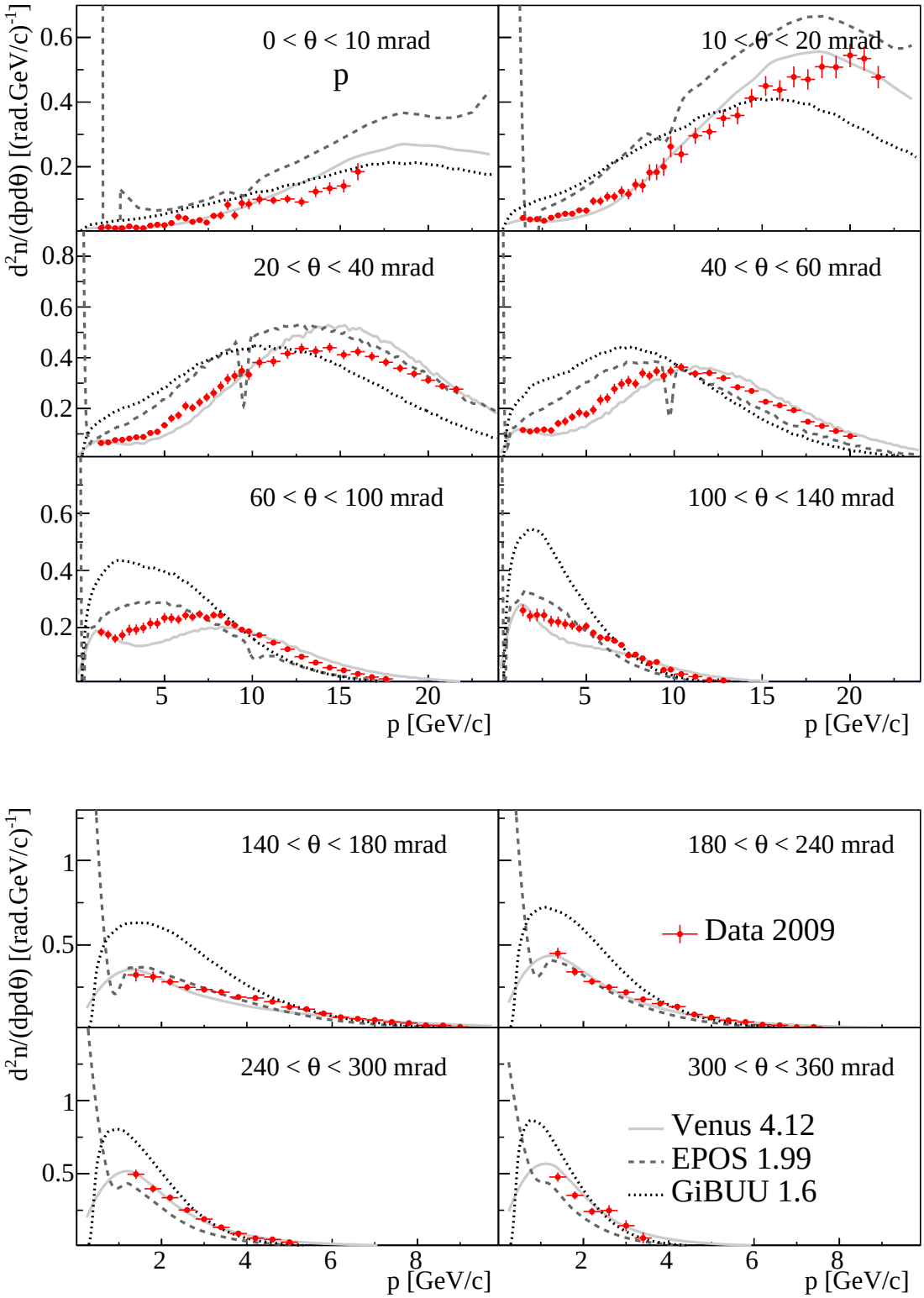

Fig. 37: (Colour online) Comparison of measured proton spectra with model (VENUS, EPOS, GIBUU) predictions. Distributions are normalized to the mean proton multiplicity in all production p+C interactions. The vertical error bars on the data points show the total (stat. and syst.) uncertainty. The horizontal bars indicate the bin size in momentum.

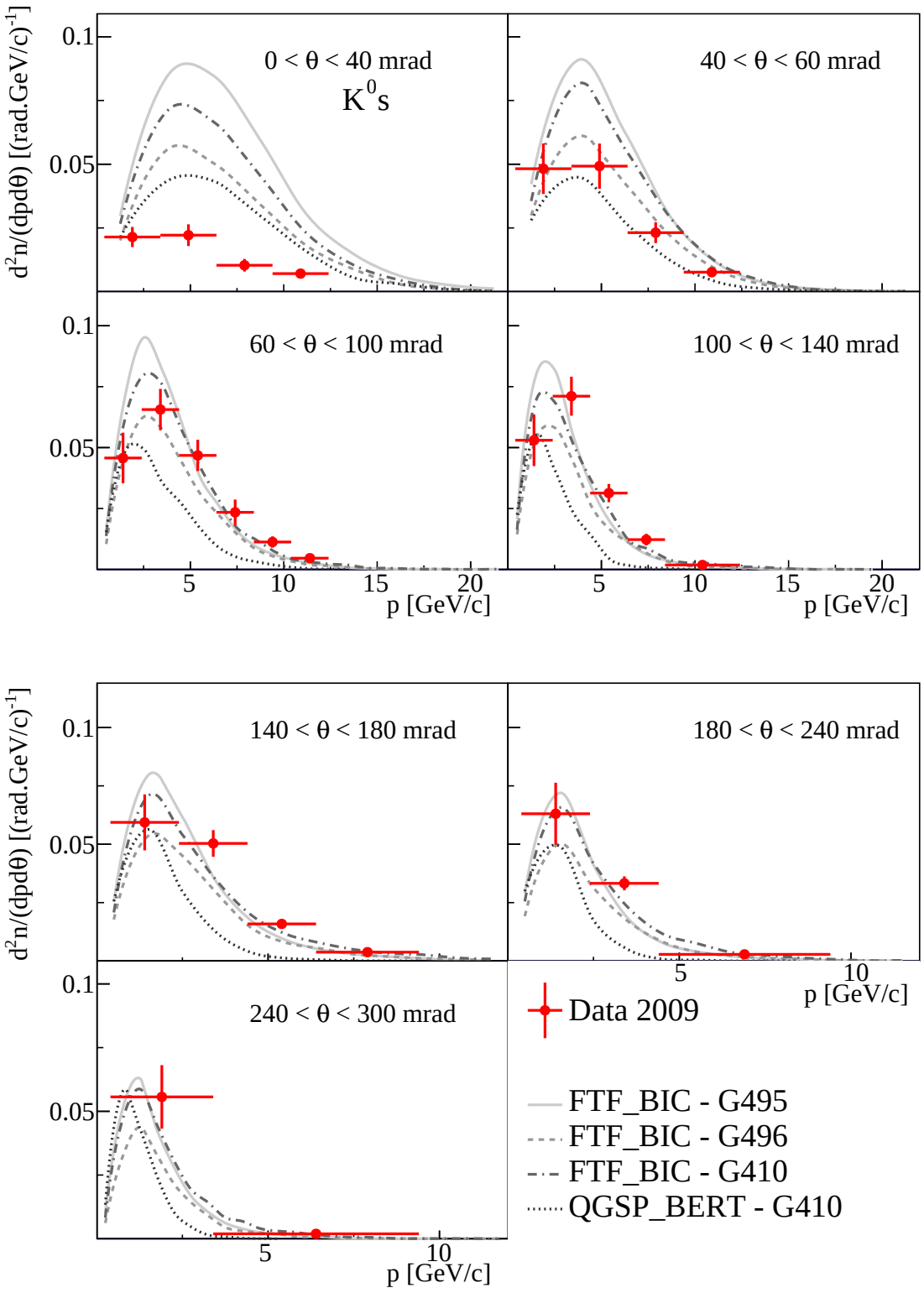

Fig. 38: (Colour online) Comparison of measured K^0_S spectra with predictions of some selected GEANT4 physics lists. Distributions are normalized to the mean K^0_S multiplicity in all production p+C interactions. The vertical error bars on the data points show the total (stat. and syst.) uncertainty. The horizontal bars indicate the bin size in momentum.

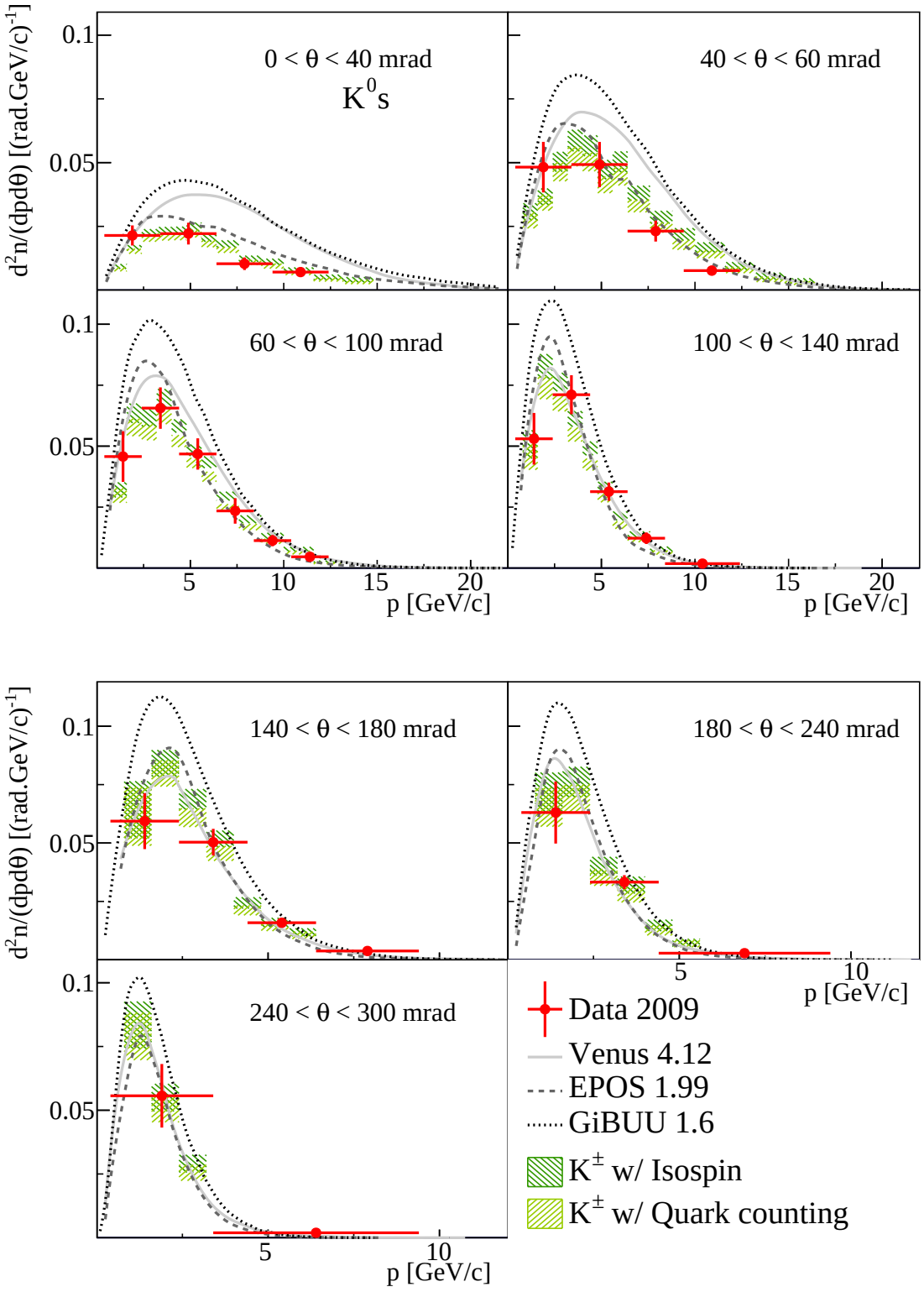

Fig. 39: (Colour online) Comparison of measured K^0_S spectra with model (VENUS, EPOS, GIBUU) Distributions are normalized to the mean K^0_S multiplicity in all production p+C interactions. The vertical error bars on the data points show the total (stat. and syst.) uncertainty. The horizontal bars indicate the bin size in momentum. The mixing of $K^{\pm}$ under isospin (dark green) and quark counting (light green) hypotheses are also presented.

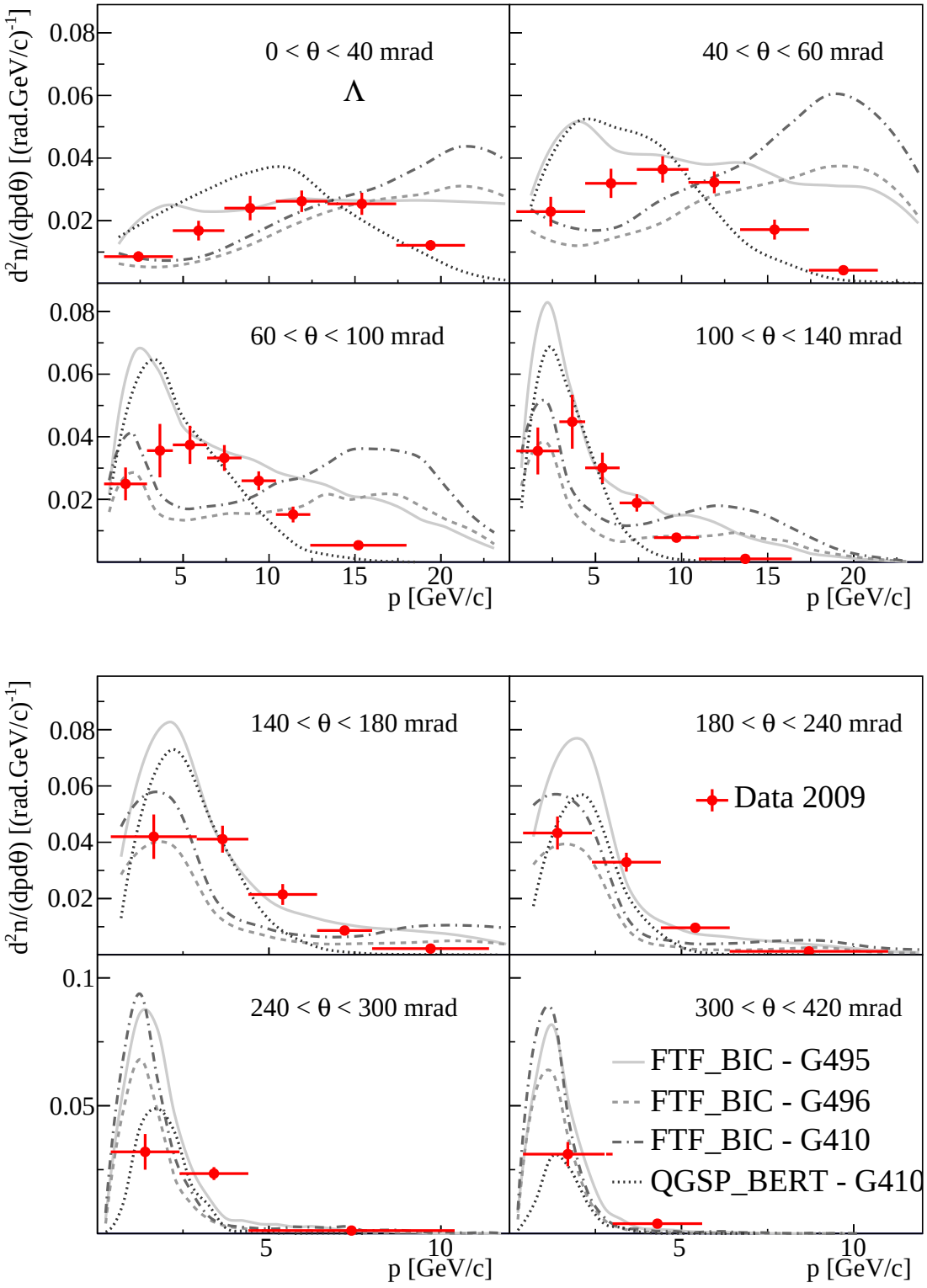

Fig. 40: (Colour online) Comparison of measured Λ spectra with predictions of some selected GEANT4 physics lists. Distributions are normalized to the mean Λ multiplicity in all production p+C interactions. The vertical error bars on the data points show the total (stat. and syst.) uncertainty. The horizontal bars indicate the bin size in momentum.

7 Summary

This work presents precise measurements of interaction and production cross sections as well as of spectra of $\pi^{\pm}$, $K^{\pm}$, protons, K^0_S and Λ in p+C interactions at 31 GeV/c. These data are crucial for predictions of the initial neutrino fluxes in the T2K long baseline neutrino oscillation experiment in Japan. Furthermore, they provide important input to improve hadron production models needed for the interpretation of air showers initiated by ultra high energy cosmic particles. The measurements were performed with the large acceptance NA61/SHINE spectrometer at the CERN SPS. A set of data collected with a 4% λ_I isotropic graphite target during the high-statistics NA61/SHINE run in 2009 was used for the analysis. The measured spectra were compared with predictions of hadron production models.

Acknowledgements We would like to thank the CERN PH, BE and EN Departments for the strong support of NA61.

This work was supported by the Hungarian Scientific Research Fund (grants OTKA 68506 and 71989), the János Bolyai Research Scholarship of the Hungarian Academy of Sciences, the Polish Ministry of Science and Higher Education (grants 667/N-CERN/2010/0, NN 202 48 4339 and NN 202 23 1837), the Polish National Center for Science (grants 2011/03/N/ST2/03691, 2012/04/M/ST2/00816 and 2013/11/N/ST2/03879), the Foundation for Polish Science — MPD program, co-financed by the European Union within the European Regional Development Fund, the Federal Agency of Education of the Ministry of Education and Science of the Russian Federation (SPbSU research grant 11.38.193.2014), the Russian Academy of Science and the Russian Foundation for Basic Research (grants 08-02-00018, 09-02-00664 and 12-02-91503-CERN), the Ministry of Education, Culture, Sports, Science and Technology, Japan, Grant-in-Aid for Scientific Research (grants 18071005, 19034011, 19740162, 20740160 and 20039012), the German Research Foundation (grant GA 1480/2-2), the EU-funded Marie Curie Outgoing Fellowship, Grant PIOF-GA-2013-624803, the Bulgarian Nuclear Regulatory Agency and the Joint Institute for Nuclear Research, Dubna (bilateral contract No. 4418-1-15/17), Ministry of Education and Science of the Republic of Serbia (grant OI171002), Swiss Nationalfonds Foundation (grant 200020117913/1) and ETH Research Grant TH-01 07-3.

References

1. N. Antoniou, et al., CERN-SPSC-2006-034 (2006)
2. N. Antoniou, et al., CERN-SPSC-2007-004 (2007)
3. N. Antoniou, et al., CERN-SPSC-2007-019 (2007)
4. N. Abgrall, et al., CERN-SPSC-2008-018 (2008)
5. N. Abgrall, et al., Phys. Rev. **C84**, 034604 (2011). DOI 10.1103/PhysRevC.84.034604
6. N. Abgrall, et al., Phys. Rev. **C85**, 035210 (2012). DOI 10.1103/PhysRevC.85.035210
7. K. Abe, et al., Nucl. Instrum. Meth. **A659**, 106 (2011). DOI 10.1016/j.nima.2011.06.067
8. S. Johnson, et al., CERN-SPSC-2014-032; SPSC-P-330-ADD-7 (2014)
9. J. Abraham, et al., Nucl. Instrum. Meth. **A523**, 50 (2004). DOI 10.1016/j.nima.2003.12.012
10. T. Antoni, et al., Nucl. Instrum. Meth. **A513**, 490 (2003). DOI 10.1016/S0168-9002(03)02076-X
11. N. Abgrall, et al., Eur. Phys. J. **C74**, 2794 (2014). DOI 10.1140/epjc/s10052-014-2794-6
12. N. Abgrall, et al., CERN-SPSC-2014-031 (2014)
13. N. Abgrall, et al., Phys. Rev. **C89**, 025205 (2014). DOI 10.1103/PhysRevC.89.025205
14. K. Abe, et al., Phys. Rev. Lett. **107**(4), 041801 (2011). DOI 10.1103/PhysRevLett.107.041801
15. K. Abe, et al., Phys. Rev. **D85**, 031103 (2012). DOI 10.1103/PhysRevD.85.031103
16. K. Abe, et al., Phys. Rev. **D87**, 012001 (2013). DOI 10.1103/PhysRevD.87.012001,10.1103/PhysRevD.87.019902
17. K. Abe, et al., Phys. Rev. **D88**, 032002 (2013). DOI 10.1103/PhysRevD.88.032002
18. K. Abe, et al., Phys. Rev. Lett. **111**, 211803 (2013). DOI 10.1103/PhysRevLett.111.211803
19. K. Abe, et al., Phys. Rev. Lett. **112**, 061802 (2014). DOI 10.1103/PhysRevLett.112.061802
20. K. Abe, et al., Phys. Rev. Lett. **112**, 181801 (2014). DOI 10.1103/PhysRevLett.112.181801
21. K. Abe, et al., Phys. Rev. **D87**, 092003 (2013). DOI 10.1103/PhysRevD.87.092003
22. K. Abe, et al., Phys. Rev. **D90**(5), 052010 (2014). DOI 10.1103/PhysRevD.90.052010
23. K. Abe, et al., Phys. Rev. Lett. **113**(24), 241803 (2014). DOI 10.1103/PhysRevLett.113.241803
24. N. Abgrall, et al., JINST **9**, P06005 (2014). DOI 10.1088/1748-0221/9/06/P06005
25. K. Abe, et al., PTEP **2015**(4), 043C01 (2014). DOI 10.1093/ptep/ptv031
26. N. Abgrall, et al., Nucl. Instrum. Meth. **A701**, 99 (2013). DOI 10.1016/j.nima.2012.10.079
27. A. Haesler, Ph.D. Thesis, University of Geneva (2015). URL https://cds.cern.ch/record/2039148
28. S. Afanasiev, et al., Nucl.Instrum.Meth. **A430**, 210 (1999). DOI 10.1016/S0168-9002(99)00239-9
29. C. Bovet, et al., (1982). CERN-YELLOW-82-13
30. N. Abgrall, Ph.D. Thesis, University of Geneva (2011). URL https://edms.cern.ch/document/1172455/1
31. B. Bobchenko, A. Buklei, A. Vlasov, L. Vorobev, N. Goryainov, et al., Sov.J.Nucl.Phys. **30**, 805 (1979)
32. D. Sgalaberna, Ph.D. Thesis, ETH Zurich (*to be defended soon*) (2015)
33. C. Strabel, Ph.D. Thesis, ETH Zurich (2011). URL https://edms.cern.ch/document/1136130/1
34. G. Bellettini, et al., Nucl. Phys. **79**(3), 609 (1966)
35. S.P. Denisov, et al., Nucl. Phys. B **61**, 62 (1973)

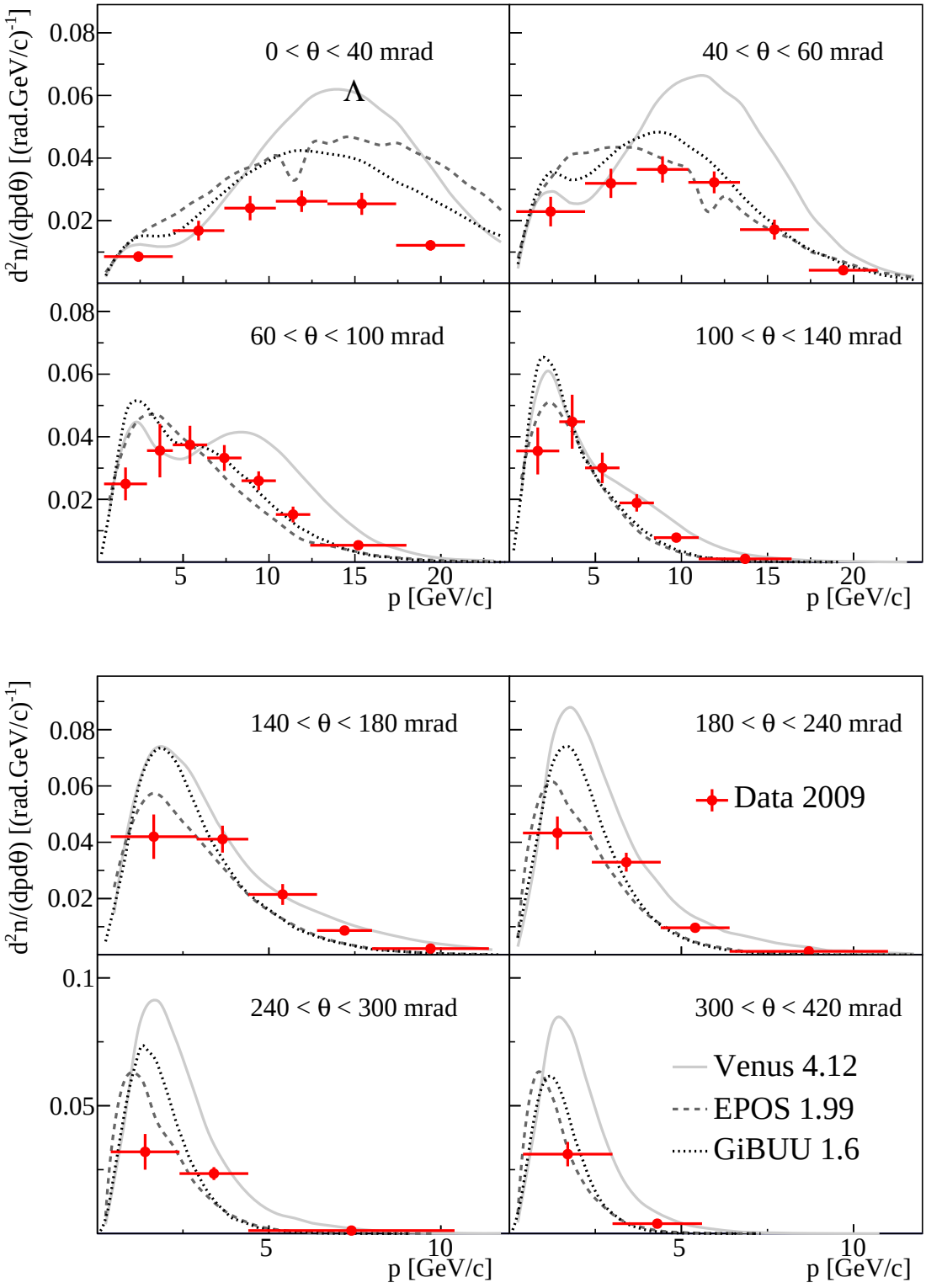

Fig. 41: (Colour online) Comparison of measured Λ spectra with model (VENUS, EPOS, GIBUU) predictions. Distributions are normalized to the mean Λ multiplicity in all production p+C interactions. The vertical error bars on the data points show the total (stat. and syst.) uncertainty. The horizontal bars indicate the bin size in momentum.

36. S. Mahajan, R. Raja, (2013). FERMILAB-CONF-13-461-E
37. A.S. Carroll, et al., Phys. Lett. B **80**, 319 (1979)
38. S. Agostinelli, et al., Nucl. Instrum. Meth. **A506**, 250 (2003)
39. J. Allison, et al., IEEE Transactions on Nuclear Science **53**(1), 270 (2006)
40. A. Schiz, et al., Phys. Rev. D **21**(11), 3010 (1980)
41. L. Zambelli, Ph.D. Thesis, University of Paris VII (2013). URL https://edms.cern.ch/document/1316278/1
42. K. Olive, et al., Chin. Phys. **C38**, 090001 (2014). DOI 10.1088/1674-1137/38/9/090001
43. J. Podolanski, R. Armenteros, Philosophical Magazine Series 7 **45:360**, 13 (1953)
44. K. Werner, Nucl. Phys. **A525**, 501 (1991). DOI 10.1016/0375-9474(91)90372-D
45. K. Werner, Phys. Rept. **232**, 87 (1993). DOI 10.1016/0370-1573(93)90078-R
46. A. Ferrari, P.R. Sala, A. Fasso, J. Ranft, CERN-2005-010, SLAC-R-773, INFN-TC-05-11 (2005)
47. G. Battistoni, et al., AIP Conf. Proc. **896**, 31 (2007). DOI 10.1063/1.2720455
48. T. Böhlen, et al., Nuclear Data Sheets 120, 211-214 (2014)
49. K. Werner, F.M. Liu, T. Pierog, Phys. Rev. **C74**, 044902 (2006). DOI 10.1103/PhysRevC.74.044902
50. S. Murphy, Ph.D. Thesis, University of Geneva (2012). URL https://edms.cern.ch/document/1218480/1
51. M. Posiadała, Ph.D. Thesis, University of Warsaw (2012). URL https://edms.cern.ch/document/1250627/1
52. R.M. Sternheimer, R.F. Peierls, Phys. Rev. **B3**, 3681 (1971). DOI 10.1103/PhysRevB.3.3681
53. M. Gazdzicki, Nucl. Instrum. Meth. **A345**, 148 (1994). DOI 10.1016/0168-9002(94)90984-9
54. T. Palczewski, Ph.D. Thesis, NCNR, Warsaw (2012). URL https://edms.cern.ch/document/1240016/1
55. O. Chvala, H. Fischer, M. Makariev, A. Rybicki, D. Varga, et al., Eur. Phys. J. **C73**, 2329 (2013). DOI 10.1140/epjc/s10052-013-2329-6
56. N. Abgrall, et al., CERN-SPSC-2012-029 (2012)
57. M. Gazdzicki, O. Hansen, Nucl.Phys. **A528**, 754 (1991)
58. M. Bonesini, A. Marchionni, F. Pietropaolo, T. Tabarelli de Fatis, Eur. Phys. J. **C20**, 13 (2001). DOI 10.1007/s100520100656
59. O. Buss, T. Gaitanos, K. Gallmeister, H. van Hees, M. Kaskulov, et al., Phys. Rept. **512**, 1 (2012). DOI 10.1016/j.physrep.2011.12.001

θ [mrad]	p [GeV/c]	$\frac{d^2\sigma}{dpd\theta}(\pi^+)$ [mb/rad/(GeV/c)]	Δ_{stat} [mb/rad/(GeV/c)]	Δ_{stat} [%]	Δ_{syst} [mb/rad/(GeV/c)]	Δ_{syst} [%]
0 - 10	0.2 - 0.3	2.8	1.4	49.7	0.3	12.2
	0.3 - 0.4	7.0	1.3	18.9	0.6	8.7
	0.4 - 0.5	8.1	1.5	18.4	0.6	7.8
	0.5 - 0.6	7.3	1.2	17.0	0.6	8.1
	0.6 - 0.7	7.1	1.4	19.2	0.6	8.1
	0.7 - 0.8	14.9	1.9	12.6	1.2	8.3
	0.8 - 0.9	10.0	1.7	16.5	0.8	7.9
	0.9 - 1.0	13.1	1.9	14.5	1.1	8.7
	1.0 - 1.2	13.4	1.9	13.9	0.8	5.7
	1.2 - 1.6	14.5	1.6	10.9	0.8	5.7
	1.6 - 2.0	18.9	2.0	10.9	0.9	5.0
	2.0 - 2.4	19.5	2.2	11.5	1.0	5.1
	2.4 - 2.8	20.7	2.3	11.3	1.0	5.0
	2.8 - 3.2	23.0	2.3	9.9	1.1	5.0
	3.2 - 3.6	20.0	2.4	12.0	1.0	5.1
	3.6 - 4.0	19.7	2.5	12.6	1.0	5.0
	4.0 - 4.4	26.0	2.7	10.5	1.3	5.0
	4.4 - 4.8	19.2	3.0	15.4	0.9	4.9
	4.8 - 5.2	25.8	4.3	16.7	1.3	5.1
	5.2 - 5.6	31.2	4.5	14.4	1.6	5.1
	5.6 - 6.0	25.3	5.0	19.6	1.3	5.2
	6.0 - 6.4	31.5	4.8	15.2	1.6	5.0
	6.4 - 6.8	26.5	5.3	19.9	1.3	5.0
	6.8 - 7.2	25.5	4.6	17.9	1.3	5.2
	7.2 - 7.6	23.9	4.5	18.6	1.3	5.3
	7.6 - 8.0	32.7	4.6	14.0	1.7	5.3
	8.0 - 8.4	24.2	4.3	17.8	2.6	10.9
	8.4 - 8.8	28.5	5.8	20.4	3.2	11.1
	8.8 - 9.2	36.9	5.6	15.1	4.1	11.2
	9.2 - 9.6	30.4	4.8	15.8	3.4	11.2
	9.6 - 10.0	21.7	5.1	23.5	2.4	11.3
	10.0 - 10.8	24.0	3.6	14.9	2.7	11.3
	10.8 - 11.6	20.8	3.4	16.5	1.2	5.9
	11.6 - 12.4	18.0	3.6	19.7	1.1	6.0
	12.4 - 13.2	16.5	4.0	24.5	1.1	6.5
	13.2 - 14.0	9.7	2.2	22.7	0.7	7.3
	14.0 - 14.8	12.4	3.5	27.9	1.0	8.4
	14.8 - 15.6	6.9	2.5	35.9	0.7	9.7
	15.6 - 16.4	3.2	2.6	80.2	0.4	11.1

θ [mrad]	p [GeV/c]	$\frac{d^2\sigma}{dpd\theta}(\pi^+)$ [mb/rad/(GeV/c)]	Δ_{stat} [mb/rad/(GeV/c)]	Δ_{stat} [%]	Δ_{syst} [mb/rad/(GeV/c)]	Δ_{syst} [%]
10 - 20	0.2 - 0.3	15.3	2.4	15.4	1.6	10.6
	0.3 - 0.4	17.4	1.9	11.2	1.4	8.1
	0.4 - 0.5	18.5	2.1	11.6	1.5	7.9
	0.5 - 0.6	32.1	2.9	8.9	2.4	7.6
	0.6 - 0.7	31.2	2.7	8.7	2.4	7.6
	0.7 - 0.8	27.1	2.6	9.6	2.1	7.7
	0.8 - 0.9	37.8	3.0	7.9	2.9	7.7
	0.9 - 1.0	36.9	2.9	7.8	2.8	7.6
	1.0 - 1.2	43.5	2.2	5.1	2.5	5.8
	1.2 - 1.6	45.6	2.2	4.9	2.4	5.3
	1.6 - 2.0	53.9	2.4	4.4	2.8	5.2
	2.0 - 2.4	58.5	2.5	4.2	3.0	5.2
	2.4 - 2.8	57.0	2.5	4.5	2.9	5.2
	2.8 - 3.2	61.4	2.8	4.6	3.1	5.1
	3.2 - 3.6	70.4	3.7	5.3	3.6	5.1
	3.6 - 4.0	75.6	3.8	5.0	3.9	5.2
	4.0 - 4.4	75.9	3.8	5.0	3.8	5.0
	4.4 - 4.8	70.5	3.8	5.3	3.5	5.0
	4.8 - 5.2	70.3	3.8	5.4	3.5	5.0
	5.2 - 5.6	79.3	4.4	5.5	3.9	5.0
	5.6 - 6.0	79.1	4.6	5.8	3.9	4.9
	6.0 - 6.4	78.3	4.6	5.9	4.0	5.1
	6.4 - 6.8	79.7	5.2	6.5	3.9	4.9
	6.8 - 7.2	78.5	5.1	6.5	3.8	4.9
	7.2 - 7.6	83.2	5.3	6.4	4.0	4.9
	7.6 - 8.0	70.4	5.2	7.3	3.5	5.0
	8.0 - 8.4	76.8	5.3	6.9	6.9	9.0
	8.4 - 8.8	69.9	5.0	7.2	6.4	9.2
	8.8 - 9.2	68.9	5.5	8.0	6.3	9.2
	9.2 - 9.6	54.5	4.5	8.2	5.0	9.2
	9.6 - 10.0	58.3	4.8	8.3	5.4	9.2
	10.0 - 10.8	58.5	3.4	5.9	5.4	9.2
	10.8 - 11.6	43.2	3.0	7.0	2.2	5.1
	11.6 - 12.4	44.4	3.0	6.8	2.2	5.0
	12.4 - 13.2	36.3	2.7	7.4	1.8	5.1
	13.2 - 14.0	29.6	2.3	7.9	1.6	5.3
	14.0 - 14.8	31.7	2.6	8.2	1.8	5.8
	14.8 - 15.6	24.7	2.1	8.6	1.6	6.4
	15.6 - 16.4	19.6	1.9	9.5	1.4	7.3
	16.4 - 17.2	14.7	1.8	12.0	1.2	8.2
	17.2 - 18.0	14.5	1.8	12.7	1.3	9.2
	18.0 - 18.8	7.0	1.6	22.8	0.7	10.2
	18.8 - 19.6	6.9	1.2	17.0	0.8	11.2
	19.6 - 20.4	7.6	1.4	18.4	0.9	12.3
	20.4 - 21.2	4.9	0.9	18.7	0.7	13.4
	21.2 - 22.0	3.3	1.6	48.8	0.5	14.6

θ [mrad]	p [GeV/c]	$\frac{d^2\sigma}{dpd\theta}(\pi^+)$ [mb/rad/(GeV/c)]	Δ_{stat} [mb/rad/(GeV/c)]	Δ_{stat} [%]	Δ_{syst} [mb/rad/(GeV/c)]	Δ_{syst} [%]
20 - 40	0.2 - 0.3	25.5	2.0	7.7	2.0	7.7
	0.3 - 0.4	32.6	2.0	6.1	2.0	6.3
	0.4 - 0.5	41.9	2.3	5.5	2.6	6.1
	0.5 - 0.6	50.1	2.4	4.8	3.1	6.2
	0.6 - 0.7	58.5	2.6	4.5	3.6	6.2
	0.7 - 0.8	60.0	2.6	4.4	3.6	6.1
	0.8 - 0.9	69.5	2.9	4.1	4.2	6.0
	0.9 - 1.0	77.6	2.9	3.7	4.8	6.2
	1.0 - 1.2	80.6	2.1	2.6	4.1	5.1
	1.2 - 1.6	96.1	2.2	2.2	4.6	4.8
	1.6 - 2.0	107.8	2.2	2.0	5.1	4.7
	2.0 - 2.4	113.9	2.4	2.1	5.1	4.5
	2.4 - 2.8	123.8	3.3	2.7	5.7	4.6
	2.8 - 3.2	127.0	3.3	2.6	5.8	4.5
	3.2 - 3.6	133.6	3.4	2.6	5.9	4.4
	3.6 - 4.0	142.4	3.5	2.5	6.3	4.4
	4.0 - 4.4	148.6	3.5	2.4	6.3	4.2
	4.4 - 4.8	143.9	3.5	2.4	6.1	4.3
	4.8 - 5.2	142.5	3.5	2.5	5.9	4.2
	5.2 - 5.6	143.0	3.5	2.5	5.9	4.1
	5.6 - 6.0	141.8	3.5	2.5	5.8	4.1
	6.0 - 6.4	135.1	3.4	2.5	5.5	4.1
	6.4 - 6.8	130.5	3.5	2.6	5.3	4.0
	6.8 - 7.2	126.8	3.4	2.7	5.1	4.0
	7.2 - 7.6	112.0	3.2	2.9	4.5	4.1
	7.6 - 8.0	105.6	3.2	3.0	4.3	4.0
	8.0 - 8.4	101.0	3.2	3.1	4.0	4.0
	8.4 - 8.8	87.4	2.9	3.3	3.5	4.0
	8.8 - 9.2	83.6	2.9	3.5	3.4	4.0
	9.2 - 9.6	80.8	2.9	3.6	3.3	4.1
	9.6 - 10.0	69.7	2.8	4.0	2.8	4.1
	10.0 - 10.8	59.5	1.8	2.9	2.4	4.1
	10.8 - 11.6	48.3	1.7	3.4	2.0	4.1
	11.6 - 12.4	42.3	1.6	3.7	1.5	3.5
	12.4 - 13.2	35.6	1.5	4.1	1.2	3.5
	13.2 - 14.0	28.1	1.3	4.7	1.0	3.6
	14.0 - 14.8	26.3	1.3	4.8	0.9	3.5
	14.8 - 15.6	19.3	1.1	5.6	0.7	3.6
	15.6 - 16.4	14.9	1.0	6.7	0.5	3.6
	16.4 - 17.2	11.3	0.9	7.7	0.4	3.7
	17.2 - 18.0	8.8	0.8	9.1	0.3	3.7
	18.0 - 18.8	7.1	0.7	9.9	0.3	3.9
	18.8 - 19.6	4.7	0.6	11.8	0.2	4.2
	19.6 - 20.4	4.4	0.6	13.3	0.2	4.8
	20.4 - 21.2	2.7	0.5	18.5	0.1	5.5
	21.2 - 22.0	1.8	0.4	20.5	0.1	6.2

θ [mrad]	p [GeV/c]	$\frac{d^2\sigma}{dpd\theta}(\pi^+)$ [mb/rad/(GeV/c)]	Δ_{stat} [mb/rad/(GeV/c)]	Δ_{stat} [%]	Δ_{syst} [mb/rad/(GeV/c)]	Δ_{syst} [%]
40 - 60	0.2 - 0.3	39.9	2.2	5.4	3.2	8.1
	0.3 - 0.4	51.3	2.6	5.0	3.4	6.7
	0.4 - 0.5	70.3	3.2	4.6	4.6	6.6
	0.5 - 0.6	77.6	2.9	3.8	5.1	6.5
	0.6 - 0.7	95.0	3.2	3.4	6.2	6.6
	0.7 - 0.8	107.3	3.5	3.3	6.8	6.3
	0.8 - 0.9	121.5	3.7	3.0	7.6	6.3
	0.9 - 1.0	138.1	3.9	2.8	8.7	6.3
	1.0 - 1.2	161.9	5.6	3.4	6.8	4.2
	1.2 - 1.4	159.8	7.1	4.4	5.9	3.7
	1.4 - 1.6	176.8	7.8	4.4	7.0	3.9
	1.6 - 1.8	177.0	7.5	4.2	6.4	3.6
	1.8 - 2.0	190.1	7.8	4.1	6.5	3.4
	2.0 - 2.2	208.4	7.8	3.8	7.1	3.4
	2.2 - 2.4	229.8	8.3	3.6	8.4	3.7
	2.4 - 2.6	207.2	7.8	3.8	7.5	3.6
	2.6 - 2.8	219.9	8.1	3.7	7.6	3.5
	2.8 - 3.0	218.7	8.1	3.7	7.1	3.2
	3.0 - 3.2	227.4	8.1	3.6	7.3	3.2
	3.2 - 3.4	232.9	8.3	3.6	7.6	3.2
	3.4 - 3.6	235.4	8.3	3.5	6.8	2.9
	3.6 - 3.8	224.1	8.2	3.6	6.6	3.0
	3.8 - 4.0	224.8	8.1	3.6	6.5	2.9
	4.0 - 4.2	211.8	7.8	3.7	6.3	3.0
	4.2 - 4.4	196.4	7.3	3.7	5.5	2.8
	4.4 - 4.6	204.3	7.7	3.8	5.8	2.8
	4.6 - 4.8	202.9	7.8	3.9	5.5	2.7
	4.8 - 5.0	194.7	7.8	4.0	5.0	2.6
	5.0 - 5.2	189.1	7.4	3.9	5.2	2.8
	5.2 - 5.6	169.9	5.0	2.9	4.6	2.7
	5.6 - 6.0	156.6	4.9	3.1	4.2	2.7
	6.0 - 6.4	143.4	4.5	3.1	3.7	2.6
	6.4 - 6.8	125.4	4.3	3.4	3.3	2.6
	6.8 - 7.2	121.2	4.2	3.5	3.1	2.6
	7.2 - 7.6	108.0	3.6	3.3	2.8	2.6
	7.6 - 8.0	104.2	3.4	3.3	2.7	2.6
	8.0 - 8.4	82.7	2.9	3.6	2.2	2.6
	8.4 - 8.8	81.0	2.9	3.6	2.2	2.7
	8.8 - 9.2	71.1	2.7	3.7	1.9	2.7
	9.2 - 9.6	66.6	2.6	3.8	1.8	2.6
	9.6 - 10.0	53.8	2.2	4.2	1.4	2.7
	10.0 - 10.8	47.5	1.5	3.1	1.3	2.7
	10.8 - 11.6	36.3	1.2	3.4	1.0	2.7
	11.6 - 12.4	30.9	1.2	3.8	0.9	2.8
	12.4 - 13.2	23.5	1.0	4.3	0.7	2.8
	13.2 - 14.0	17.4	1.0	5.5	0.5	2.9
	14.0 - 14.8	13.2	0.8	6.0	0.4	2.8
	14.8 - 15.6	8.0	0.6	7.3	0.2	2.9
	15.6 - 16.4	7.6	0.6	7.6	0.2	3.0
	16.4 - 17.2	5.1	0.5	9.1	0.2	3.0
	17.2 - 18.0	3.3	0.4	11.8	0.1	2.9
	18.0 - 18.8	2.2	0.3	14.1	0.1	3.0
	18.8 - 19.6	1.8	0.3	19.3	0.1	3.2
	19.6 - 20.4	1.2	0.3	20.8	0.04	3.1

θ [mrad]	p [GeV/c]	$\frac{d^2\sigma}{dpd\theta}(\pi^+)$ [mb/rad/(GeV/c)]	Δ_{stat} [mb/rad/(GeV/c)]	Δ_{stat} [%]	Δ_{syst} [mb/rad/(GeV/c)]	Δ_{syst} [%]
60 - 100	0.2 - 0.3	57.2	1.9	3.3	3.6	6.3
	0.3 - 0.4	80.3	2.5	3.1	4.2	5.2
	0.4 - 0.5	107.6	3.3	3.1	5.5	5.1
	0.5 - 0.6	128.8	3.2	2.5	6.3	4.9
	0.6 - 0.7	153.8	3.3	2.2	7.4	4.8
	0.7 - 0.8	172.8	3.5	2.0	8.1	4.7
	0.8 - 0.9	182.7	3.6	2.0	8.5	4.7
	0.9 - 1.0	207.7	3.9	1.9	9.8	4.7
	1.0 - 1.2	254.1	6.5	2.6	10.4	4.1
	1.2 - 1.4	249.5	6.2	2.5	9.3	3.7
	1.4 - 1.6	267.7	8.0	3.0	10.0	3.7
	1.6 - 1.8	280.6	7.8	2.8	9.7	3.5
	1.8 - 2.0	273.7	7.5	2.7	9.9	3.6
	2.0 - 2.2	300.4	8.2	2.7	9.8	3.3
	2.2 - 2.4	289.0	7.9	2.7	9.4	3.3
	2.4 - 2.6	286.6	7.7	2.7	9.4	3.3
	2.6 - 2.8	283.3	7.6	2.7	8.7	3.1
	2.8 - 3.0	268.6	7.4	2.8	8.4	3.1
	3.0 - 3.2	264.8	6.8	2.6	8.0	3.0
	3.2 - 3.4	267.3	6.7	2.5	7.7	2.9
	3.4 - 3.6	251.8	6.3	2.5	7.3	2.9
	3.6 - 3.8	233.2	5.9	2.5	6.6	2.8
	3.8 - 4.0	231.4	5.7	2.5	6.6	2.8
	4.0 - 4.2	226.8	5.6	2.4	6.4	2.8
	4.2 - 4.4	213.1	5.3	2.5	6.0	2.8
	4.4 - 4.6	202.8	5.1	2.5	5.6	2.8
	4.6 - 4.8	181.2	4.7	2.6	5.0	2.8
	4.8 - 5.0	165.4	4.4	2.7	4.6	2.8
	5.0 - 5.2	154.4	4.3	2.8	4.3	2.8
	5.2 - 5.6	140.0	2.8	2.0	3.9	2.8
	5.6 - 6.0	126.5	2.6	2.1	3.4	2.7
	6.0 - 6.4	106.6	2.4	2.2	2.9	2.7
	6.4 - 6.8	93.5	2.2	2.4	2.6	2.7
	6.8 - 7.2	78.6	2.1	2.6	2.1	2.6
	7.2 - 7.6	67.1	1.9	2.8	1.8	2.7
	7.6 - 8.0	60.2	1.9	3.1	1.6	2.6
	8.0 - 8.4	52.1	1.7	3.3	1.3	2.5
	8.4 - 8.8	42.0	1.5	3.5	1.1	2.6
	8.8 - 9.2	36.7	1.4	3.9	1.0	2.6
	9.2 - 9.6	32.6	1.4	4.2	0.9	2.7
	9.6 - 10.0	27.2	1.3	4.7	0.7	2.6
	10.0 - 10.8	19.6	0.8	3.8	0.5	2.6
	10.8 - 11.6	14.4	0.6	4.4	0.4	2.6
	11.6 - 12.4	9.0	0.5	5.4	0.2	2.6
	12.4 - 13.2	7.1	0.5	6.6	0.2	2.8
	13.2 - 14.0	4.6	0.4	7.9	0.1	2.7
	14.0 - 14.8	3.1	0.3	10.4	0.1	2.8
	14.8 - 15.6	1.6	0.2	14.0	0.05	2.9
	15.6 - 16.4	1.0	0.2	17.3	0.03	2.9
	16.4 - 17.2	0.8	0.2	20.2	0.02	2.8
	17.2 - 18.0	0.4	0.1	30.0	0.01	3.0

θ [mrad]			p [GeV/c]			$\frac{d^2\sigma}{dpd\theta}(\pi^+)$ [mb/rad/(GeV/c)]	Δ_{stat} [mb/rad/(GeV/c)]	Δ_{stat} [%]	Δ_{syst} [mb/rad/(GeV/c)]	Δ_{syst} [%]
100	-	140	0.2	-	0.3	76.5	2.9	3.8	4.9	6.5
			0.3	-	0.4	118.4	3.9	3.3	6.5	5.5
			0.4	-	0.5	158.5	4.5	2.8	8.5	5.4
			0.5	-	0.6	183.3	4.0	2.2	9.4	5.1
			0.6	-	0.7	217.2	4.4	2.0	10.7	4.9
			0.7	-	0.8	238.1	4.4	1.9	11.5	4.8
			0.8	-	0.9	267.8	4.7	1.8	13.0	4.8
			0.9	-	1.0	292.6	4.9	1.7	14.8	5.1
			1.0	-	1.2	318.6	13.2	4.1	13.1	4.1
			1.2	-	1.4	354.2	10.5	3.0	13.2	3.7
			1.4	-	1.6	359.0	10.7	3.0	13.4	3.7
			1.6	-	1.8	334.2	10.3	3.1	11.7	3.5
			1.8	-	2.0	346.2	10.0	2.9	12.0	3.5
			2.0	-	2.2	332.6	8.9	2.7	10.5	3.2
			2.2	-	2.4	328.6	8.2	2.5	10.8	3.3
			2.4	-	2.6	284.2	7.0	2.5	8.7	3.1
			2.6	-	2.8	275.7	6.8	2.5	8.9	3.2
			2.8	-	3.0	259.4	6.5	2.5	7.3	2.8
			3.0	-	3.2	226.3	6.1	2.7	6.8	3.0
			3.2	-	3.4	218.6	5.9	2.7	6.3	2.9
			3.4	-	3.6	186.4	5.5	2.9	5.5	3.0
			3.6	-	3.8	167.8	5.1	3.0	4.7	2.8
			3.8	-	4.0	164.1	5.2	3.2	4.7	2.8
			4.0	-	4.2	144.0	4.8	3.3	4.2	2.9
			4.2	-	4.4	137.7	4.8	3.5	3.8	2.8
			4.4	-	4.6	118.4	4.3	3.6	3.3	2.8
			4.6	-	4.8	105.2	4.1	3.9	2.8	2.6
			4.8	-	5.0	87.2	3.6	4.2	2.4	2.7
			5.0	-	5.2	93.3	4.1	4.4	2.5	2.6
			5.2	-	5.6	77.3	2.6	3.4	2.0	2.6
			5.6	-	6.0	57.6	2.1	3.7	1.5	2.7
			6.0	-	6.4	45.9	1.9	4.2	1.2	2.6
			6.4	-	6.8	36.3	1.7	4.8	1.0	2.8
			6.8	-	7.2	30.6	1.6	5.3	0.8	2.5
			7.2	-	7.6	25.0	1.5	6.0	0.6	2.6
			7.6	-	8.0	17.9	1.2	6.8	0.5	2.7
			8.0	-	8.4	14.1	1.0	7.4	0.4	2.6
			8.4	-	8.8	12.9	1.1	8.4	0.3	2.5
			8.8	-	9.2	9.1	0.9	10.0	0.2	2.4
			9.2	-	9.6	5.9	0.7	11.4	0.1	2.5
			9.6	-	10.0	4.7	0.6	13.6	0.1	2.4
			10.0	-	10.8	3.3	0.4	11.3	0.1	2.6
			10.8	-	11.6	2.2	0.3	13.4	0.1	2.5
			11.6	-	12.4	0.7	0.1	22.3	0.02	2.8
			12.4	-	13.2	0.4	0.1	27.6	0.01	2.5
			13.2	-	14.0	0.2	0.1	54.9	0.01	4.5

θ [mrad]			p [GeV/c]			$\frac{d^2\sigma}{dpd\theta}(\pi^+)$ [mb/rad/(GeV/c)]	Δ_{stat} [mb/rad/(GeV/c)]	Δ_{stat} [%]	Δ_{syst} [mb/rad/(GeV/c)]	Δ_{syst} [%]
140	-	180	0.2	-	0.3	105.0	4.2	4.0	6.3	6.0
			0.3	-	0.4	146.5	4.7	3.2	7.5	5.1
			0.4	-	0.5	190.9	4.2	2.2	9.4	4.9
			0.5	-	0.6	240.2	4.5	1.9	12.0	5.0
			0.6	-	0.7	270.5	4.8	1.8	12.7	4.7
			0.7	-	0.8	311.2	5.1	1.6	14.9	4.8
			0.8	-	0.9	319.7	5.0	1.6	14.8	4.6
			0.9	-	1.0	345.5	5.2	1.5	15.6	4.5
			1.0	-	1.2	340.6	23.7	6.9	16.5	4.8
			1.2	-	1.4	362.3	50.7	14.0	19.2	5.3
			1.4	-	1.6	402.1	19.2	4.8	31.0	7.7
			1.6	-	1.8	365.1	12.2	3.3	27.6	7.5
			1.8	-	2.0	305.4	9.5	3.1	15.4	5.0
			2.0	-	2.2	308.1	9.4	3.0	9.7	3.2
			2.2	-	2.4	259.9	8.4	3.2	7.7	2.9
			2.4	-	2.6	219.8	7.7	3.5	6.6	3.0
			2.6	-	2.8	216.5	8.1	3.8	6.6	3.0
			2.8	-	3.0	172.6	6.9	4.0	5.2	3.0
			3.0	-	3.2	156.1	6.6	4.2	5.0	3.2
			3.2	-	3.4	133.9	6.0	4.5	3.9	2.9
			3.4	-	3.6	124.7	5.8	4.6	3.5	2.8
			3.6	-	3.8	98.3	5.1	5.2	2.9	2.9
			3.8	-	4.0	100.3	5.3	5.3	2.9	2.9
			4.0	-	4.2	81.5	4.7	5.8	2.3	2.8
			4.2	-	4.4	74.3	4.5	6.1	2.2	3.0
			4.4	-	4.6	59.1	4.0	6.8	1.6	2.7
			4.6	-	4.8	50.1	3.8	7.5	1.6	3.3
			4.8	-	5.0	41.8	3.4	8.1	1.0	2.3
			5.0	-	5.2	43.9	3.6	8.2	1.2	2.7
			5.2	-	5.6	30.3	2.0	6.7	0.9	2.9
			5.6	-	6.0	20.9	1.7	8.2	0.6	3.0
			6.0	-	6.4	14.9	1.3	9.1	0.4	2.9
			6.4	-	6.8	12.5	1.3	10.5	0.3	2.7
			6.8	-	7.2	9.9	1.3	13.2	0.2	2.5
			7.2	-	7.6	6.4	0.9	14.4	0.2	3.0
			7.6	-	8.0	4.3	0.7	16.2	0.1	2.6
			8.0	-	8.4	4.2	0.8	19.5	0.2	3.6
			8.4	-	8.8	2.3	0.6	28.1	0.1	2.8
			8.8	-	9.2	2.3	0.6	25.4	0.1	2.5
			9.2	-	9.6	0.9	0.4	40.4	0.02	2.7
			9.6	-	10.0	0.7	0.3	36.4	0.02	2.7
			10.0	-	10.8	0.2	0.2	65.9	0.01	2.4

θ [mrad]	p [GeV/c]	$\frac{d^2\sigma}{dpd\theta}(\pi^+)$ [mb/rad/(GeV/c)]	Δ_{stat} [mb/rad/(GeV/c)]	Δ_{stat} [%]	Δ_{syst} [mb/rad/(GeV/c)]	Δ_{syst} [%]
180 - 240	0.2 - 0.3	133.0	3.2	2.4	7.6	5.7
	0.3 - 0.4	183.3	3.4	1.9	9.5	5.2
	0.4 - 0.5	243.5	3.7	1.5	12.5	5.1
	0.5 - 0.6	284.7	4.0	1.4	14.2	5.0
	0.6 - 0.7	327.3	4.3	1.3	16.3	5.0
	0.7 - 0.8	340.7	4.3	1.3	16.3	4.8
	0.8 - 0.9	374.5	4.6	1.2	18.1	4.8
	0.9 - 1.0	368.3	4.6	1.3	22.3	6.1
	1.0 - 1.2	395.9	18.9	4.8	18.1	4.6
	1.2 - 1.4	366.8	13.7	3.7	14.4	3.9
	1.4 - 1.6	310.0	12.0	3.9	11.3	3.6
	1.6 - 1.8	271.0	11.2	4.1	9.1	3.4
	1.8 - 2.0	256.4	10.7	4.2	8.3	3.3
	2.0 - 2.2	196.9	9.0	4.5	5.8	2.9
	2.2 - 2.4	181.8	8.1	4.5	6.7	3.7
	2.4 - 2.6	145.3	6.8	4.7	4.4	3.0
	2.6 - 2.8	119.0	5.8	4.9	3.5	3.0
	2.8 - 3.0	104.2	5.5	5.3	3.4	3.3
	3.0 - 3.2	84.6	4.8	5.6	2.7	3.2
	3.2 - 3.4	71.6	4.4	6.1	2.7	3.8
	3.4 - 3.6	66.4	4.3	6.4	1.8	2.8
	3.6 - 3.8	47.6	3.5	7.4	1.7	3.5
	3.8 - 4.0	43.4	3.4	7.8	1.7	3.9
	4.0 - 4.2	29.2	2.6	8.8	1.1	3.8
	4.2 - 4.4	30.0	2.8	9.2	0.9	3.0
	4.4 - 4.6	26.4	2.7	10.0	0.9	3.3
	4.6 - 4.8	20.8	2.3	10.8	0.5	2.6
	4.8 - 5.0	18.5	2.3	12.6	0.4	2.4
	5.0 - 5.2	14.4	1.9	13.2	0.5	3.7
	5.2 - 5.6	12.0	1.3	10.9	0.3	2.8
	5.6 - 6.0	6.0	0.8	13.9	0.2	2.6
	6.0 - 6.4	4.7	0.7	15.3	0.1	2.4
	6.4 - 6.8	2.4	0.5	19.2	0.1	2.4
	6.8 - 7.2	0.8	0.2	30.6	0.02	2.3
	7.2 - 7.6	1.7	0.5	26.9	0.05	2.9
	7.6 - 8.0	1.3	0.5	38.5	0.04	2.8
240 - 300	0.2 - 0.3	146.4	3.5	2.4	8.6	5.8
	0.3 - 0.4	226.0	4.1	1.8	12.4	5.5
	0.4 - 0.5	284.4	4.5	1.6	15.4	5.4
	0.5 - 0.6	323.6	4.7	1.5	17.1	5.3
	0.6 - 0.7	343.8	4.9	1.4	17.9	5.2
	0.7 - 0.8	353.3	5.0	1.4	18.2	5.2
	0.8 - 0.9	352.7	5.0	1.4	18.0	5.1
	0.9 - 1.0	357.2	5.1	1.4	18.6	5.2
	1.0 - 1.2	351.9	13.3	3.8	13.4	3.8
	1.2 - 1.4	283.2	11.7	4.1	10.1	3.6
	1.4 - 1.6	229.7	10.1	4.4	7.3	3.2
	1.6 - 1.8	211.2	10.1	4.8	7.7	3.7
	1.8 - 2.0	162.9	8.5	5.2	5.9	3.6
	2.0 - 2.2	132.8	7.8	5.9	5.0	3.7
	2.2 - 2.4	118.2	7.7	6.5	3.9	3.3
	2.4 - 2.6	81.0	6.1	7.6	3.0	3.7
	2.6 - 2.8	60.9	5.1	8.3	2.3	3.8
	2.8 - 3.0	68.2	6.2	9.1	2.6	3.9
	3.0 - 3.2	40.2	4.5	11.3	1.5	3.8
	3.2 - 3.4	29.3	3.5	12.0	1.1	3.7
	3.4 - 3.6	26.1	3.4	12.9	1.1	4.4
	3.6 - 3.8	14.8	2.5	16.9	0.8	5.1
	3.8 - 4.0	14.5	2.6	18.2	0.7	4.9
	4.0 - 4.2	9.9	2.1	21.1	0.6	6.0
	4.2 - 4.4	9.8	2.5	25.6	0.3	2.7
	4.4 - 4.6	8.3	2.0	24.3	0.2	2.1
	4.6 - 4.8	3.3	1.1	33.2	0.1	3.3
	4.8 - 5.0	3.0	1.2	38.7	0.1	3.4

θ [mrad]	p [GeV/c]	$\frac{d^2\sigma}{dpd\theta}(\pi^+)$ [mb/rad/(GeV/c)]	Δ_{stat} [mb/rad/(GeV/c)]	Δ_{stat} [%]	Δ_{syst} [mb/rad/(GeV/c)]	Δ_{syst} [%]
300 - 360	0.2 - 0.3	192.7	6.2	3.2	10.5	5.4
	0.3 - 0.4	267.9	7.1	2.6	13.5	5.0
	0.4 - 0.5	274.7	5.0	1.8	13.8	5.0
	0.5 - 0.6	319.1	5.4	1.7	15.4	4.8
	0.6 - 0.7	334.3	5.5	1.7	16.0	4.8
	0.7 - 0.8	340.2	5.6	1.7	16.3	4.8
	0.8 - 0.9	323.5	5.5	1.7	18.1	5.6
	0.9 - 1.0	303.9	5.4	1.8	18.6	6.1
	1.0 - 1.2	259.8	12.8	4.9	9.8	3.8
	1.2 - 1.4	249.0	13.5	5.4	8.6	3.5
	1.4 - 1.6	186.2	12.3	6.6	5.9	3.2
	1.6 - 1.8	149.2	12.5	8.4	5.0	3.4
	1.8 - 2.0	102.3	10.4	10.2	3.8	3.7
	2.0 - 2.2	76.7	9.8	12.8	3.2	4.2
	2.2 - 2.4	55.6	9.7	17.5	2.0	3.6
	2.4 - 2.6	39.2	8.2	21.1	1.6	4.0
	2.6 - 2.8	29.4	8.2	28.0	1.4	4.9
	2.8 - 3.0	23.0	8.9	38.8	2.0	8.8
360 - 420	0.2 - 0.3	190.5	6.5	3.4	11.1	5.8
	0.3 - 0.4	250.0	7.2	2.9	14.0	5.6
	0.4 - 0.5	303.2	8.0	2.6	16.6	5.5
	0.5 - 0.6	305.5	8.0	2.6	16.3	5.3
	0.6 - 0.7	305.0	8.1	2.7	15.9	5.2
	0.7 - 0.8	311.3	8.4	2.7	15.7	5.1
	0.8 - 0.9	283.4	8.2	2.9	14.2	5.0
	0.9 - 1.0	244.7	7.5	3.1	11.9	4.9

Table 4: The NA61/SHINE results on the π^+ double differential cross section, $d^2\sigma_{\pi^+}/(dpd\theta)$, in the laboratory system for p+C interactions at 31 GeV/c. The results are presented as a function of momentum in different angular intervals. The statistical Δ_{stat} and systematic Δ_{syst} errors are quoted.

θ [mrad]	p [GeV/c]	$\frac{d^2\sigma}{dpd\theta}(\pi^-)$ [mb/rad/(GeV/c)]	Δ_{stat} [mb/rad/(GeV/c)]	Δ_{stat} [%]	Δ_{syst} [mb/rad/(GeV/c)]	Δ_{syst} [%]
0 - 10	0.3 - 0.4	5.0	0.8	16.4	0.4	7.8
	0.4 - 0.5	6.6	1.0	15.5	0.6	8.7
	0.5 - 0.6	9.3	1.3	14.1	0.7	7.3
	0.6 - 0.7	8.0	1.1	14.1	0.6	7.9
	0.7 - 0.8	8.7	1.0	11.8	0.7	8.6
	0.8 - 0.9	10.2	1.2	11.7	0.9	8.4
	0.9 - 1.0	10.8	1.2	11.6	0.9	8.1
	1.0 - 1.2	11.3	0.9	7.8	0.9	8.4
	1.2 - 1.4	13.1	1.0	7.6	1.0	7.8
	1.4 - 1.6	15.7	1.1	6.9	1.2	7.7
	1.6 - 1.8	15.2	1.0	6.8	1.0	6.9
	1.8 - 2.0	16.1	1.1	6.7	1.0	6.3
	2.0 - 2.2	14.9	1.0	6.7	1.0	6.8
	2.2 - 2.4	17.8	1.1	6.2	1.1	6.3
	2.4 - 2.6	20.7	1.3	6.1	1.2	6.0
	2.6 - 2.8	18.6	1.2	6.2	1.1	5.7
	2.8 - 3.2	18.9	0.8	4.3	1.2	6.2
	3.2 - 3.6	15.9	0.9	5.9	0.9	5.8
	3.6 - 4.0	19.3	0.8	4.3	1.1	5.5
	4.0 - 4.4	18.8	0.8	4.4	1.0	5.6
	4.4 - 4.8	17.5	0.8	4.5	0.9	5.4
	4.8 - 5.2	18.7	0.8	4.5	1.0	5.6
	5.2 - 5.6	17.4	0.8	4.7	0.9	5.4
	5.6 - 6.0	15.9	0.8	4.9	0.9	5.7
	6.0 - 6.4	18.1	0.9	4.7	1.0	5.6
	6.4 - 6.8	17.6	0.8	4.7	1.1	6.3
	6.8 - 7.2	17.6	0.8	4.7	1.1	6.4
	7.2 - 7.6	15.5	0.8	5.1	1.0	6.3
	7.6 - 8.0	13.2	0.7	5.5	0.8	6.2
	8.0 - 8.4	13.2	0.8	5.9	0.8	6.3
	8.4 - 8.8	13.0	0.8	6.1	0.8	6.4
	8.8 - 9.2	12.8	0.8	6.2	0.8	6.1
	9.2 - 9.6	11.0	0.8	7.2	0.7	6.2
	9.6 - 10.0	10.9	0.9	8.1	0.7	6.1
	10.0 - 10.8	11.4	0.6	5.7	0.7	5.8
	10.8 - 11.6	9.3	0.6	6.5	0.5	5.9
	11.6 - 12.4	9.7	0.7	7.0	0.6	5.7
	12.4 - 13.2	7.7	0.6	8.4	0.4	5.9
	13.2 - 14.0	6.0	0.6	10.6	0.4	5.9
	14.0 - 14.8	5.7	0.7	11.6	0.4	6.9
	14.8 - 15.6	4.4	0.6	14.4	0.3	7.1
	15.6 - 16.4	4.6	0.8	16.6	0.3	7.0

θ [mrad]	p [GeV/c]	$\frac{d^2\sigma}{dpd\theta}(\pi^-)$ [mb/rad/(GeV/c)]	Δ_{stat} [mb/rad/(GeV/c)]	Δ_{stat} [%]	Δ_{syst} [mb/rad/(GeV/c)]	Δ_{syst} [%]
10 - 20	0.2 - 0.3	9.1	1.2	13.4	0.7	7.8
	0.3 - 0.4	17.0	2.2	12.9	1.2	6.8
	0.4 - 0.5	17.2	1.7	10.0	1.2	7.1
	0.5 - 0.6	21.4	1.7	8.1	1.4	6.4
	0.6 - 0.7	25.0	1.9	7.4	2.0	7.8
	0.7 - 0.8	26.5	1.9	7.0	2.1	7.9
	0.8 - 0.9	31.4	2.1	6.6	2.5	8.0
	0.9 - 1.0	33.7	2.1	6.2	2.5	7.3
	1.0 - 1.2	34.1	1.5	4.4	2.5	7.3
	1.2 - 1.4	37.5	1.6	4.1	2.6	6.9
	1.4 - 1.6	41.8	1.6	3.9	2.8	6.7
	1.6 - 1.8	46.7	1.8	3.8	2.9	6.3
	1.8 - 2.0	47.3	1.8	3.7	2.9	6.1
	2.0 - 2.2	46.5	2.0	4.4	2.5	5.4
	2.2 - 2.4	45.5	2.1	4.5	2.5	5.6
	2.4 - 2.6	54.0	1.9	3.6	2.8	5.3
	2.6 - 2.8	57.4	2.0	3.4	3.0	5.2
	2.8 - 3.2	49.4	1.5	3.0	2.5	5.0
	3.2 - 3.6	48.9	1.5	3.0	2.4	4.9
	3.6 - 4.0	49.9	1.6	3.2	2.3	4.5
	4.0 - 4.4	52.8	1.7	3.2	2.3	4.3
	4.4 - 4.8	49.5	1.8	3.6	2.2	4.4
	4.8 - 5.2	50.2	1.9	3.7	2.2	4.3
	5.2 - 5.6	44.5	1.7	3.9	1.8	4.2
	5.6 - 6.0	45.1	1.8	3.9	1.8	4.1
	6.0 - 6.4	40.4	1.6	4.1	1.6	4.0
	6.4 - 6.8	40.6	1.7	4.1	1.6	3.9
	6.8 - 7.2	41.6	1.8	4.2	1.6	3.7
	7.2 - 7.6	36.7	1.6	4.4	1.4	3.8
	7.6 - 8.0	33.9	1.6	4.6	1.3	3.8
	8.0 - 8.4	36.2	1.6	4.5	1.4	3.9
	8.4 - 8.8	33.1	1.6	4.7	1.2	3.7
	8.8 - 9.2	30.1	1.5	5.0	1.1	3.8
	9.2 - 9.6	26.0	1.4	5.2	1.0	3.7
	9.6 - 10.0	25.4	1.4	5.3	1.0	3.7
	10.0 - 10.8	24.2	1.0	3.9	0.9	3.7
	10.8 - 11.6	19.7	0.8	4.3	0.8	3.9
	11.6 - 12.4	18.1	0.8	4.7	0.7	3.9
	12.4 - 13.2	14.3	0.8	5.3	0.5	3.7
	13.2 - 14.0	13.3	0.8	5.9	0.5	3.8
	14.0 - 14.8	10.4	0.7	6.5	0.4	4.1
	14.8 - 15.6	8.8	0.7	7.4	0.3	3.9
	15.6 - 16.4	8.6	0.7	7.9	0.3	3.9
	16.4 - 17.2	7.4	0.6	8.4	0.3	3.9
	17.2 - 18.0	5.5	0.6	10.1	0.2	4.0
	18.0 - 18.8	3.7	0.5	12.2	0.1	4.0
	18.8 - 19.6	3.7	0.5	12.9	0.2	5.3
	19.6 - 20.4	1.9	0.3	16.3	0.1	5.3
	20.4 - 21.2	1.7	0.3	17.6	0.1	5.6

θ [mrad]	p [GeV/c]	$\frac{d^2\sigma}{dpd\theta}(\pi^-)$ [mb/rad/(GeV/c)]	Δ_{stat} [mb/rad/(GeV/c)]	Δ_{stat} [%]	Δ_{syst} [mb/rad/(GeV/c)]	Δ_{syst} [%]
20 - 40	0.2 - 0.3	15.9	1.1	7.2	1.2	7.3
	0.3 - 0.4	23.2	1.7	7.3	1.6	7.0
	0.4 - 0.5	34.8	1.8	5.1	2.5	7.2
	0.5 - 0.6	43.8	1.8	4.1	3.3	7.5
	0.6 - 0.7	54.3	2.0	3.6	4.0	7.4
	0.7 - 0.8	54.2	1.9	3.4	4.0	7.3
	0.8 - 0.9	59.7	2.0	3.4	4.6	7.7
	0.9 - 1.0	59.4	2.0	3.3	4.6	7.8
	1.0 - 1.2	64.9	1.6	2.5	4.8	7.4
	1.2 - 1.4	72.4	1.7	2.4	5.0	6.9
	1.4 - 1.6	77.1	1.8	2.3	5.3	6.9
	1.6 - 1.8	83.5	1.8	2.2	5.5	6.6
	1.8 - 2.0	88.3	1.8	2.1	5.4	6.1
	2.0 - 2.2	88.6	1.9	2.1	5.3	6.0
	2.2 - 2.4	91.4	1.9	2.1	5.3	5.8
	2.4 - 2.6	94.5	2.0	2.1	5.2	5.5
	2.6 - 2.8	98.7	2.2	2.2	5.3	5.3
	2.8 - 3.2	97.9	1.7	1.7	5.1	5.2
	3.2 - 3.6	95.1	1.9	2.0	4.8	5.1
	3.6 - 4.0	92.4	1.9	2.1	4.3	4.7
	4.0 - 4.4	91.6	1.9	2.1	4.0	4.4
	4.4 - 4.8	89.3	1.9	2.1	4.0	4.5
	4.8 - 5.2	85.4	1.9	2.2	3.6	4.2
	5.2 - 5.6	76.4	1.8	2.3	3.2	4.2
	5.6 - 6.0	74.3	1.7	2.3	3.0	4.1
	6.0 - 6.4	74.1	1.7	2.2	3.0	4.0
	6.4 - 6.8	66.8	1.6	2.3	2.7	4.0
	6.8 - 7.2	64.3	1.5	2.4	2.5	3.8
	7.2 - 7.6	58.5	1.5	2.5	2.3	3.9
	7.6 - 8.0	53.0	1.4	2.6	2.0	3.8
	8.0 - 8.4	48.4	1.3	2.8	1.8	3.8
	8.4 - 8.8	45.4	1.3	2.9	1.7	3.7
	8.8 - 9.2	42.9	1.3	3.0	1.6	3.8
	9.2 - 9.6	36.1	1.2	3.2	1.3	3.7
	9.6 - 10.0	37.1	1.2	3.2	1.4	3.7
	10.0 - 10.8	30.0	0.7	2.5	1.1	3.6
	10.8 - 11.6	22.6	0.6	2.9	0.8	3.6
	11.6 - 12.4	19.5	0.6	3.1	0.7	3.6
	12.4 - 13.2	15.6	0.6	3.5	0.5	3.5
	13.2 - 14.0	12.5	0.5	4.0	0.4	3.5
	14.0 - 14.8	9.6	0.4	4.6	0.3	3.6
	14.8 - 15.6	8.1	0.4	5.1	0.3	3.4
	15.6 - 16.4	6.4	0.4	5.8	0.2	3.4
	16.4 - 17.2	4.5	0.3	7.0	0.2	3.4
	17.2 - 18.0	3.2	0.3	8.2	0.1	3.8
	18.0 - 18.8	3.0	0.3	8.5	0.1	3.4
	18.8 - 19.6	2.4	0.2	10.1	0.1	3.5
	19.6 - 20.4	1.0	0.1	14.8	0.03	3.4
	20.4 - 21.2	0.9	0.1	14.5	0.04	3.8

θ [mrad]	p [GeV/c]	$\frac{d^2\sigma}{dpd\theta}(\pi^-)$ [mb/rad/(GeV/c)]	Δ_{stat} [mb/rad/(GeV/c)]	Δ_{stat} [%]	Δ_{syst} [mb/rad/(GeV/c)]	Δ_{syst} [%]
40 - 60	0.2 - 0.3	29.0	2.3	8.0	2.4	8.3
	0.3 - 0.4	43.9	2.8	6.4	3.0	6.8
	0.4 - 0.5	61.9	2.8	4.6	4.1	6.6
	0.5 - 0.6	74.3	2.8	3.7	5.3	7.1
	0.6 - 0.7	92.1	3.0	3.3	6.6	7.2
	0.7 - 0.8	96.8	3.0	3.1	6.9	7.1
	0.8 - 0.9	92.7	2.9	3.1	6.4	6.9
	0.9 - 1.0	106.2	3.0	2.9	7.7	7.2
	1.0 - 1.2	114.1	2.4	2.1	7.8	6.8
	1.2 - 1.4	118.2	2.4	2.0	7.8	6.6
	1.4 - 1.6	134.0	2.5	1.9	8.9	6.7
	1.6 - 1.8	135.2	2.5	1.9	9.5	7.1
	1.8 - 2.0	142.6	2.6	1.9	9.9	7.0
	2.0 - 2.2	151.0	2.8	1.8	10.3	6.8
	2.2 - 2.4	148.3	2.7	1.8	9.6	6.5
	2.4 - 2.6	150.8	2.8	1.8	7.6	5.0
	2.6 - 2.8	146.0	2.8	1.9	7.4	5.1
	2.8 - 3.0	152.4	3.8	2.5	7.4	4.8
	3.0 - 3.2	145.2	2.9	2.0	6.9	4.7
	3.2 - 3.4	149.2	2.9	1.9	6.8	4.5
	3.4 - 3.6	144.4	3.1	2.2	6.3	4.4
	3.6 - 3.8	140.4	3.0	2.1	6.1	4.3
	3.8 - 4.0	138.4	3.0	2.2	5.8	4.2
	4.0 - 4.2	136.6	3.2	2.3	5.6	4.1
	4.2 - 4.4	138.6	3.1	2.2	5.5	4.0
	4.4 - 4.6	126.1	2.9	2.3	4.9	3.9
	4.6 - 4.8	118.5	2.8	2.4	4.6	3.9
	4.8 - 5.0	118.2	2.8	2.4	4.4	3.7
	5.0 - 5.2	109.0	2.7	2.5	4.1	3.8
	5.2 - 5.6	100.7	1.9	1.9	3.7	3.7
	5.6 - 6.0	90.7	1.8	2.0	3.2	3.5
	6.0 - 6.4	86.1	1.7	1.9	3.0	3.5
	6.4 - 6.8	75.7	1.5	2.0	2.6	3.5
	6.8 - 7.2	68.1	1.5	2.3	2.2	3.3
	7.2 - 7.6	62.7	1.4	2.2	2.1	3.3
	7.6 - 8.0	55.2	1.3	2.3	1.9	3.4
	8.0 - 8.4	49.5	1.2	2.5	1.6	3.3
	8.4 - 8.8	42.4	1.1	2.6	1.4	3.3
	8.8 - 9.2	40.0	1.1	2.7	1.3	3.2
	9.2 - 9.6	33.2	1.0	2.9	1.1	3.2
	9.6 - 10.0	31.1	1.0	3.1	1.0	3.2
	10.0 - 10.8	25.4	0.6	2.4	0.8	3.1
	10.8 - 11.6	19.9	0.5	2.7	0.6	3.1
	11.6 - 12.4	14.6	0.5	3.1	0.4	3.1
	12.4 - 13.2	11.4	0.4	3.5	0.3	3.0
	13.2 - 14.0	8.6	0.3	4.1	0.3	3.0
	14.0 - 14.8	6.3	0.3	4.7	0.2	3.2
	14.8 - 15.6	4.0	0.2	5.8	0.1	2.8
	15.6 - 16.4	3.2	0.2	6.6	0.1	3.0
	16.4 - 17.2	2.2	0.2	7.8	0.1	3.1
	17.2 - 18.0	1.5	0.1	9.4	0.04	2.7
	18.0 - 18.8	1.0	0.1	11.3	0.04	3.9
	18.8 - 19.6	0.8	0.1	13.1	0.03	3.3
	19.6 - 20.4	0.4	0.1	16.6	0.01	3.1

θ [mrad]	p [GeV/c]	$\frac{d^2\sigma}{dpd\theta}(\pi^-)$ [mb/rad/(GeV/c)]	Δ_{stat} [mb/rad/(GeV/c)]	Δ_{stat} [%]	Δ_{syst} [mb/rad/(GeV/c)]	Δ_{syst} [%]
60 - 100	0.2 - 0.3	47.2	2.4	5.1	3.4	7.2
	0.3 - 0.4	74.2	2.8	3.8	5.1	6.8
	0.4 - 0.5	89.8	2.8	3.1	6.1	6.8
	0.5 - 0.6	109.5	2.8	2.6	7.1	6.5
	0.6 - 0.7	135.9	3.1	2.3	9.2	6.7
	0.7 - 0.8	155.5	3.6	2.3	10.2	6.6
	0.8 - 0.9	166.6	3.4	2.1	10.9	6.5
	0.9 - 1.0	181.6	3.6	2.0	11.7	6.5
	1.0 - 1.2	174.9	2.5	1.5	11.0	6.3
	1.2 - 1.4	188.8	2.6	1.4	11.6	6.2
	1.4 - 1.6	200.8	3.0	1.5	11.7	5.8
	1.6 - 1.8	209.9	3.6	1.7	11.5	5.5
	1.8 - 2.0	225.4	3.7	1.6	11.8	5.2
	2.0 - 2.2	225.1	3.8	1.7	11.2	5.0
	2.2 - 2.4	220.6	3.7	1.7	10.8	4.9
	2.4 - 2.6	215.4	3.7	1.7	10.2	4.7
	2.6 - 2.8	214.6	3.7	1.7	9.5	4.4
	2.8 - 3.0	195.4	2.8	1.4	8.3	4.2
	3.0 - 3.2	190.9	2.8	1.4	8.1	4.2
	3.2 - 3.4	183.7	2.6	1.4	7.5	4.1
	3.4 - 3.6	174.0	2.6	1.5	6.9	4.0
	3.6 - 3.8	167.8	2.5	1.5	6.7	4.0
	3.8 - 4.0	155.9	2.4	1.5	6.2	4.0
	4.0 - 4.2	146.3	2.3	1.6	5.8	4.0
	4.2 - 4.4	138.6	2.2	1.6	5.4	3.9
	4.4 - 4.6	131.5	2.2	1.6	4.9	3.7
	4.6 - 4.8	118.0	2.0	1.7	4.4	3.8
	4.8 - 5.0	113.9	2.0	1.8	4.1	3.6
	5.0 - 5.2	105.6	1.9	1.8	3.9	3.7
	5.2 - 5.6	94.8	1.3	1.4	3.5	3.7
	5.6 - 6.0	78.8	1.2	1.5	2.8	3.6
	6.0 - 6.4	67.4	1.1	1.6	2.4	3.6
	6.4 - 6.8	59.2	1.0	1.7	2.1	3.5
	6.8 - 7.2	51.1	0.9	1.8	1.8	3.6
	7.2 - 7.6	42.3	0.9	2.0	1.5	3.5
	7.6 - 8.0	37.1	0.8	2.2	1.3	3.6
	8.0 - 8.4	29.8	0.7	2.4	1.0	3.5
	8.4 - 8.8	26.1	0.7	2.6	0.9	3.4
	8.8 - 9.2	22.4	0.6	2.7	0.7	3.3
	9.2 - 9.6	18.4	0.6	3.1	0.6	3.4
	9.6 - 10.0	15.3	0.5	3.4	0.5	3.5
	10.0 - 10.8	11.8	0.3	2.7	0.4	3.3
	10.8 - 11.6	7.8	0.3	3.3	0.3	3.4
	11.6 - 12.4	5.4	0.2	4.0	0.2	3.1
	12.4 - 13.2	3.7	0.2	4.8	0.1	3.3
	13.2 - 14.0	2.6	0.1	5.8	0.1	3.0
	14.0 - 14.8	1.5	0.1	7.5	0.05	3.0
	14.8 - 15.6	1.1	0.1	9.1	0.03	3.1
	15.6 - 16.4	0.6	0.1	12.3	0.02	3.0
	16.4 - 17.2	0.4	0.1	14.5	0.01	2.9
	17.2 - 18.0	0.3	0.0	17.2	0.01	3.3

θ [mrad]	p [GeV/c]	$\frac{d^2\sigma}{dpd\theta}(\pi^-)$ [mb/rad/(GeV/c)]	Δ_{stat} [mb/rad/(GeV/c)]	Δ_{stat} [%]	Δ_{syst} [mb/rad/(GeV/c)]	Δ_{syst} [%]
100 - 140	0.2 - 0.3	61.3	3.0	4.9	4.2	6.9
	0.3 - 0.4	96.9	3.5	3.6	6.5	6.7
	0.4 - 0.5	131.4	3.4	2.6	9.0	6.8
	0.5 - 0.6	158.2	3.5	2.2	10.6	6.7
	0.6 - 0.7	180.5	3.6	2.0	11.1	6.2
	0.7 - 0.8	204.1	3.9	1.9	12.8	6.3
	0.8 - 0.9	221.6	4.0	1.8	14.3	6.4
	0.9 - 1.0	229.3	4.0	1.8	14.3	6.2
	1.0 - 1.2	262.8	3.2	1.2	15.2	5.8
	1.2 - 1.4	279.8	3.2	1.2	15.0	5.4
	1.4 - 1.6	284.3	3.2	1.1	14.6	5.1
	1.6 - 1.8	283.5	3.2	1.1	13.4	4.7
	1.8 - 2.0	263.8	3.0	1.2	12.5	4.7
	2.0 - 2.2	259.0	3.0	1.2	11.8	4.5
	2.2 - 2.4	242.3	2.9	1.2	10.5	4.3
	2.4 - 2.6	228.7	2.8	1.2	9.6	4.2
	2.6 - 2.8	213.5	2.7	1.3	9.0	4.2
	2.8 - 3.0	194.3	2.5	1.3	8.0	4.1
	3.0 - 3.2	186.2	2.5	1.3	7.3	3.9
	3.2 - 3.4	169.0	2.4	1.4	6.5	3.8
	3.4 - 3.6	146.5	2.2	1.5	5.7	3.9
	3.6 - 3.8	137.3	2.1	1.6	5.3	3.8
	3.8 - 4.0	123.2	2.0	1.6	4.6	3.8
	4.0 - 4.2	107.6	1.9	1.7	4.1	3.8
	4.2 - 4.4	103.0	1.9	1.8	3.9	3.8
	4.4 - 4.6	86.5	1.7	1.9	3.3	3.8
	4.6 - 4.8	82.7	1.7	2.0	3.2	3.9
	4.8 - 5.0	73.0	1.6	2.1	2.7	3.8
	5.0 - 5.2	66.2	1.5	2.3	2.4	3.7
	5.2 - 5.6	54.9	1.0	1.8	2.1	3.8
	5.6 - 6.0	44.5	0.9	1.9	1.7	3.9
	6.0 - 6.4	32.7	0.7	2.3	1.2	3.7
	6.4 - 6.8	26.2	0.7	2.5	1.0	3.7
	6.8 - 7.2	22.0	0.6	2.8	0.8	3.8
	7.2 - 7.6	16.6	0.5	3.1	0.6	3.7
	7.6 - 8.0	13.6	0.5	3.6	0.5	3.7
	8.0 - 8.4	10.1	0.4	4.0	0.4	3.8
	8.4 - 8.8	8.3	0.4	4.6	0.3	3.6
	8.8 - 9.2	6.8	0.3	5.1	0.3	3.9
	9.2 - 9.6	4.8	0.3	5.9	0.2	4.3
	9.6 - 10.0	3.4	0.2	6.9	0.1	3.7
	10.0 - 10.8	2.6	0.1	5.6	0.1	4.2
	10.8 - 11.6	1.4	0.1	7.6	0.1	4.5
	11.6 - 12.4	0.9	0.1	9.8	0.03	3.9
	12.4 - 13.2	0.5	0.1	12.4	0.02	4.0
	13.2 - 14.0	0.3	0.0	15.2	0.01	4.4

θ [mrad]			p [GeV/c]			$\frac{d^2\sigma}{dpd\theta}(\pi^-)$ [mb/rad/(GeV/c)]	Δ_{stat} [mb/rad/(GeV/c)]	Δ_{stat} [%]	Δ_{syst} [mb/rad/(GeV/c)]	Δ_{syst} [%]
140	-	180	0.2	-	0.3	80.6	3.4	4.2	5.7	7.1
			0.3	-	0.4	134.3	3.6	2.7	9.4	7.0
			0.4	-	0.5	166.3	3.6	2.1	11.1	6.7
			0.5	-	0.6	199.9	3.8	1.9	12.9	6.5
			0.6	-	0.7	225.5	3.9	1.7	13.4	5.9
			0.7	-	0.8	252.6	4.2	1.7	14.5	5.8
			0.8	-	0.9	281.1	4.4	1.6	16.1	5.7
			0.9	-	1.0	288.9	4.4	1.5	16.1	5.6
			1.0	-	1.2	302.7	3.2	1.1	15.7	5.2
			1.2	-	1.4	301.0	3.2	1.1	14.4	4.8
			1.4	-	1.6	289.8	3.2	1.1	13.9	4.8
			1.6	-	1.8	276.2	3.1	1.1	12.4	4.5
			1.8	-	2.0	259.9	3.0	1.2	11.2	4.3
			2.0	-	2.2	236.4	2.9	1.2	10.0	4.2
			2.2	-	2.4	218.2	2.8	1.3	8.8	4.1
			2.4	-	2.6	188.7	2.6	1.4	7.7	4.1
			2.6	-	2.8	169.1	2.5	1.5	6.8	4.0
			2.8	-	3.0	144.3	2.3	1.6	5.8	4.0
			3.0	-	3.2	130.2	2.2	1.7	5.2	4.0
			3.2	-	3.4	114.0	2.0	1.8	4.5	4.0
			3.4	-	3.6	95.2	1.8	1.9	3.7	3.9
			3.6	-	3.8	85.4	1.7	2.0	3.3	3.8
			3.8	-	4.0	73.1	1.6	2.2	2.9	4.0
			4.0	-	4.2	61.6	1.5	2.4	2.5	4.0
			4.2	-	4.4	53.8	1.4	2.5	2.1	3.9
			4.4	-	4.6	49.0	1.3	2.7	2.0	4.0
			4.6	-	4.8	42.1	1.2	2.9	1.6	3.8
			4.8	-	5.0	37.0	1.1	3.1	1.5	4.2
			5.0	-	5.2	30.2	1.0	3.3	1.3	4.2
			5.2	-	5.6	24.6	0.7	2.7	1.1	4.3
			5.6	-	6.0	17.8	0.6	3.1	0.7	4.1
			6.0	-	6.4	12.7	0.5	3.7	0.5	4.1
			6.4	-	6.8	10.1	0.4	4.2	0.4	4.2
			6.8	-	7.2	6.7	0.3	5.1	0.3	4.5
			7.2	-	7.6	4.8	0.3	5.8	0.2	4.2
			7.6	-	8.0	4.0	0.3	6.8	0.2	3.9
			8.0	-	8.4	2.5	0.2	8.0	0.1	4.0
			8.4	-	8.8	1.7	0.2	9.5	0.1	4.6
			8.8	-	9.2	1.5	0.2	10.6	0.1	4.7
			9.2	-	9.6	1.0	0.1	13.4	0.1	5.2
			9.6	-	10.0	0.6	0.1	16.4	0.03	4.6
			10.0	-	10.8	0.4	0.1	12.7	0.02	5.0
			10.8	-	11.6	0.3	0.0	17.8	0.01	5.1

θ [mrad]	p [GeV/c]	$\frac{d^2\sigma}{dpd\theta}(\pi^-)$ [mb/rad/(GeV/c)]	Δ_{stat} [mb/rad/(GeV/c)]	Δ_{stat} [%]	Δ_{syst} [mb/rad/(GeV/c)]	Δ_{syst} [%]
180 - 240	0.2 - 0.3	111.8	2.6	2.3	7.8	7.0
	0.3 - 0.4	176.8	3.0	1.7	11.5	6.5
	0.4 - 0.5	223.2	3.3	1.5	14.3	6.4
	0.5 - 0.6	261.7	3.5	1.4	15.9	6.1
	0.6 - 0.7	287.1	3.7	1.3	16.9	5.9
	0.7 - 0.8	308.5	3.9	1.3	17.0	5.5
	0.8 - 0.9	321.0	4.0	1.3	16.8	5.2
	0.9 - 1.0	323.5	4.1	1.3	16.1	5.0
	1.0 - 1.2	317.4	2.9	0.9	15.0	4.7
	1.2 - 1.4	290.2	2.7	0.9	13.2	4.6
	1.4 - 1.6	264.2	2.6	1.0	11.2	4.3
	1.6 - 1.8	242.1	2.5	1.0	10.3	4.3
	1.8 - 2.0	206.8	2.3	1.1	8.7	4.2
	2.0 - 2.2	178.8	2.2	1.2	7.7	4.3
	2.2 - 2.4	147.8	2.0	1.3	6.1	4.1
	2.4 - 2.6	125.2	1.8	1.4	5.2	4.2
	2.6 - 2.8	103.1	1.6	1.6	4.4	4.3
	2.8 - 3.0	88.8	1.5	1.7	3.8	4.3
	3.0 - 3.2	74.2	1.4	1.9	3.2	4.3
	3.2 - 3.4	62.3	1.3	2.1	2.6	4.2
	3.4 - 3.6	50.0	1.1	2.3	2.2	4.4
	3.6 - 3.8	39.0	1.0	2.5	1.7	4.5
	3.8 - 4.0	35.1	1.0	2.8	1.5	4.3
	4.0 - 4.2	28.4	0.9	3.1	1.2	4.1
	4.2 - 4.4	24.7	0.8	3.3	1.2	4.7
	4.4 - 4.6	19.0	0.7	3.7	0.9	4.8
	4.6 - 4.8	16.3	0.6	4.0	0.8	4.9
	4.8 - 5.0	14.0	0.6	4.5	0.7	4.7
	5.0 - 5.2	10.4	0.5	4.9	0.5	4.7
	5.2 - 5.6	8.7	0.3	3.8	0.4	4.6
	5.6 - 6.0	5.0	0.2	4.9	0.2	4.9
	6.0 - 6.4	3.4	0.2	5.8	0.2	4.6
	6.4 - 6.8	2.5	0.2	7.1	0.1	5.0
	6.8 - 7.2	1.7	0.1	8.0	0.1	5.4
	7.2 - 7.6	0.9	0.1	11.1	0.1	5.7
	7.6 - 8.0	0.6	0.1	13.4	0.03	5.2
	8.0 - 8.4	0.5	0.1	14.7	0.02	4.2
	8.4 - 8.8	0.3	0.1	18.5	0.02	5.9

θ [mrad]	p [GeV/c]	$\frac{d^2\sigma}{dpd\theta}(\pi^-)$ [mb/rad/(GeV/c)]	Δ_{stat} [mb/rad/(GeV/c)]	Δ_{stat} [%]	Δ_{syst} [mb/rad/(GeV/c)]	Δ_{syst} [%]
240 - 300	0.2 - 0.3	166.6	4.9	2.9	12.0	7.2
	0.3 - 0.4	219.6	5.1	2.3	15.1	6.9
	0.4 - 0.5	285.3	5.8	2.0	20.0	7.0
	0.5 - 0.6	313.2	6.0	1.9	21.1	6.7
	0.6 - 0.7	329.9	6.2	1.9	21.6	6.5
	0.7 - 0.8	310.9	5.9	1.9	18.4	5.9
	0.8 - 0.9	331.6	4.7	1.4	17.6	5.3
	0.9 - 1.0	303.4	4.4	1.5	15.9	5.3
	1.0 - 1.2	292.4	3.1	1.1	14.3	4.9
	1.2 - 1.4	253.2	2.9	1.1	11.7	4.6
	1.4 - 1.6	206.1	2.6	1.3	9.3	4.5
	1.6 - 1.8	168.4	2.4	1.4	7.6	4.5
	1.8 - 2.0	139.0	2.1	1.5	6.1	4.4
	2.0 - 2.2	110.4	1.9	1.7	5.0	4.6
	2.2 - 2.4	86.1	1.7	2.0	4.0	4.7
	2.4 - 2.6	65.8	1.5	2.2	3.0	4.6
	2.6 - 2.8	55.0	1.4	2.5	2.7	4.9
	2.8 - 3.0	40.2	1.1	2.8	1.8	4.5
	3.0 - 3.2	37.1	1.6	4.4	1.7	4.7
	3.2 - 3.4	28.6	1.5	5.1	1.4	4.8
	3.4 - 3.6	23.2	1.3	5.5	1.1	4.7
	3.6 - 3.8	19.7	1.3	6.3	0.9	4.8
	3.8 - 4.0	14.1	1.0	7.0	0.6	4.4
	4.0 - 4.2	9.6	0.8	8.1	0.4	4.4
	4.2 - 4.4	9.1	0.8	8.5	0.4	4.4
	4.4 - 4.6	6.2	0.6	10.4	0.4	5.8
	4.6 - 4.8	6.3	0.7	11.1	0.4	5.9
	4.8 - 5.0	4.8	0.6	12.2	0.2	3.9
	5.0 - 5.2	2.9	0.4	14.7	0.1	4.5
	5.2 - 5.6	2.9	0.3	11.1	0.1	4.4
	5.6 - 6.0	1.5	0.2	14.2	0.1	4.3
	6.0 - 6.4	1.0	0.2	17.8	0.1	6.5
	6.4 - 6.8	1.7	0.3	17.7	0.1	4.1

θ [mrad]			p [GeV/c]			$\frac{d^2\sigma}{dpd\theta}(\pi^-)$ [mb/rad/(GeV/c)]	Δ_{stat} [mb/rad/(GeV/c)]	Δ_{stat} [%]	Δ_{syst} [mb/rad/(GeV/c)]	Δ_{syst} [%]
300	-	360	0.2	-	0.3	178.6	5.5	3.1	12.2	6.8
			0.3	-	0.4	240.9	6.1	2.6	16.8	7.0
			0.4	-	0.5	290.1	6.7	2.3	22.8	7.9
			0.5	-	0.6	342.3	7.7	2.2	24.3	7.1
			0.6	-	0.7	339.2	7.4	2.2	22.0	6.5
			0.7	-	0.8	318.9	7.2	2.3	19.7	6.2
			0.8	-	0.9	302.4	7.0	2.3	17.5	5.8
			0.9	-	1.0	276.6	6.7	2.4	15.4	5.6
			1.0	-	1.2	238.8	4.4	1.8	12.8	5.4
			1.2	-	1.4	194.4	4.0	2.1	9.1	4.7
			1.4	-	1.6	153.0	3.6	2.3	6.8	4.5
			1.6	-	1.8	112.1	3.0	2.7	5.2	4.6
			1.8	-	2.0	80.4	2.5	3.1	3.7	4.6
			2.0	-	2.2	55.7	2.1	3.7	2.9	5.2
			2.2	-	2.4	42.4	1.8	4.3	2.2	5.2
			2.4	-	2.6	29.1	1.5	5.1	1.4	4.9
			2.6	-	2.8	19.6	1.2	6.2	1.0	5.2
			2.8	-	3.0	14.3	1.0	7.0	0.7	5.1
			3.0	-	3.2	9.9	0.9	8.8	0.5	4.6
			3.2	-	3.4	7.3	0.7	9.9	0.4	5.5
			3.4	-	3.6	3.9	0.5	13.0	0.2	5.4
			3.6	-	3.8	2.6	0.4	15.5	0.1	5.6
			3.8	-	4.0	2.8	0.4	16.1	0.2	6.7
360	-	420	0.2	-	0.3	183.2	5.4	2.9	13.7	7.5
			0.3	-	0.4	257.7	6.4	2.5	19.4	7.5
			0.4	-	0.5	326.1	7.6	2.3	21.6	6.6
			0.5	-	0.6	295.2	6.9	2.3	19.2	6.5
			0.6	-	0.7	302.2	7.1	2.3	18.7	6.2
			0.7	-	0.8	275.9	6.7	2.4	16.3	5.9
			0.8	-	0.9	255.6	6.5	2.5	18.0	7.0
			0.9	-	1.0	232.8	6.3	2.7	16.3	7.0
			1.0	-	1.2	187.8	4.0	2.1	14.9	8.0
			1.2	-	1.4	129.2	3.3	2.6	10.1	7.8
			1.4	-	1.6	87.8	2.7	3.1	7.0	7.9
			1.6	-	1.8	59.2	2.2	3.7	4.9	8.3
			1.8	-	2.0	36.3	1.7	4.6	2.9	8.1
			2.0	-	2.2	23.8	1.3	5.7	2.1	8.9
			2.2	-	2.4	15.3	1.1	6.9	1.4	9.0
			2.4	-	2.6	9.9	0.9	8.6	0.9	9.1
			2.6	-	2.8	6.3	0.7	10.7	0.6	9.2
			2.8	-	3.0	4.1	0.5	13.1	0.4	9.2
			3.0	-	3.2	3.1	0.5	15.2	0.3	10.0

Table 5: The NA61/SHINE results on the π^- double differential cross section, $d^2\sigma_{\pi^-}/(dpd\theta)$, in the laboratory system for p+C interactions at 31 GeV/c. The results are presented as a function of momentum in different angular intervals. The statistical Δ_{stat} and systematic Δ_{syst} errors are quoted.

θ [mrad]	p [GeV/c]	$\frac{d^2\sigma}{dpd\theta}(K^+)$ [mb/rad/(GeV/c)]	Δ_{stat} [mb/rad/(GeV/c)]	Δ_{stat} [%]	Δ_{syst} [mb/rad/(GeV/c)]	Δ_{syst} [%]
0 - 20	0.8 - 1.6	2.1	0.5	23.8	0.1	5.7
	1.6 - 2.4	2.8	0.4	15.0	0.2	5.4
	2.4 - 3.2	4.6	0.6	13.9	0.2	5.4
	3.2 - 4.0	3.7	0.7	19.1	0.2	5.4
	4.0 - 4.8	3.5	0.6	17.1	0.2	5.5
	4.8 - 5.6	3.8	0.7	19.1	0.2	5.8
	5.6 - 6.4	4.3	0.7	16.5	0.3	6.3
	6.4 - 7.6	3.5	0.6	17.8	0.3	7.2
	7.6 - 8.8	3.1	0.7	23.8	0.3	8.7
	8.8 - 10.0	3.0	0.7	24.6	0.3	10.7
	10.0 - 11.6	3.2	0.6	20.0	0.4	13.3
	11.6 - 13.2	2.3	1.0	42.3	0.4	16.6
	13.2 - 14.8	1.4	1.3	93.8	0.3	19.9
	14.8 - 16.4	1.6	1.6	95.2	0.4	22.9
20 - 40	0.8 - 1.6	4.3	0.6	13.3	0.2	4.3
	1.6 - 2.4	7.6	0.6	7.9	0.3	4.1
	2.4 - 3.2	10.6	0.8	7.2	0.4	4.1
	3.2 - 4.0	11.9	0.9	7.9	0.5	4.1
	4.0 - 4.8	12.2	1.0	8.0	0.5	4.1
	4.8 - 5.6	12.9	1.1	8.9	0.6	4.3
	5.6 - 6.4	10.3	1.1	10.4	0.5	4.8
	6.4 - 7.6	9.7	0.9	9.1	0.5	5.6
	7.6 - 8.8	8.6	0.9	10.1	0.6	7.3
	8.8 - 10.0	8.5	0.8	9.8	0.8	9.7
	10.0 - 11.6	5.8	0.7	11.7	0.8	13.1
	11.6 - 13.2	4.1	0.7	16.6	0.7	16.9
	13.2 - 14.8	3.7	0.7	18.1	0.8	20.5
	14.8 - 16.4	2.4	0.6	25.1	0.5	23.1
40 - 60	0.8 - 1.6	10.4	1.3	12.4	0.4	3.6
	1.6 - 2.4	10.9	1.1	10.5	0.3	2.9
	2.4 - 3.2	15.7	1.4	9.0	0.4	2.7
	3.2 - 4.0	19.9	1.6	8.2	0.5	2.6
	4.0 - 4.8	19.5	1.6	8.0	0.5	2.7
	4.8 - 5.6	17.0	1.6	9.2	0.5	3.0
	5.6 - 6.4	17.4	1.6	9.4	0.6	3.4
	6.4 - 7.6	13.8	1.2	8.5	0.6	4.2
	7.6 - 8.8	10.7	1.0	9.0	0.6	5.6
	8.8 - 10.0	9.2	0.9	10.1	0.7	7.4
	10.0 - 11.6	6.5	0.7	10.8	0.6	9.9
	11.6 - 13.2	3.7	0.6	16.0	0.5	13.0
	13.2 - 14.8	2.5	0.5	21.2	0.4	16.1
	14.8 - 16.4	1.7	0.4	22.1	0.3	18.8
	16.4 - 18.0	0.4	0.2	51.6	0.1	20.9
	18.0 - 19.6	0.4	0.2	55.9	0.1	22.4
60 - 100	0.8 - 1.6	9.7	1.1	11.2	0.3	3.4
	1.6 - 2.4	20.5	1.4	7.0	0.6	3.0
	2.4 - 3.2	20.0	1.3	6.6	0.5	2.7
	3.2 - 4.0	23.3	1.4	5.9	0.6	2.7
	4.0 - 4.8	19.8	1.0	4.9	0.6	2.8
	4.8 - 5.6	16.5	0.9	5.2	0.5	3.1
	5.6 - 6.4	16.1	0.9	5.7	0.5	3.4
	6.4 - 7.6	11.6	0.7	5.9	0.5	4.0
	7.6 - 8.8	7.8	0.6	7.9	0.4	5.0
	8.8 - 10.0	5.2	0.5	9.9	0.3	6.2
	10.0 - 11.6	3.2	0.4	12.1	0.2	7.8
	11.6 - 13.2	1.2	0.2	17.0	0.1	9.8
	13.2 - 14.8	0.9	0.2	22.3	0.1	11.8
	14.8 - 16.4	0.3	0.1	44.3	0.04	13.6

θ [mrad]			p [GeV/c]			$\frac{d^2\sigma}{dpd\theta}(K^+)$ [mb/rad/(GeV/c)]	Δ_{stat} [mb/rad/(GeV/c)]	Δ_{stat} [%]	Δ_{syst} [mb/rad/(GeV/c)]	Δ_{syst} [%]
100	-	140	0.8	-	1.6	16.9	2.2	13.0	0.6	3.5
			1.6	-	2.4	27.7	2.0	7.1	0.8	3.0
			2.4	-	3.2	26.3	1.4	5.2	0.7	2.8
			3.2	-	4.0	20.7	1.2	5.8	0.6	2.7
			4.0	-	4.8	18.0	1.1	6.2	0.5	2.8
			4.8	-	5.6	11.8	0.9	7.5	0.4	3.0
			5.6	-	6.4	8.6	0.8	9.0	0.3	3.3
			6.4	-	7.6	5.2	0.5	10.3	0.2	3.9
			7.6	-	8.8	3.1	0.5	15.0	0.2	4.9
			8.8	-	10.0	1.5	0.4	25.6	0.1	6.1
			10.0	-	11.6	0.6	0.2	31.0	0.05	7.8
			11.6	-	13.2	0.3	0.1	39.1	0.03	9.8
140	-	180	0.8	-	1.6	18.1	4.1	22.5	0.6	3.2
			1.6	-	2.4	24.2	1.9	8.0	0.7	2.8
			2.4	-	3.2	23.7	1.7	7.2	0.6	2.7
			3.2	-	4.0	18.2	1.4	7.7	0.5	2.6
			4.0	-	4.8	8.8	1.0	11.1	0.2	2.7
			4.8	-	5.6	5.6	0.8	13.6	0.2	2.9
			5.6	-	6.4	4.0	0.7	16.6	0.1	3.3
			6.4	-	7.6	1.6	0.4	24.6	0.1	4.0
			7.6	-	8.8	0.6	0.3	44.6	0.03	5.0
			8.8	-	10.0	0.2	0.1	65.8	0.01	6.7
180	-	240	0.8	-	1.6	22.9	3.3	14.4	0.8	3.5
			1.6	-	2.4	24.9	2.4	9.7	0.8	3.2
			2.4	-	3.2	14.0	1.6	11.4	0.4	2.5
			3.2	-	4.0	11.5	1.4	12.5	0.3	2.5
			4.0	-	4.8	5.4	1.0	18.0	0.1	2.6
			4.8	-	5.6	2.0	0.6	29.3	0.1	3.1
			5.6	-	6.4	2.4	0.8	31.4	0.1	3.3
			6.4	-	7.6	0.4	0.2	52.5	0.02	4.2
240	-	300	0.8	-	1.6	24.0	3.2	13.3	0.7	2.9
			1.6	-	2.4	17.4	2.0	11.8	0.5	2.7
			2.4	-	3.2	10.2	1.4	13.4	0.3	2.9
			3.2	-	4.0	5.5	1.2	21.1	0.1	2.6
			4.0	-	4.8	2.2	0.8	35.6	0.1	2.7
			4.8	-	5.6	0.5	0.3	54.8	0.01	2.8

Table 6: The NA61/SHINE results on the K^+ double differential cross section, $d^2\sigma_{K^+}/(dpd\theta)$, in the laboratory system for p+C interactions at 31 GeV/c. The results are presented as a function of momentum in different angular intervals. The statistical Δ_{stat} and systematic Δ_{syst} errors are quoted.

θ [mrad]	p [GeV/c]	$\frac{d^2\sigma}{dpd\theta}(K^-)$ [mb/rad/(GeV/c)]	Δ_{stat} [mb/rad/(GeV/c)]	Δ_{stat} [%]	Δ_{syst} [mb/rad/(GeV/c)]	Δ_{syst} [%]
0 - 20	0.8 - 1.6	0.5	0.2	50.6	0.03	6.0
	1.6 - 2.4	1.5	0.3	20.9	0.1	5.7
	2.4 - 3.2	0.9	0.3	34.8	0.1	11.1
	3.2 - 4.0	1.7	0.4	26.0	0.2	11.1
	4.0 - 4.8	1.7	0.3	19.6	0.2	11.1
	4.8 - 5.6	1.7	0.3	19.7	0.2	11.2
	5.6 - 6.4	1.2	0.3	28.2	0.1	11.3
	6.4 - 7.6	1.2	0.3	22.5	0.1	11.6
	7.6 - 8.8	1.2	0.2	16.5	0.1	12.2
	8.8 - 10.0	0.5	0.2	30.9	0.04	8.5
	10.0 - 11.6	0.7	0.2	23.9	0.1	10.3
	11.6 - 13.2	0.2	0.1	84.9	0.02	12.6
	13.2 - 14.8	0.4	0.1	34.3	0.1	15.0
	14.8 - 16.4	0.1	0.2	141.5	0.02	17.2
20 - 40	0.8 - 1.6	1.9	0.4	18.7	0.1	4.4
	1.6 - 2.4	3.9	0.5	12.0	0.2	4.2
	2.4 - 3.2	5.5	0.6	10.4	0.2	4.1
	3.2 - 4.0	4.9	0.6	11.6	0.2	4.1
	4.0 - 4.8	5.0	0.6	12.8	0.2	4.1
	4.8 - 5.6	5.4	0.6	12.0	0.2	4.2
	5.6 - 6.4	4.1	0.6	13.5	0.2	4.4
	6.4 - 7.6	3.0	0.4	12.9	0.1	4.7
	7.6 - 8.8	3.2	0.4	12.1	0.2	5.2
	8.8 - 10.0	2.2	0.3	12.6	0.1	5.9
	10.0 - 11.6	1.7	0.2	14.3	0.1	7.0
	11.6 - 13.2	0.7	0.2	22.3	0.1	8.1
	13.2 - 14.8	0.2	0.1	61.2	0.02	9.6
	14.8 - 16.4	0.1	0.1	52.8	0.01	11.0
	16.4 - 18.0	0.1	0.1	46.9	0.02	12.1
	18.0 - 19.6	0.1	0.1	46.3	0.02	12.9
40 - 60	0.8 - 1.6	4.1	0.9	21.0	0.1	3.4
	1.6 - 2.4	6.5	0.9	14.4	0.2	3.3
	2.4 - 3.2	8.2	1.1	13.1	0.2	2.7
	3.2 - 4.0	8.0	1.0	12.6	0.2	2.7
	4.0 - 4.8	7.5	1.0	13.0	0.2	2.7
	4.8 - 5.6	5.6	0.7	12.9	0.2	2.9
	5.6 - 6.4	6.6	0.9	13.2	0.2	3.1
	6.4 - 7.6	4.4	0.6	12.7	0.2	3.4
	7.6 - 8.8	3.0	0.4	12.7	0.1	3.9
	8.8 - 10.0	1.2	0.2	17.5	0.1	4.3
	10.0 - 11.6	1.5	0.2	13.8	0.1	4.8
	11.6 - 13.2	0.8	0.1	17.3	0.04	5.1
	13.2 - 14.8	0.1	0.1	55.8	0.01	5.4
	14.8 - 16.4	0.1	0.04	57.0	0.00	5.5
	16.4 - 18.0	0.1	0.04	60.9	0.00	5.5
60 - 100	0.8 - 1.6	5.5	0.9	16.2	0.2	3.5
	1.6 - 2.4	9.6	1.0	10.2	0.3	3.1
	2.4 - 3.2	9.1	0.9	9.9	0.3	2.8
	3.2 - 4.0	9.7	0.9	9.2	0.3	2.8
	4.0 - 4.8	8.0	0.6	7.5	0.2	2.8
	4.8 - 5.6	6.6	0.5	7.6	0.2	2.9
	5.6 - 6.4	4.7	0.4	8.9	0.1	3.1
	6.4 - 7.6	2.5	0.2	9.8	0.1	3.4
	7.6 - 8.8	1.7	0.2	13.3	0.1	3.9
	8.8 - 10.0	1.1	0.2	15.1	0.05	4.3
	10.0 - 11.6	0.5	0.1	18.1	0.03	4.7
	11.6 - 13.2	0.1	0.03	47.4	0.00	5.1
	13.2 - 14.8	0.1	0.1	41.6	0.01	5.3
	14.8 - 16.4	0.01	0.01	238.7	0.00	5.6
	16.4 - 18.0	0.01	0.01	135.4	0.00	5.5

θ [mrad]			p [GeV/c]			$\frac{d^2\sigma}{dpd\theta}(K^-)$ [mb/rad/(GeV/c)]	Δ_{stat} [mb/rad/(GeV/c)]	Δ_{stat} [%]	Δ_{syst} [mb/rad/(GeV/c)]	Δ_{syst} [%]
100	-	140	0.8	-	1.6	7.3	1.5	20.8	0.2	3.3
			1.6	-	2.4	11.4	1.2	10.4	0.4	3.2
			2.4	-	3.2	10.0	0.9	8.6	0.3	3.0
			3.2	-	4.0	8.5	0.7	8.5	0.2	2.8
			4.0	-	4.8	5.4	0.6	10.3	0.1	2.8
			4.8	-	5.6	3.9	0.5	12.2	0.1	2.8
			5.6	-	6.4	1.5	0.3	18.1	0.05	3.0
			6.4	-	7.6	1.4	0.2	16.9	0.05	3.3
			7.6	-	8.8	0.6	0.1	26.2	0.02	3.8
			8.8	-	10.0	0.2	0.1	34.9	0.01	4.3
			10.0	-	11.6	0.02	0.02	96.2	0.00	4.9
			11.6	-	13.2	0.3	0.3	109.5	0.01	5.0
140	-	180	0.8	-	1.6	12.7	4.1	32.6	0.4	2.8
			1.6	-	2.4	15.9	1.7	10.5	0.5	3.2
			2.4	-	3.2	8.9	1.0	11.7	0.2	2.6
			3.2	-	4.0	6.4	0.8	12.7	0.2	2.6
			4.0	-	4.8	2.7	0.5	19.3	0.1	2.7
			4.8	-	5.6	2.0	0.5	24.8	0.1	2.8
			5.6	-	6.4	1.6	0.4	27.4	0.05	2.9
			6.4	-	7.6	0.4	0.2	37.5	0.02	4.0
			7.6	-	8.8	0.5	0.5	90.7	0.02	4.0
180	-	240	0.8	-	1.6	11.3	2.5	21.6	0.4	3.6
			1.6	-	2.4	11.3	1.7	15.0	0.4	3.7
			2.4	-	3.2	5.0	0.9	18.9	0.1	2.9
			3.2	-	4.0	3.6	0.9	23.8	0.1	2.6
			4.0	-	4.8	1.5	0.6	39.1	0.04	2.6
			4.8	-	5.6	1.4	0.5	35.0	0.04	2.7
			5.6	-	6.4	0.1	0.1	76.7	0.00	2.9

Table 7: The NA61/SHINE results on the K^- double differential cross section, $d^2\sigma_{K^-}/(dpd\theta)$, in the laboratory system for p+C interactions at 31 GeV/c. The results are presented as a function of momentum in different angular intervals. The statistical Δ_{stat} and systematic Δ_{syst} errors are quoted.

θ [mrad]	p [GeV/c]	$\frac{d^2\sigma}{dpd\theta}(p)$ [mb/rad/(GeV/c)]	Δ_{stat} [mb/rad/(GeV/c)]	Δ_{stat} [%]	Δ_{syst} [mb/rad/(GeV/c)]	Δ_{syst} [%]
0 - 10	1.2 - 1.6	2.4	0.5	19.0	0.2	8.7
	1.6 - 2.0	3.1	0.5	17.8	0.3	8.9
	2.0 - 2.4	2.2	0.4	19.9	0.2	10.3
	2.4 - 2.8	2.3	0.4	17.8	0.3	14.0
	2.8 - 3.2	3.6	0.5	14.8	0.5	14.0
	3.2 - 3.6	2.7	0.6	20.9	0.3	11.5
	3.6 - 4.0	2.3	0.5	22.9	0.2	9.3
	4.0 - 4.4	4.1	0.7	16.0	0.5	11.1
	4.4 - 4.8	4.8	0.8	16.9	0.5	9.6
	4.8 - 5.2	4.5	1.2	27.3	0.4	9.5
	5.2 - 5.6	6.0	1.7	28.0	0.4	6.7
	5.6 - 6.0	10.3	2.2	21.1	0.9	8.3
	6.0 - 6.4	9.3	1.9	19.9	0.8	8.4
	6.4 - 6.8	6.8	1.5	22.0	0.6	8.5
	6.8 - 7.2	8.1	1.7	20.5	0.6	7.0
	7.2 - 7.6	6.4	1.5	24.4	0.5	7.5
	7.6 - 8.0	11.1	2.0	17.8	0.7	6.4
	8.0 - 8.4	11.4	2.6	22.6	1.3	11.8
	8.4 - 8.8	19.0	3.0	15.6	2.3	11.8
	8.8 - 9.2	11.5	2.8	24.6	1.4	11.8
	9.2 - 9.6	20.2	3.0	14.7	2.4	11.9
	9.6 - 10.0	19.5	2.9	15.1	2.3	11.6
	10.0 - 10.8	22.9	2.4	10.4	2.7	11.6
	10.8 - 11.6	22.2	2.3	10.2	1.4	6.4
	11.6 - 12.4	23.1	2.7	11.5	1.5	6.5
	12.4 - 13.2	21.0	3.1	14.7	1.4	6.6
	13.2 - 14.0	28.4	3.4	12.0	1.9	6.5
	14.0 - 14.8	30.8	3.7	12.1	2.1	6.8
	14.8 - 15.6	32.4	4.0	12.4	2.3	7.0
	15.6 - 16.4	42.6	5.3	12.5	3.0	7.1

θ [mrad]	p [GeV/c]	$\frac{d^2\sigma}{dpd\theta}(p)$ [mb/rad/(GeV/c)]	Δ_{stat} [mb/rad/(GeV/c)]	Δ_{stat} [%]	Δ_{syst} [mb/rad/(GeV/c)]	Δ_{syst} [%]
10 - 20	1.2 - 1.6	9.6	0.9	8.9	0.8	8.7
	1.6 - 2.0	8.6	0.8	9.1	0.8	9.1
	2.0 - 2.4	8.8	0.8	8.8	1.0	11.5
	2.4 - 2.8	7.6	0.8	10.7	0.8	10.8
	2.8 - 3.2	9.8	1.4	14.5	1.0	10.2
	3.2 - 3.6	11.4	1.3	11.6	1.3	11.7
	3.6 - 4.0	12.6	1.6	12.4	1.5	11.7
	4.0 - 4.4	12.6	1.4	11.2	1.3	10.0
	4.4 - 4.8	15.0	1.5	10.0	1.4	9.3
	4.8 - 5.2	14.9	1.6	11.0	1.5	9.9
	5.2 - 5.6	21.6	2.2	10.4	1.8	8.5
	5.6 - 6.0	21.6	2.4	11.2	1.8	8.5
	6.0 - 6.4	24.8	2.7	10.9	1.9	7.8
	6.4 - 6.8	24.8	2.6	10.5	1.8	7.4
	6.8 - 7.2	28.5	3.0	10.5	2.2	7.7
	7.2 - 7.6	26.7	3.3	12.2	1.7	6.4
	7.6 - 8.0	33.4	3.5	10.6	2.1	6.4
	8.0 - 8.4	32.6	3.5	10.8	3.2	9.8
	8.4 - 8.8	42.0	4.3	10.2	4.1	9.8
	8.8 - 9.2	42.3	3.9	9.2	4.2	9.8
	9.2 - 9.6	46.2	4.6	10.0	4.5	9.8
	9.6 - 10.0	60.5	4.7	7.8	5.8	9.7
	10.0 - 10.8	55.1	3.5	6.4	5.3	9.6
	10.8 - 11.6	68.3	4.3	6.3	3.9	5.7
	11.6 - 12.4	71.2	3.9	5.6	3.9	5.5
	12.4 - 13.2	80.8	4.4	5.4	4.4	5.4
	13.2 - 14.0	82.7	4.3	5.2	4.5	5.4
	14.0 - 14.8	95.1	4.3	4.5	5.0	5.3
	14.8 - 15.6	103.8	4.4	4.3	5.5	5.3
	15.6 - 16.4	101.0	4.5	4.5	5.3	5.3
	16.4 - 17.2	110.3	4.8	4.3	5.8	5.3
	17.2 - 18.0	108.5	4.6	4.2	5.7	5.3
	18.0 - 18.8	117.6	5.2	4.4	6.2	5.3
	18.8 - 19.6	117.2	5.0	4.3	6.2	5.3
	19.6 - 20.4	125.6	5.1	4.1	6.7	5.3
	20.4 - 21.2	123.4	5.4	4.4	6.6	5.4
	21.2 - 22.0	110.2	5.3	4.8	6.0	5.4

θ [mrad]	p [GeV/c]	$\frac{d^2\sigma}{dpd\theta}(p)$ [mb/rad/(GeV/c)]	Δ_{stat} [mb/rad/(GeV/c)]	Δ_{stat} [%]	Δ_{syst} [mb/rad/(GeV/c)]	Δ_{syst} [%]
20 - 40	1.2 - 1.6	14.8	0.7	4.7	1.3	8.5
	1.6 - 2.0	15.4	0.7	4.6	1.6	10.2
	2.0 - 2.4	17.5	0.8	4.4	2.0	11.3
	2.4 - 2.8	17.7	1.0	5.7	2.0	11.4
	2.8 - 3.2	18.9	1.1	5.8	2.1	11.0
	3.2 - 3.6	20.1	1.1	5.7	2.0	9.8
	3.6 - 4.0	20.3	1.2	5.8	1.9	9.3
	4.0 - 4.4	23.9	1.2	5.1	1.9	8.1
	4.4 - 4.8	25.0	1.3	5.3	2.4	9.5
	4.8 - 5.2	31.0	1.6	5.0	2.4	7.8
	5.2 - 5.6	37.3	1.8	4.8	3.1	8.3
	5.6 - 6.0	40.0	1.9	4.8	3.0	7.4
	6.0 - 6.4	48.4	1.9	4.0	3.5	7.2
	6.4 - 6.8	46.8	2.0	4.3	3.1	6.5
	6.8 - 7.2	51.8	2.3	4.4	3.3	6.3
	7.2 - 7.6	56.3	2.2	4.0	3.3	5.8
	7.6 - 8.0	60.3	2.4	4.0	3.6	5.9
	8.0 - 8.4	66.3	2.4	3.7	3.8	5.7
	8.4 - 8.8	73.0	2.7	3.7	3.8	5.2
	8.8 - 9.2	75.8	2.8	3.7	4.0	5.2
	9.2 - 9.6	80.4	2.8	3.5	4.1	5.1
	9.6 - 10.0	76.9	2.9	3.8	3.8	4.9
	10.0 - 10.8	88.0	2.2	2.5	4.2	4.8
	10.8 - 11.6	89.0	2.2	2.5	4.2	4.7
	11.6 - 12.4	96.1	2.3	2.4	3.8	4.0
	12.4 - 13.2	100.7	2.5	2.4	3.9	3.9
	13.2 - 14.0	98.4	2.5	2.5	3.7	3.8
	14.0 - 14.8	101.5	2.5	2.5	3.8	3.7
	14.8 - 15.6	95.0	2.5	2.6	3.5	3.6
	15.6 - 16.4	97.9	2.5	2.5	3.5	3.6
	16.4 - 17.2	93.5	2.4	2.6	3.3	3.5
	17.2 - 18.0	88.2	2.4	2.7	3.1	3.5
	18.0 - 18.8	82.8	2.3	2.8	2.9	3.5
	18.8 - 19.6	77.7	2.3	3.0	2.7	3.4
	19.6 - 20.4	71.9	2.3	3.2	2.5	3.4
	20.4 - 21.2	66.5	2.1	3.2	2.3	3.4
	21.2 - 22.0	63.8	2.2	3.5	2.2	3.4

θ [mrad]	p [GeV/c]	$\frac{d^2\sigma}{dpd\theta}(p)$ [mb/rad/(GeV/c)]	Δ_{stat} [mb/rad/(GeV/c)]	Δ_{stat} [%]	Δ_{syst} [mb/rad/(GeV/c)]	Δ_{syst} [%]
40 - 60	1.2 - 1.6	26.6	1.3	4.8	1.9	7.2
	1.6 - 2.0	25.3	1.3	5.2	2.3	9.3
	2.0 - 2.4	26.5	1.4	5.4	2.5	9.5
	2.4 - 2.8	27.0	1.6	6.0	2.5	9.3
	2.8 - 3.2	26.2	1.6	6.3	2.5	9.7
	3.2 - 3.6	32.7	2.0	6.0	2.8	8.5
	3.6 - 4.0	34.5	2.1	6.0	3.2	9.3
	4.0 - 4.4	38.4	2.2	5.7	2.8	7.3
	4.4 - 4.8	42.5	2.4	5.5	3.5	8.3
	4.8 - 5.2	40.9	2.2	5.4	2.8	6.8
	5.2 - 5.6	45.0	2.5	5.5	3.3	7.4
	5.6 - 6.0	54.0	2.8	5.2	3.8	7.0
	6.0 - 6.4	55.6	2.8	5.0	3.5	6.2
	6.4 - 6.8	64.0	3.1	4.8	3.6	5.6
	6.8 - 7.2	68.5	3.1	4.6	3.5	5.1
	7.2 - 7.6	71.0	3.2	4.6	3.6	5.0
	7.6 - 8.0	68.7	2.8	4.0	3.1	4.6
	8.0 - 8.4	78.2	2.9	3.6	3.4	4.4
	8.4 - 8.8	76.0	2.7	3.5	3.1	4.1
	8.8 - 9.2	80.1	2.9	3.6	3.3	4.1
	9.2 - 9.6	75.8	2.6	3.5	3.0	4.0
	9.6 - 10.0	80.3	2.7	3.4	3.1	3.9
	10.0 - 10.8	83.8	1.9	2.3	3.1	3.7
	10.8 - 11.6	77.9	1.9	2.4	2.7	3.4
	11.6 - 12.4	78.5	1.9	2.4	2.6	3.3
	12.4 - 13.2	73.8	1.8	2.4	2.4	3.2
	13.2 - 14.0	65.5	1.6	2.5	2.1	3.1
	14.0 - 14.8	62.1	1.6	2.6	1.9	3.0
	14.8 - 15.6	52.3	1.4	2.7	1.6	3.0
	15.6 - 16.4	49.0	1.4	2.9	1.4	2.9
	16.4 - 17.2	44.6	1.3	3.0	1.3	2.8
	17.2 - 18.0	34.2	1.1	3.3	0.9	2.8
	18.0 - 18.8	30.3	1.1	3.6	0.8	2.7
	18.8 - 19.6	25.7	1.0	3.9	0.7	2.7
	19.6 - 20.4	21.0	0.9	4.3	0.6	2.7
60 - 100	1.2 - 1.6	42.3	1.6	3.8	3.1	7.2
	1.6 - 2.0	40.3	1.6	3.9	3.2	7.9
	2.0 - 2.4	37.1	1.7	4.5	3.1	8.3
	2.4 - 2.8	39.9	1.7	4.3	3.9	9.8
	2.8 - 3.2	44.1	1.9	4.4	3.9	9.0
	3.2 - 3.6	44.4	1.6	3.6	3.9	8.7
	3.6 - 4.0	45.8	1.6	3.5	3.9	8.6
	4.0 - 4.4	49.5	1.6	3.3	4.1	8.3
	4.4 - 4.8	49.4	1.6	3.1	3.9	7.9
	4.8 - 5.2	53.8	1.7	3.1	3.7	6.9
	5.2 - 5.6	53.6	1.6	3.0	3.6	6.8
	5.6 - 6.0	52.6	1.6	3.0	3.2	6.2
	6.0 - 6.4	56.0	1.7	3.0	3.3	5.8
	6.4 - 6.8	54.7	1.7	3.0	2.9	5.4
	6.8 - 7.2	56.9	1.7	3.0	2.8	4.9
	7.2 - 7.6	53.9	1.7	3.1	2.4	4.5
	7.6 - 8.0	56.2	1.7	3.1	2.5	4.4
	8.0 - 8.4	56.0	1.7	3.1	2.3	4.0
	8.4 - 8.8	49.9	1.6	3.3	1.9	3.9
	8.8 - 9.2	47.9	1.5	3.2	1.9	4.0
	9.2 - 9.6	44.4	1.5	3.5	1.6	3.7
	9.6 - 10.0	43.0	1.5	3.5	1.5	3.5
	10.0 - 10.8	40.0	1.0	2.6	1.4	3.5
	10.8 - 11.6	33.8	0.9	2.8	1.1	3.2
	11.6 - 12.4	28.6	0.9	3.0	0.9	3.2
	12.4 - 13.2	22.5	0.8	3.4	0.7	3.0
	13.2 - 14.0	17.7	0.7	3.8	0.5	2.9
	14.0 - 14.8	13.6	0.6	4.5	0.4	2.9
	14.8 - 15.6	11.4	0.5	4.8	0.3	2.9
	15.6 - 16.4	8.6	0.5	5.5	0.2	2.8
	16.4 - 17.2	6.0	0.4	6.1	0.2	2.8
	17.2 - 18.0	4.5	0.3	7.1	0.1	2.7

θ [mrad]			p [GeV/c]			$\frac{d^2\sigma}{dpd\theta}(p)$ [mb/rad/(GeV/c)]	Δ_{stat} [mb/rad/(GeV/c)]	Δ_{stat} [%]	Δ_{syst} [mb/rad/(GeV/c)]	Δ_{syst} [%]
100	-	140	1.2	-	1.6	60.0	2.7	4.5	4.0	6.6
			1.6	-	2.0	55.4	2.5	4.5	3.7	6.7
			2.0	-	2.4	56.4	2.1	3.7	4.7	8.3
			2.4	-	2.8	56.0	1.9	3.4	4.5	8.0
			2.8	-	3.2	51.2	1.8	3.5	4.0	7.9
			3.2	-	3.6	50.7	1.8	3.5	3.9	7.7
			3.6	-	4.0	48.9	1.8	3.7	3.7	7.5
			4.0	-	4.4	47.9	1.8	3.7	3.4	7.0
			4.4	-	4.8	45.3	1.8	4.0	2.8	6.2
			4.8	-	5.2	47.2	1.9	4.0	2.7	5.7
			5.2	-	5.6	41.8	1.7	4.2	2.2	5.2
			5.6	-	6.0	38.0	1.7	4.4	1.9	5.0
			6.0	-	6.4	37.3	1.7	4.5	1.6	4.2
			6.4	-	6.8	35.4	1.6	4.7	1.5	4.2
			6.8	-	7.2	32.0	1.6	5.0	1.3	4.1
			7.2	-	7.6	23.6	1.3	5.3	1.0	4.2
			7.6	-	8.0	24.2	1.4	5.6	0.9	3.6
			8.0	-	8.4	21.2	1.3	6.0	0.7	3.5
			8.4	-	8.8	17.1	1.1	6.5	0.6	3.5
			8.8	-	9.2	18.2	1.2	6.8	0.6	3.3
			9.2	-	9.6	11.8	1.0	8.2	0.4	3.3
			9.6	-	10.0	12.0	0.9	7.9	0.4	3.2
			10.0	-	10.8	8.4	0.6	6.8	0.3	3.1
			10.8	-	11.6	6.3	0.5	7.6	0.2	3.0
			11.6	-	12.4	3.7	0.4	10.0	0.1	2.8
			12.4	-	13.2	3.2	0.3	10.0	0.1	2.8
140	-	180	1.2	-	1.6	74.5	6.2	8.3	6.5	8.8
			1.6	-	2.0	71.7	3.0	4.2	6.8	9.5
			2.0	-	2.4	65.0	2.6	4.0	4.6	7.0
			2.4	-	2.8	57.4	2.4	4.2	3.9	6.7
			2.8	-	3.2	54.4	2.4	4.4	3.6	6.6
			3.2	-	3.6	50.8	2.3	4.5	3.4	6.6
			3.6	-	4.0	44.2	2.2	5.0	2.7	6.0
			4.0	-	4.4	42.9	2.2	5.2	2.9	6.7
			4.4	-	4.8	37.9	2.1	5.6	1.9	5.0
			4.8	-	5.2	30.6	1.8	6.0	1.4	4.5
			5.2	-	5.6	27.6	1.8	6.5	1.5	5.4
			5.6	-	6.0	21.8	1.6	7.4	0.9	4.2
			6.0	-	6.4	16.6	1.4	8.6	0.7	4.0
			6.4	-	6.8	14.4	1.3	9.2	0.5	3.4
			6.8	-	7.2	12.8	1.3	10.2	0.5	3.7
			7.2	-	7.6	10.1	1.0	10.0	0.3	3.3
			7.6	-	8.0	8.7	1.1	12.2	0.3	3.9
			8.0	-	8.4	5.6	0.8	14.0	0.2	3.6
			8.4	-	8.8	5.4	0.7	13.6	0.2	4.5
			8.8	-	9.2	3.3	0.6	17.7	0.1	3.4
			9.2	-	9.6	1.3	0.4	33.0	0.04	3.1
			9.6	-	10.0	1.3	0.4	28.5	0.05	3.6

θ [mrad]			p [GeV/c]			$\frac{d^2\sigma}{dpd\theta}(p)$ [mb/rad/(GeV/c)]	Δ_{stat} [mb/rad/(GeV/c)]	Δ_{stat} [%]	Δ_{syst} [mb/rad/(GeV/c)]	Δ_{syst} [%]
180	-	240	1.2	-	1.6	104.0	4.4	4.3	5.9	5.7
			1.6	-	2.0	78.5	3.6	4.5	4.2	5.4
			2.0	-	2.4	65.4	3.1	4.7	3.6	5.5
			2.4	-	2.8	57.5	2.7	4.6	3.4	5.9
			2.8	-	3.2	50.7	2.5	4.8	2.7	5.4
			3.2	-	3.6	41.1	2.1	5.2	2.0	4.9
			3.6	-	4.0	35.3	2.0	5.7	1.7	4.9
			4.0	-	4.4	31.1	1.9	6.0	1.4	4.5
			4.4	-	4.8	20.4	1.4	6.9	0.9	4.3
			4.8	-	5.2	16.1	1.2	7.7	0.6	3.8
			5.2	-	5.6	12.4	1.2	9.3	0.5	3.8
			5.6	-	6.0	10.1	1.0	10.0	0.4	3.8
			6.0	-	6.4	6.4	0.8	12.4	0.2	3.5
			6.4	-	6.8	5.6	0.7	12.7	0.2	3.7
			6.8	-	7.2	3.0	0.5	17.7	0.1	3.8
			7.2	-	7.6	3.4	0.6	17.5	0.1	3.7
240	-	300	1.2	-	1.6	114.5	4.5	3.9	5.8	5.1
			1.6	-	2.0	91.6	4.0	4.4	4.4	4.8
			2.0	-	2.4	77.5	3.8	4.9	3.5	4.6
			2.4	-	2.8	58.1	3.3	5.6	2.6	4.4
			2.8	-	3.2	43.8	2.9	6.6	1.9	4.4
			3.2	-	3.6	30.7	2.4	7.9	1.3	4.3
			3.6	-	4.0	20.9	2.0	9.6	0.9	4.3
			4.0	-	4.4	13.6	1.6	12.1	0.6	4.4
			4.4	-	4.8	11.6	1.7	14.4	0.4	3.6
			4.8	-	5.2	7.2	1.2	17.3	0.2	3.4
300	-	360	1.2	-	1.6	110.2	5.4	4.9	4.9	4.4
			1.6	-	2.0	81.2	5.5	6.8	3.2	3.9
			2.0	-	2.4	55.7	5.5	9.8	2.2	3.9
			2.4	-	2.8	57.3	8.1	14.2	2.6	4.5
			2.8	-	3.2	33.3	8.2	24.5	3.0	9.1
			3.2	-	3.6	13.9	8.8	63.6	0.3	2.1

Table 8: The NA61/SHINE results on the proton double differential cross section, $d^2\sigma_p/(dpd\theta)$, in the laboratory system for p+C interactions at 31 GeV/c. The results are presented as a function of momentum in different angular intervals. The statistical Δ_{stat} and systematic Δ_{syst} errors are quoted.

θ [mrad]	p [GeV/c]	$\frac{d^2\sigma}{dpd\theta}(K^0_S)$ [mb/rad/(GeV/c)]	Δ_{stat} [mb/rad/(GeV/c)]	Δ_{stat} [%]	Δ_{syst} [mb/rad/(GeV/c)]	Δ_{syst} [%]
0 - 40	0.4 - 3.4	4.9	0.6	11.9	0.7	14.4
	3.4 - 6.4	5.1	0.5	9.0	0.9	16.6
	6.4 - 9.4	2.4	0.3	13.0	0.5	19.9
	9.4 - 12.4	1.6	0.2	13.9	0.3	19.9
40 - 60	0.4 - 3.4	11.1	1.3	11.5	1.9	17.4
	3.4 - 6.4	11.4	0.9	8.3	1.8	16.3
	6.4 - 9.4	5.3	0.6	10.8	0.7	13.5
	9.4 - 12.4	1.8	0.3	16.3	0.3	18.6
60 - 100	0.4 - 2.4	10.6	1.1	10.8	2.1	20.5
	2.4 - 4.4	15.1	1.0	6.8	1.7	10.6
	4.4 - 6.4	10.8	0.7	6.7	1.3	12.0
	6.4 - 8.4	5.4	0.4	7.6	1.1	20.9
	8.4 - 10.4	2.6	0.3	9.8	0.5	17.9
	10.4 - 12.4	1.1	0.2	14.2	0.2	16.5
100 - 140	0.4 - 2.4	12.2	1.3	10.5	2.1	16.7
	2.4 - 4.4	16.4	1.0	6.0	1.6	9.5
	4.4 - 6.4	7.2	0.5	6.6	0.7	10.0
	6.4 - 8.4	2.8	0.3	9.3	0.5	16.9
	8.4 - 12.4	0.4	0.1	14.7	0.1	21.5
140 - 180	0.4 - 2.4	13.7	1.8	13.5	2.1	14.8
	2.4 - 4.4	11.6	0.8	6.8	1.1	9.1
	4.4 - 6.4	3.7	0.3	8.3	0.3	7.7
	6.4 - 9.4	0.9	0.1	13.5	0.1	16.0
180 - 240	0.4 - 2.4	14.5	1.8	12.5	2.5	17.3
	2.4 - 4.4	7.7	0.5	6.3	0.5	6.4
	4.4 - 9.4	0.7	0.1	9.3	0.1	17.9
240 - 300	0.4 - 3.4	12.8	1.3	10.1	2.6	20.1
	3.4 - 9.4	0.4	0.1	11.5	0.1	17.1

Table 9: The NA61/SHINE results on the K^0_S double differential cross section, $d^2\sigma_{K^0_S}/(dpd\theta)$, in the laboratory system for p+C interactions at 31 GeV/c. The results are presented as a function of momentum in different angular intervals. The statistical Δ_{stat} and systematic Δ_{syst} errors are quoted.

θ [mrad]			p [GeV/c]			$\frac{d^2\sigma}{dpd\theta}(\Lambda)$ [mb/rad/(GeV/c)]	Δ_{stat} [mb/rad/(GeV/c)]	Δ_{stat} [%]	Δ_{syst} [mb/rad/(GeV/c)]	Δ_{syst} [%]
0	-	40	0.4	-	4.4	2.0	0.3	15.5	0.2	11.9
			4.4	-	7.4	3.9	0.4	9.7	0.6	16.3
			7.4	-	10.4	5.5	0.4	8.1	0.8	14.1
			10.4	-	13.4	6.0	0.4	7.1	0.7	10.7
			13.4	-	17.4	5.9	0.4	7.0	0.7	11.7
			17.4	-	21.4	2.8	0.3	10.7	0.2	8.9
40	-	60	0.4	-	4.4	5.3	0.8	15.1	0.7	14.1
			4.4	-	7.4	7.4	0.7	9.6	0.8	11.1
			7.4	-	10.4	8.4	0.6	7.0	0.8	9.2
			10.4	-	13.4	7.4	0.5	6.6	0.6	8.6
			13.4	-	17.4	4.0	0.3	7.4	0.7	16.7
			17.4	-	21.4	1.0	0.1	13.7	0.1	11.7
60	-	100	0.4	-	2.9	5.8	0.9	15.7	0.8	14.0
			2.9	-	4.4	8.2	0.8	9.6	1.8	22.1
			4.4	-	6.4	8.6	0.5	6.4	1.3	14.9
			6.4	-	8.4	7.7	0.4	5.7	0.8	11.4
			8.4	-	10.4	6.0	0.3	5.8	0.6	10.0
			10.4	-	12.4	3.5	0.3	7.2	0.5	14.7
			12.4	-	18.0	1.2	0.1	6.9	0.1	10.8
100	-	140	0.4	-	2.9	8.2	0.9	11.1	1.5	18.2
			2.9	-	4.4	10.3	0.7	6.8	1.9	17.8
			4.4	-	6.4	6.9	0.4	6.1	1.0	14.6
			6.4	-	8.4	4.4	0.3	6.8	0.6	13.4
			8.4	-	11.0	1.8	0.2	9.1	0.3	16.5
			11.0	-	16.4	0.2	0.0	17.5	0.0	11.8
140	-	180	0.4	-	2.9	9.7	1.0	9.8	1.5	16.0
			2.9	-	4.4	9.5	0.6	6.3	0.9	9.8
			4.4	-	6.4	5.0	0.3	6.3	0.8	15.8
			6.4	-	8.0	2.0	0.2	11.2	0.3	14.2
			8.0	-	11.4	0.5	0.1	14.3	0.1	11.2
180	-	240	0.4	-	2.4	10.0	1.0	10.0	0.9	9.1
			2.4	-	4.4	7.6	0.4	5.3	0.7	8.7
			4.4	-	6.4	2.2	0.2	7.6	0.3	12.9
			6.4	-	11.0	0.3	0.1	17.4	0.1	21.7
240	-	300	0.4	-	2.4	7.4	1.0	13.7	1.3	16.9
			2.4	-	4.4	5.4	0.4	6.5	0.5	8.5
			4.4	-	10.4	0.3	0.0	13.8	0.1	23.0
300	-	420	0.4	-	3.0	7.2	0.7	9.6	0.9	12.2
			3.0	-	5.6	0.9	0.1	12.4	0.2	19.3

Table 10: The NA61/SHINE results on the Λ double differential cross section, $d^2\sigma_\Lambda/(dpd\theta)$, in the laboratory system for p+C interactions at 31 GeV/c. The results are presented as a function of momentum in different angular intervals. The statistical Δ_{stat} and systematic Δ_{syst} errors are quoted.